

W.C.

TR-231

AD 759352

TECHNICAL REPORT

THE SOUND VELOCITY STRUCTURE
OF THE NORTH INDIAN OCEAN

DECEMBER 1972



NATIONAL TECHNICAL
INFORMATION SERVICE

DDC
RECEIVED
MAY 2 1973
B

Approved for public release;
distribution unlimited.

U. S. NAVAL OCEANOGRAPHIC OFFICE
WASHINGTON, D. C. 20373

Price \$1.00

104

UNCLASSIFIED

Security Classification

DOCUMENT CONTROL DATA - R & D

Security classification of title, body of abstract and indexing annotation must be entered when the overall report is classified

1. ORIGINATING ACTIVITY (Corporate author) U.S. NAVAL OCEANOGRAPHIC OFFICE WASHINGTON, D.C. 20390	2a. REPORT SECURITY CLASSIFICATION UNCLASSIFIED
	2b. GROUP N.A.

3. REPORT TITLE
THE SOUND VELOCITY STRUCTURE OF THE NORTH INDIAN OCEAN

4. DESCRIPTIVE NOTES (Type of report and inclusive dates)
Technical Report

5. AUTHOR(S) (First name, middle initial, last name)
Don F. Fenner and Paul J. Bucca

6. REPORT DATE December 1972	7a. TOTAL NO. OF PAGES 98	b. NO. OF FIGS. 39
---------------------------------	------------------------------	-----------------------

8. ABSTRACT OR GRANT NO. 714-GT-HKE	9. ORIGINATOR'S REPORT NUMBER TR-231
10. PROJECT NO.	11. OTHER REFERENCE: Any other number that may be associated with this report none

12. DISTRIBUTION STATEMENT
Approved for public release; distribution unlimited.

13. ELEMENTARY NOTES	14. DISTRIBUTION STATEMENT U.S. NAVAL OCEANOGRAPHIC OFFICE WASHINGTON, D. C. 20390
----------------------	--

15. ABSTRACT

All available sound velocity data in the North Indian Ocean (north of 10°S latitude) have been analyzed in terms of annual areal extent and depth of perturbations above deep axial depth, annual average depth and velocity of the deep sound channel and critical depth for the northeast and southwest monsoons. The vertical extent of these and other sound velocity features is shown on six north-south and six east-west cross-sections that extend to a maximum depth of 5000 meters. These analyses indicate that highly saline Red Sea Intermediate Water (RSIW) is the major factor controlling sound velocity structures in the North Indian Ocean. Mixing of RSIW with low salinity water masses causes either sporadic perturbations or an essentially isovelocity layer above deep axial depth. In relatively high concentrations, RSIW causes an anomalously deep (greater than 1700 meters) and narrow sound channel with velocities greater than 1493 meters/second (Gulf of Aden, Arabian Sea, and Arabian Basin). In relatively low concentrations, RSIW causes a somewhat shoaler (1200-1600 meters) and broader sound channel at velocities between 1490 and 1493 meters/second. The deep sound channel along the southern boundary of the area (less than 1100 meters at velocities less than 1490 meters/second) is controlled by low salinity Banda Intermediate Water. Critical depths show the effects of reversing monsoon circulation north of about 10°N latitude, in the western Somali Basin, and south of Java. In the remainder of the area, critical depths are similar during both monsoons. In addition, sound velocity/temperature-salinity comparisons for 36 locations and circulation diagrams for the surface (both monsoons) and for subsurface and intermediate water masses are presented.

REF ID	L N P A		L N P B		N P	
	MOLE	WT	MOLE	WT	MOLE	WT
North Indian Ocean						
Sound Velocity Profiles						
Temperature-Salinity Profiles						
Deep Sound Channel						
Sound Velocity Perturbations						
Critical Depth						
Red Sea Intermediate Water						
Banda Intermediate Water						
Antarctic Intermediate Water						
Subtropical Subsurface Water						
Underwater Sound						
Oceanographic Data						
Oceanography						

ja

FOREWORD

An understanding of sound velocity structure is necessary for effective antisubmarine warfare in any oceanic area. This report summarizes the vertical and horizontal sound velocity structure for the North Indian Ocean, including representative sound velocity profiles. In addition, the total sound velocity structure is related to more commonly understood physical oceanographic variables. Comments on the usefulness of this report are welcomed.


P.V. PURKRABEK

Captain, U.S. Navy

Commander

U.S. Naval Oceanographic Office

PREFACE

The data analysis contained in this report was completed prior to the release of the Oceanographic Atlas of the Indian Ocean (K. Wyrski, E. B. Bennet, and D. J. Rochford, published for the National Science Foundation by the Government Printing Office, Washington, D.C., Nov 1971). Core flow diagrams for Persian Gulf Intermediate Water, Red Sea Intermediate Water, and Antarctic Intermediate Water shown in Appendix C differ in some small details from those given in the above atlas. The diagrams shown in Appendix C adequately explain the observed variations in sound velocity structure; therefore no attempt has been made to incorporate Rochford's recently published core flow diagrams.

The authors wish to thank J. J. Audet, Jr. of the Naval Oceanographic Office for aid in retrieval of data used in this report and Dr. R. L. Fisher of Scripps Institution of Oceanography for providing bathymetric charts for most of the area.

This project was funded and supported by the Long Range Acoustic Propagation Project, Dr. R.D. Gaul, manager.

TABLE OF CONTENTS

	Page
FOREWORD	iii
PREFACE	v
LIST OF FIGURES AND TABLES	viii
INTRODUCTION	1
SOURCES AND TREATMENT OF DATA	1
GENERAL OCEANOGRAPHY AS RELATED TO SOUND VELOCITY STRUCTURES	3
Surface Water Masses	
Subsurface Water Masses	
Intermediate Water Masses	
Deep Water Masses	
SOUND VELOCITY PERTURBATIONS	7
DEEP SOUND CHANNEL	13
DEEP SOUND VELOCITY PROFILES	18
SEASONAL CRITICAL DEPTHS	21
SUMMARY	27
CONCLUSIONS	28
APPENDICES	
A. SELECTED SOUND VELOCITY CROSS-SECTIONS	31
B. SELECTED SOUND VELOCITY AND T-S PROFILES	49
T-S Relations in the North Indian Ocean	
General Comments	
Treatment of Data	
C. GENERAL FLOW AT THE SURFACE AND AT SUBSURFACE AND INTERMEDIATE DEPTHS	83
REFERENCES	95

LIST OF FIGURES AND TABLES

Figure	Page
1. Names of Selected Physical Features	2
2. Annual Approximate Depth and Average Areal Extent of Upper Sound Velocity Minimum	8
3. Annual Approximate Depth and Average Areal Extent of Intermediate Sound Velocity Maximum	9
4. Number of Observations Analyzed for Upper Sound Velocity Minimum and Intermediate Sound Velocity Maximum (all months)	10
5. Annual Average Depth of Deep Sound Channel Axis	14
6. Annual Average Deep Axial Velocity	15
7. Number of Observations Deeper than Deep Sound Channel Axis (all months)	16
8. Basins with Different Sound Velocity Structure Below 2000 Meters	19
9. Average Critical Depth for Northeast Monsoon (Nov-Apr)	22
10. Total Number of Observations for Northeast Monsoon (Nov-Apr)	23
11. Average Critical Depth for Southwest Monsoon (May-Oct)	24
12. Total Number of Observations for Southwest Monsoon (May-Oct)	25

APPENDIX A

A-1. Location of Selected Sound Velocity Cross-sections (Figures A-2 through A-13).	35
A-2. Sound Velocity Cross-section Between 15° and 16° N. Latitude and into the Gulf of Aden for Southwest Monsoon (Jul-Sep)	36

LIST OF FIGURES AND TABLES (cont'd)

Figure	Page
A-3. Sound Velocity Cross-section Between 15° and 16° N. Latitude (Bay of Bengal) for Northeast Monsoon (Mar)	37
A-4. Sound Velocity Cross-sections Between 9° and 10° N. Latitude for Northeast and Southwest Monsoons (Somali Basin)	38
A-5. Sound Velocity Cross-section Along 10° N. Latitude (Andaman Sea) for Northeast Monsoon (Dec-Apr)	39
A-6. Sound Velocity Cross-section Between 5° and 6° N. Latitude for Southwest Monsoon (Jun-Oct)	40
A-7. Sound Velocity Cross-section Between 4° and 5° S. Latitude for Southwest Monsoon (Jun-Oct)	41
A-8. Sound Velocity Cross-section Between 45° and 46° E. Longitude for Southwest Monsoon (Jul-Sep)	42
A-9. Sound Velocity Cross-section Between 55° and 56° E. Longitude for Southwest Monsoon (Jul-Oct)	43
A-10. Sound Velocity Cross-section Between 66° and 67° E. Longitude for Northeast Monsoon (Nov-Apr)	44
A-11. Sound Velocity Cross-section Between 77° and 78° E. Longitude for Southwest Monsoon (Sep-Oct)	45
A-12. Sound Velocity Cross-section Between 86° and 87° E. Longitude for Northeast Monsoon (Nov-Mar)	46
A-13. Sound Velocity Cross-section Between 94° and 95° E. Longitude for Northeast Monsoon (Dec-Apr)	47

APPENDIX B

B-1. T-S Relations in the North Indian Ocean	53
B-2. Location of Selected Sound Velocity/T-S Comparisons (Figures B-3 through B-38)	54

LIST OF FIGURES AND TABLES (cont'd)

Figure	Page
B-3. Sound Velocity/T-S Comparison for Southwest Monsoon	55
B-4. Seasonal Sound Velocity/T-S Comparison	55
B-5. Sound Velocity/T-S Comparison for Southwest Monsoon	56
B-6. Sound Velocity/T-S Comparison for Southwest Monsoon	56
B-7. Seasonal Sound Velocity/T-S Comparison	57
B-8. Sound Velocity/T-S Comparison for Northeast Monsoon	58
B-9. Seasonal Sound Velocity/T-S Comparison	59
B-10. Sound Velocity/T-S Comparison for Northeast Monsoon	60
B-11. Seasonal Sound Velocity/T-S Comparison	60
B-12. Sound Velocity/T-S Comparison for Northeast Monsoon	61
B-13. Seasonal Sound Velocity/T-S Comparison	62
B-14. Seasonal Sound Velocity/T-S Comparison	63
B-15. Sound Velocity/T-S Comparison for Northeast Monsoon	64
B-16. Sound Velocity/T-S Comparison for Northeast Monsoon	64
B-17. Sound Velocity/T-S Comparison for Northeast Monsoon	65
B-18. Sound Velocity/T-S Comparison for Southwest Monsoon	65
B-19. Sound Velocity/T-S Comparison for Southwest Monsoon	66
B-20. Sound Velocity/T-S Comparison for Southwest Monsoon	66
B-21. Seasonal Sound Velocity/T-S Comparison	67
B-22. Sound Velocity/T-S Comparison for Southwest Monsoon	68

LIST OF FIGURES AND TABLES (cont'd)

Figure	Page
B-23. Seasonal Sound Velocity/T-S Comparison	69
B-24. Sound Velocity/T-S Comparison for Southwest Monsoon	70
B-25. Seasonal Sound Velocity/T-S Comparison	71
B-26. Seasonal Sound Velocity/T-S Comparison	72
B-27. Sound Velocity/T-S Comparison for Southwest Monsoon	73
B-28. Seasonal Sound Velocity/T-S Comparison	74
B-29. Sound Velocity/T-S Comparison for Northeast Monsoon	75
B-30. Sound Velocity/T-S Comparison for Southwest Monsoon	75
B-31. Sound Velocity/T-S Comparison for Northeast Monsoon	76
B-32. Sound Velocity/T-S Comparison for Southwest Monsoon	76
B-33. Sound Velocity/T-S Comparison for Southwest Monsoon	77
B-34. Sound Velocity/T-S Comparison for Northeast Monsoon	77
B-35. Seasonal Sound Velocity/T-S Comparison	78
B-36. Sound Velocity/T-S Comparison for Northeast Monsoon	79
B-37. Sound Velocity/T-S Comparison for Northeast Monsoon	80
B-38. Seasonal Sound Velocity/T-S Comparison	81

APPENDIX C

C-1. Generalized Surface Circulation for Northeast Monsoon (Nov-Apr)	86
C-2. Generalized Surface Circulation for Southwest Monsoon (May-Oct)	87

LIST OF FIGURES AND TABLES (cont'd)

Figure	Page
B-23. Seasonal Sound Velocity/T-S Comparison	69
B-24. Sound Velocity/T-S Comparison for Southwest Monsoon	70
B-25. Seasonal Sound Velocity/T-S Comparison	71
B-26. Seasonal Sound Velocity/T-S Comparison	72
B-27. Sound Velocity/T-S Comparison for Southwest Monsoon	73
B-28. Seasonal Sound Velocity/T-S Comparison	74
B-29. Sound Velocity/T-S Comparison for Northeast Monsoon	75
B-30. Sound Velocity/T-S Comparison for Southwest Monsoon	75
B-31. Sound Velocity/T-S Comparison for Northeast Monsoon	76
B-32. Sound Velocity/T-S Comparison for Southwest Monsoon	76
B-33. Sound Velocity/T-S Comparison for Southwest Monsoon	77
B-34. Sound Velocity/T-S Comparison for Northeast Monsoon	77
B-35. Seasonal Sound Velocity/T-S Comparison	78
B-36. Sound Velocity/T-S Comparison for Northeast Monsoon	79
B-37. Sound Velocity/T-S Comparison for Northeast Monsoon	80
B-38. Seasonal Sound Velocity/T-S Comparison	81

APPENDIX C

C-1. Generalized Surface Circulation for Northeast Monsoon (Nov-Apr)	86
C-2. Generalized Surface Circulation for Southwest Monsoon (May-Oct)	87

LIST OF FIGURES AND TABLES (cont'd)

Figure	Page
C-3. Generalized Flow of Persian Gulf Intermediate Water (PGIW) High Salinity Core	88
C-4. Generalized Flow of Subtropical Subsurface Water (SSW) Low Salinity Core	89
C-5. Generalized Flow of Red Sea Intermediate Water (RSIW) High Salinity Core	90
C-6. Generalized Flow of Antarctic Intermediate Water (AAIW) Low Salinity Core	92
C-7. Generalized Flow of Banda Intermediate Water (BIW) Low Salinity Core	93

TABLES

Table	Page
I. Typical Sound Velocities for Major North Indian Basins	20

INTRODUCTION

Events of the past few years have shown increased Naval interest in the Indian Ocean. However, despite extensive data collected by the International Indian Ocean Expedition (IIOE), there has been no systematic description of the sound velocity structure of the Indian Ocean. In an effort to correct this discrepancy, the Naval Oceanographic Office (NAVOCEANO) prepared a paper (Fenner and Bucca, Jan 1971) in which areal contour charts of various sound velocity features and a limited number of sound velocity/temperature-salinity (T-S) comparisons were used to define the complex sound velocity structure of the northwest Indian Ocean (north of 10° S. latitude, west of 80° E. longitude). This report supplements the above paper in terms of sound velocity cross-sections, additional sound velocity/T-S comparisons, and analysis and extends east to the Malay Peninsula and Indonesia. This report also explains the temporal and spatial distribution of various sound velocity features in terms of water mass analysis and circulation patterns. For purposes of this report, deep axial depth is defined as the deepest sound velocity minimum (usually absolute minimum). Sound velocity perturbations are defined as changes from a negative to a positive sound velocity gradient (or vice versa) that are less effective channels for sound transmission than the deep sound channel. Critical (limiting) depth is that depth where the sound velocity is equal to the maximum sound velocity at the surface or in the surface mixed layer. The names of selected physical features used in this report are given on Figure 1. Locations of sound velocity cross-sections are shown on Figure A-1. Locations of sound velocity/T-S comparisons are given on Figure B-2.

SOURCES AND TREATMENT OF DATA

All available data from the National Oceanographic Data Center (NODC) were analyzed during the preparation of this report. Additional Nansen cast data collected by the HMAS DIAMANTINA in 1964 and 1966 also are included (Commonwealth Scientific and Industrial Research Organization, Australia, 1967 and Scully-Power, Apr 1969, respectively). All data were converted into sound velocity using the equation of Wilson, 1960.

These data were analyzed for the depth and axial velocity of the deep sound channel, the depth of various sound velocity minima and maxima (perturbations) lying above deep axial depth, and for critical depth. The data were compiled by one-degree square and season. One-degree square compilations were averaged by two-degree square (i.e., four one-degree squares) on an annual basis for deep axial depth, deep axial velocity, and the depth of the maxima and minima associated with sound velocity perturbations. Critical depths were averaged similarly on a seasonal basis. The two-degree square

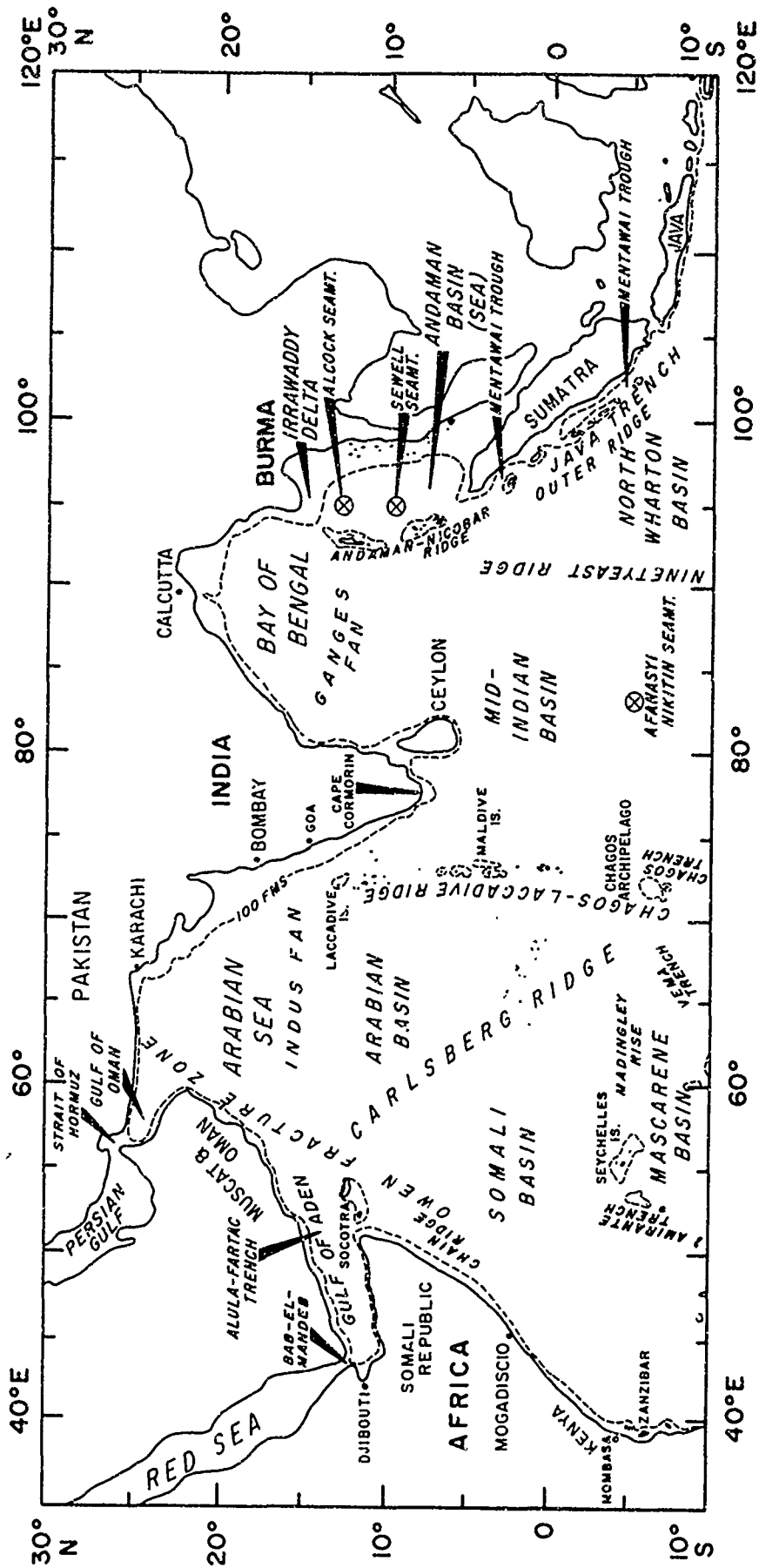


FIGURE 1. NAMES OF SELECTED PHYSICAL FEATURES

averages of these parameters then were contoured or generalized on an areal basis. Regions where sound velocity perturbations are present more than 80% of the time, 20-80% of the time, and less than 20% of the time also were derived on a two-degree square basis and generalized on an areal basis. Throughout this report, the first type of region above will be referred to as having a PERMANENT upper sound velocity minimum or intermediate sound velocity maximum, the second as TRANSITORY. In the third region, sound velocity perturbations effectively are ABSENT. The treatment of data used in the construction of the sound velocity cross-sections and sound velocity/T-S comparisons is discussed in Appendices A and B, respectively.

All available T S data were analyzed for the depth of salinity maxima and minima in order to determine the causes of various sound velocity features and the circulation of various high and low salinity water masses. Core salinity depths were generalized on an areal basis for the following water masses:

- high salinity Persian Gulf Intermediate Water (PGIW)
- low salinity Subtropical Subsurface Water (SSW)
- high salinity Red Sea Intermediate Water (RSIW)
- low salinity Antarctic Intermediate Water (AAIW)
- low salinity Banda Intermediate Water (BIW).

T-S indices for each of these water masses are shown on Figure B-1 and generalized flow diagrams are presented in Appendix C.

The two seasons of winter (November through April) and summer (May through October) are used in this report. These seasons correspond to the maximum duration of the NORTHEAST and SOUTHWEST MONSOONS, respectively. However, April-May and October-November often are representative of inter-monsoonal periods (Duing, 1970). This fact was taken into account during data analysis. Two monsoonal seasons exist throughout the area, but generally are not found south of 10° S. latitude except along major land mass boundaries (Duing, 1970).

GENERAL OCEANOGRAPHY AS RELATED TO SOUND VELOCITY STRUCTURES

A general knowledge of the circulation and water mass structure is a prerequisite to the understanding of sound velocity structures. This is particularly true in the North Indian Ocean due to the reversing monsoonal circulation at the

surface and the highly complex and interdependent circulation and mixing of high and low salinity water masses at subsurface and intermediate depths. The figures in Appendix C show surface circulation for the northeast and southwest monsoons and the circulation of the two high salinity and three low salinity water masses that markedly effect sound velocity structure at depth. T-S indices for the water masses discussed in the following paragraphs are given on Figure B-1.

Surface Water Masses

During the northeast monsoon (Figure C-1), surface circulation is essentially counterclockwise except in the Arabian Sea, Bay of Bengal, and along the southern boundary of the area (South Equatorial Current). During most of the southwest monsoon (Figure C-2), surface circulation is clockwise throughout the area. The seasonal reversal of surface circulation has noticeable effects on water properties south of about 10° N. latitude. In the Somali Basin, high salinity Arabian Sea Water (ArSW) is carried by the Northeast Monsoon Current, while during the Southwest monsoon lower salinity Indian Equatorial Water (IEW) is brought into this region by the South Equatorial and Somali Currents. Therefore surface and near-surface sound velocities are somewhat higher during the northeast monsoon (Figure B-25). The exact opposite is true in the Mid-Indian Basin, where the Southwest Monsoon Current replaces less saline Bay of Bengal Water (BBW) and IEW with more saline ArSW. This results in somewhat higher velocities during the southwest monsoon (Figure B-23). North of about 10° N. latitude, surface and near-surface sound velocities are more temperature dependent, resulting in higher velocities during the southwest monsoon (Figures B-9 and B-14), except in areas of southwest monsoon upwelling. Figures B-5, B-16, and B-35 show sound velocity and T-S profiles typical for ArSW, BBW, and IEW, respectively.

Substantial regions of upwelling during the southwest monsoon have been documented off Muscat and Oman by Ryther and Menzel, 1965; off the Somali Republic by Warren, et al., 1966; and south of Java by Wyrski, 1962 (Figures B-4, B-11, and B-38 respectively). In all three cases, surface velocities are less during the southwest monsoon. Off the Somali Republic, velocities are less to depths exceeding 1000 meters (Figure B-11). During the northeast monsoon, regions of upwelling are found at the northern end of the Arabian Sea, off the coast of Kenya, off the east coast of India, and off the coast of Burma. During the northeast monsoon, upwelling is confined to or near the continental shelf.

Subsurface Water Masses

At subsurface depths, sound velocity structures throughout most of the area are altered by intrusions of PGIW (Rochford, 1964) and SSW (Ivanenkov and Gubin, 1960). PGIW is characterized by a salinity maximum between 250 and 400 meters (Figure C-3), and enters the Gulf of Oman across the Straits of Hormuz. SSW is formed at the Subtropical Convergence (approximately 40° S. latitude) and initially is characterized by an oxygen minimum in a layer of decreasing salinity. However, as SSW flows north into regions with increasing concentrations of RSIW, a salinity minimum is formed at a depth somewhat deeper than the characteristic oxygen minimum (Warren, et al., 1966). In the North Indian Ocean, this salinity minimum generally is found between 400 and 700 meters (Figure C-4). South of 5° S. latitude, SSW often cannot be distinguished by T-S analysis alone.

In the Gulf of Oman and the northern Arabian Sea, high concentrations of PGIW cause the formation of a sound velocity minimum at the interface with ArSW and a sound velocity maximum at the approximate depth of the high salinity core (Figures B-3 and B-4). However, throughout most of the area, lesser concentrations of PGIW retard the formation of negative velocity gradients below the surface mixed layer (e.g., see Figures B-5, B-8, B-16, B-22, and B-36). Intrusion of SSW tends to block the southward spread of PGIW, particularly in the Somali Basin. In the Somali Basin, SSW can cause the formation of a strong sound velocity minimum (Figures B-8, B-18, and B-30). However, throughout much of the area, SSW interacts with PGIW above and RSIW below to form an essentially isovelocity layer between the strong subsurface negative velocity gradient and the deep sound channel axis (Figures B-19, B-22, B-26, B-28, and B-33).

Intermediate Water Masses

At intermediate depths, sound velocity structures throughout most of the area are modified by intrusions of RSIW (Rochford, 1964), AAIW (Sverdrup, et al., 1942), and BIW (Rochford, 1966a). RSIW is characterized by a salinity maximum between about 500 and 1000 meters (Figure C-5) and enters the Gulf of Aden through Bab-el-Mandeb. Two preferential RSIW flows are apparent in the North Indian Ocean, one south along the east coast of Africa and another east into the Mid-Indian Basin between the Maldivé Islands and the Chagos Archipelago. Larger concentrations of RSIW apparently enter the Gulf of Aden during the northeast monsoon due to the lack of a northward flowing current in Bab-el-Mandeb (Seri, 1968). AAIW is characterized by a salinity minimum between about 700 and 900 meters (Figure C-6) and enters the area from the south.

Northward flow of AAIW is blocked by the Chagos-Laccadive Ridge, the westward flow of BIW, and the preponderance of RSIW to the north. BIW is characterized by a salinity minimum between about 900 and 1200 meters (Figure C-7) and enters the area from the east. Although the southward spread of RSIW and the Chagos-Laccadive Ridge divert the main BIW flow to south of 10° S. latitude, substantial concentrations are observed north and south of the Seychelles Islands.

In the Gulf of Aden, west central Arabian Basin, and western Somali Basin, high RSIW concentrations cause the formation of a strong sound velocity maximum at the approximate depth of the high salinity core (e.g., see Figures B-6, B-7, B-8, and B-18). As previously shown (Fenner and Bucca, Jan 1971), high concentrations of RSIW in the presence of SSW can cause the formation of a "meaningful" upper sound channel in the Gulf of Aden and a limited region east and south of Socotra. In this context, a "meaningful" upper sound channel is defined as having an average velocity at the upper sound velocity minimum that is at least 1.5 meters/second greater than the comparable velocity at the intermediate sound velocity maximum. Figures B-7, B-8, and B-11 show good examples of a "meaningful" upper sound channel. This sound velocity structure is much less widespread in the northwest Indian Ocean than that observed in the North Atlantic Ocean (Fenner and Bucca, Dec 1969), largely due to the rapid dilution of RSIW in Bab-el-Mandeb and the Gulf of Aden. Less than 200 nautical miles east of Bab-el-Mandeb, only 35% RSIW remains unmixed (Figure B-6). In contrast, more than 95% unmixed Mediterranean Intermediate Water (MIW; upper North Atlantic Deep Water of Defant, 1961) was found approximately 250 nautical miles west of the Straits of Gibraltar (Fenner and Bucca, Dec 1969).

Throughout much of the area, RSIW depresses the deep sound channel axis and, in concentrations less than 15%, broadens the channel by interacting with various low salinity water masses to form an essentially isovelocity layer between the subsurface negative velocity gradient and deep axial depth. Figures B-21, B-26 and B-28 show such interactions with AAIW and/or SSW in the Arabian, Somali, and Mid-Indian Basins, respectively. Interaction of RSIW with either AAIW or BIW can split RSIW into two lobes, both with a salinity maximum and weak sound velocity maximum (Figures B-25 and B-31, respectively). The lower RSIW lobe formed by interaction with BIW often lies at depths below 1100 meters (Figure B-29). In such cases, it is called North Indian Deep Water (NIDW).

The effects of AAIW on sound velocity structures in the North Indian Ocean are minor due to its sporadic occurrence and relatively small unmixed concentrations. AAIW either can cause the formation of a weak sound velocity minimum below the RSIW induced maximum (Figure B-11) or interact with RSIW and SSW to form an essentially isovelocity gradient above deep axial depth

(Figures B-12 and B-33). In contrast, BIW has marked effects in forming a shoaler and narrower sound channel at lesser velocities (Figures B-34 and B-36). Along the southern boundary of the area, the deep sound channel structure is controlled by BIW. Mixing of BIW and RSIW can form sound velocity perturbations below deep axial depth (Figure B-31).

Deep Water Masses

The circulation of NIDW (formed by sinking of RSIW south of the North Indian Equatorial Front, Shcherbinin, 1969a) and North Indian Bottom Water does not change the basic shape of the positive sound velocity gradient below about 2000 meters. Although sound velocity varies somewhat from basin to basin (see Table I), deep sound velocity profiles are quite similar throughout most of the area. However, in the Andaman Basin, sound velocity values below 2000 meters are 10- to 17-meters/second (m/sec) greater than those in the rest of the North Indian Ocean (Table I). In addition, T-S values below 2000 meters in the Andaman Basin are essentially isothermal and isohaline (Figure B-17). Andaman Sea Deep and Bottom Water is considerably warmer and more saline than NIDW, and probably is formed by sinking and local modification of RSIW and IEW trapped inside the Andaman Basin.

SOUND VELOCITY PERTURBATIONS

Highly sporadic perturbations in the sound velocity structure above deep axial depth were found throughout most of the northwest Indian Ocean, in a band between about 5° N. and 5° S. latitude across the Mid-Indian and North Wharton Basins, and in the region south of Java. Sound velocity minima associated with these perturbations generally occur at the approximate depth of the SSW or AAIW low salinity core (Figure B-11). Sound velocity maxima associated with such structures generally occur at the approximate depth of the RSIW high salinity core (Figure B-11). Sound velocity maxima associated with the PGIW high salinity core were found only in the Gulf of Oman and northern Arabian Sea (Figures B-3 and B-4).

Figures 2 and 3 show the annual approximate depth and average areal extent of the upper sound velocity minimum and intermediate sound velocity maximum. The data base for both figures is shown on Figure 4. Throughout most of the area, sound velocity perturbations were highly sporadic, particularly in terms of depth. More than one perturbation often was found on a given sound velocity profile. Therefore, it was impossible to contour the depth of either the upper sound velocity minimum or intermediate sound velocity maximum. Rather, Figures 2 and 3 show regions of similar average depth of the most pronounced minimum and maximum (i.e., minimum with least sound velocity and maximum

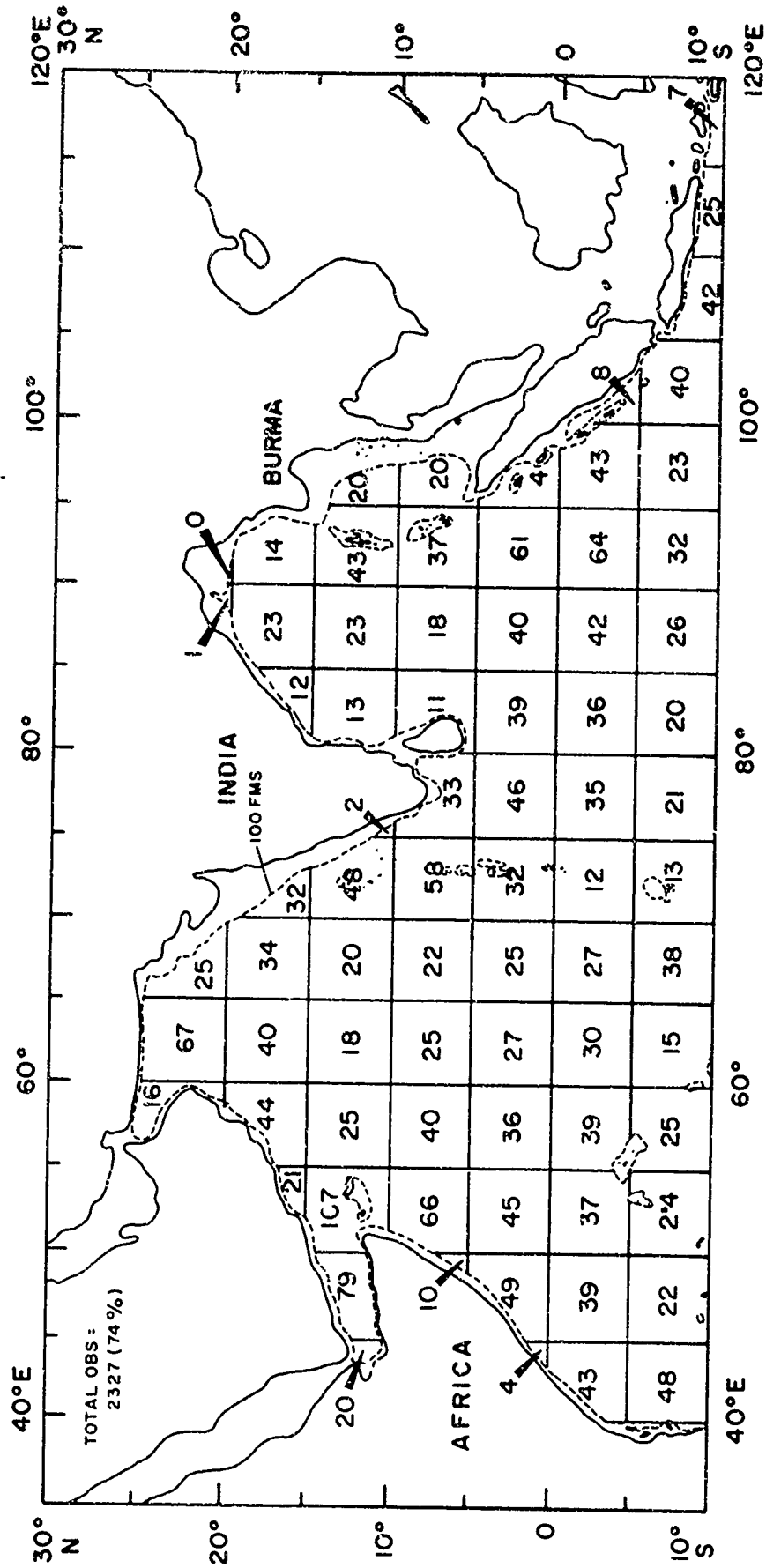


FIGURE 4. NUMBER OF OBSERVATIONS ANALYZED FOR UPPER SOUND VELOCITY MINIMUM AND INTERMEDIATE SOUND VELOCITY MAXIMUM (ALL MONTHS)

with greatest sound velocity). The duration of both features was somewhat less sporadic. Therefore, identical permanent (greater than 80%) and transitory (20-80%) regions are shown on both figures.

The three fingerlike regions with deepening permanent perturbations extending from the Gulf of Aden into the Somali Basin correspond well with flows of RSIW (Figure C-5), as does the region with deepening transitory perturbations that spans the Mid-Indian and North Wharton Basins between about 5° N. and 5° S. latitude. The two fingerlike regions with shoaling transitory perturbations extending from about 5° S. latitude into the Somali Basin correspond with flows of SSW and AAIW (Figures C-4 and C-6, respectively). The three regions where sound velocity perturbations effectively are absent (Arabian Sea, Bay of Bengal, and Mid-Indian and North Wharton Basins south of about 5° S. latitude) all correspond to regions without RSIW (Figures B-5, B-16, and B-36, respectively).

The complex nature of perturbations in the vertical dimension is best seen on the various sound velocity cross-sections. Figure A-2 shows a permanent upper sound velocity minimum at velocities less than 1510 m/sec and a permanent intermediate sound velocity maximum at velocities between 1510 and 1515 m/sec that extends the length of the Gulf of Aden and terminates near the Owen Fracture Zone. Minima are associated with SSW, maxima with RSIW. East of 60° E. longitude, only sporadic perturbations are found (lesser concentrations of RSIW). Figure A-3 shows that perturbations are absent in the Bay of Bengal except along the India and Irrawaddy Delta continental slopes (probably caused by local northeast monsoon upwelling). The effects of upwelling on sound velocity perturbations is demonstrated well on Figure A-4 (northern Somali Basin). During the northeast monsoon, a single minimum and maximum is found on both sides of the Owen Fracture Zone (caused by SSW and RSIW, respectively). However, during the southwest monsoon in the presence of extensive upwelling, two distinct sets of perturbations are found west of 55° E. longitude at velocities up to 5 m/sec less than those during the northeast monsoon (also see Figure B-11).

Figure A-6 shows a double set of perturbations at velocities greater than 1495 m/sec west of the Chain Ridge (southwest monsoon upwelling) that merges into a single minimum/maximum structure at about 56° E. longitude. Only sporadic perturbations are found east of the Carlsberg Ridge at velocities less than 1495 m/sec (lesser RSIW concentrations). Figure A-7 shows a single minimum/maximum structure at velocities less than 1495 m/sec over the southern Somali Basin (interaction of SSW and RSIW). However, on either side of the Seychelles Islands a more complicated pattern of perturbations is associated with intermixing of RSIW, SSW, AAIW, and BIW. East of the Seychelles Islands and

over the Carlsberg Ridge there are perturbations below the deep sound channel axis (mixing of RSIW and BIW) as well as above. Perturbations are absent over the Mid-Indian Basin, but recur sporadically east of the Ninetyeast Ridge above and below deep axial depth.

In the north-south direction, Figure A-8 shows a single perturbation structure that shoals and becomes better defined north of 5° S. latitude (caused by interaction of SSW and RSIW). Farther east, Figure A-9 shows a well defined minimum/maximum structure north of the Equator. However, between the Equator and about 5° N. latitude, 3 separate sets of perturbations are found at velocities from greater than 1500 to less than 1495 m/sec (intermixing of RSIW, SSW, AAIW, and BIW). South of Cape Cormerin, Figure A-11 shows transitory perturbations north of the Equator at velocities less than 1495 m/sec, including one perturbation below deep axial depth. In the eastern part of the area, Figure A-13 shows an extremely complex pattern of perturbations between 5° S. and the Andaman-Nicobar Ridge at velocities greater and less than 1495 m/sec. Perturbations at greater than 1495 m/sec probably are caused by mixing of RSIW with SSW; those at less than 1495 m/sec by mixing of RSIW and/or NIDW with BIW. At approximately 2° S. latitude, perturbations above and below deep axial depth merge with the deep sound channel axis. The complicated perturbations north of the Equator also are related to bathymetric interference by the Andaman-Nicobar Ridge to the eastward flow of RSIW and the northward flow of SSW and BIW.

The highly significant role of RSIW in forming sound velocity perturbations in the North Indian Ocean is analogous to that of MIW in forming an upper sound channel and subsurface sound velocity maximum in the North Atlantic Ocean (Fenner and Bucca, Nov 1971). In the North Atlantic, relatively high to intermediate concentrations of MIW (greater than about 60%) are necessary for the formation of an upper sound channel and subsurface sound velocity maximum. However, sound velocity perturbations frequently are found at greater than 30% MIW concentrations. Using the curve of Defant, 1961, 30% unmixed MIW lies at approximately the same salinity as 10% unmixed RSIW (Figure B-1). RSIW concentrations greater than 10% generally are found in the Gulf of Aden, east and south of Socotra, and along the east coast of Africa (Figures B-7, B-8 and B-11, and B-25, respectively). Therefore, the relative absence of RSIW (due to intensive mixing with low salinity water masses in the Somali and northern Arabian Basins) is largely responsible for the absence of a "meaningful" upper sound channel and well defined intermediate (subsurface) sound velocity maximum in the North Indian Ocean.

DEEP SOUND CHANNEL

Figures 5 and 6 show the annual average depth and velocity of the deep sound channel axis. The data base for both figures (number of observations deeper than deep axial depth) is shown on Figure 7. These values of depth and velocity are larger than those at similar latitudes in the Pacific Ocean (Johnson and Norris, Apr 1967). However, the deep axial depths throughout most of the area are similar to those in the North Atlantic Ocean in the presence of unmixed MIW (Fenner and Bucca, Nov 1971). Deep axial depths and velocities greater than 1200 meters and 1490 m/sec, respectively, are controlled by RSIW, that (like MIW) depresses the deep sound channel. Deep axial depths and velocities less than 1200 meters and 1490 m/sec are controlled by BIW that causes a shoaler and narrower sound channel. AAIW does not have a marked effect on deep channel structure in the North Indian Ocean since it is present only sporadically and in slight concentrations. Deep axial depths and velocities less than 1200 meters and greater than 1493 m/sec found in the Andaman Basin are intermediate between those controlled by RSIW and BIW. Here, the deep channel structure probably is controlled by locally modified RSIW and IEW that enter the Andaman Basin north of Sumatra and at about 10° N. latitude.

Deep axial depths and velocities greater than 1700 meters and 1494 m/sec consistently are found in the Gulf of Aden, Arabian Sea, and north Arabian Basin in the presence of RSIW and ArSW. The marked southward tendency of the 1600- through 1800-meter and 1494- through 1496-m/sec isolines along about 55° E. longitude corresponds well to preferential flows of RSIW (Figure C-5). The relatively tight packing of deep axial depth and velocity isolines south of the Equator corresponds roughly to the northern limit of persistent BIW occurrence (Figure C-7) and the position of the North Indian Equatorial Front (Shcherbinin, 1969a). The northward tendency of the 1500- and 1600-meter deep axial depth isolines along about 90° E. longitude corresponds to a flow of RSIW into the Bay of Bengal (Figure C-5). Deep axial depth isolines shown on Figure 5 are accurate to ± 100 meters north of the Equator, but are somewhat less accurate between the Equator and 10° S. latitude (± 100 to 200 meters). The same is true of the deep axial velocity isolines shown on Figure 6 (accurate to ± 0.5 m/sec north of Equator, to ± 1.0 m/sec south of Equator). The greater variability of both parameters south of the Equator is related to mixing between various intermediate water masses.

The sound velocity cross-sections illustrate these and other features of the deep axial depth and velocity distribution. Figure A-2 shows a relatively stable deep sound channel at approximately 1800 meters extending across the Gulf of Aden and northern Arabian Basin. Axial velocities less than 1495 m/sec probably represent regions lacking substantial RSIW flows (Figure C-5). Figure A-3 shows

DEEP SOUND CHANNEL

Figures 5 and 6 show the annual average depth and velocity of the deep sound channel axis. The data base for both figures (number of observations deeper than deep axial depth) is shown on Figure 7. These values of depth and velocity are larger than those at similar latitudes in the Pacific Ocean (Johnson and Norris, Apr 1967). However, the deep axial depths throughout most of the area are similar to those in the North Atlantic Ocean in the presence of unmixed MIW (Fenner and Bucca, Nov 1971). Deep axial depths and velocities greater than 1200 meters and 1490 m/sec, respectively, are controlled by RSIW, that (like MIW) depresses the deep sound channel. Deep axial depths and velocities less than 1200 meters and 1490 m/sec are controlled by BIW that causes a shoaler and narrower sound channel. AAIW does not have a marked effect on deep channel structure in the North Indian Ocean since it is present only sporadically and in slight concentrations. Deep axial depths and velocities less than 1200 meters and greater than 1493 m/sec found in the Andaman Basin are intermediate between those controlled by RSIW and BIW. Here, the deep channel structure probably is controlled by locally modified RSIW and IEW that enter the Andaman Basin north of Sumatra and at about 10° N. latitude.

Deep axial depths and velocities greater than 1700 meters and 1494 m/sec consistently are found in the Gulf of Aden, Arabian Sea, and north Arabian Basin in the presence of RSIW and ArSW. The marked southward tendency of the 1600- through 1800-meter and 1494- through 1496-m/sec isolines along about 55° E. longitude corresponds well to preferential flows of RSIW (Figure C-5). The relatively tight packing of deep axial depth and velocity isolines south of the Equator corresponds roughly to the northern limit of persistent BIW occurrence (Figure C-7) and the position of the North Indian Equatorial Front (Shcherbinin, 1969a). The northward tendency of the 1500- and 1600-meter deep axial depth isolines along about 90° E. longitude corresponds to a flow of RSIW into the Bay of Bengal (Figure C-5). Deep axial depth isolines shown on Figure 5 are accurate to ±100 meters north of the Equator, but are somewhat less accurate between the Equator and 10° S. latitude (±100 to 200 meters). The same is true of the deep axial velocity isolines shown on Figure 6 (accurate to ±0.5 m/sec north of Equator, to ±1.0 m/sec south of Equator). The greater variability of both parameters south of the Equator is related to mixing between various intermediate water masses.

The sound velocity cross-sections illustrate these and other features of the deep axial depth and velocity distribution. Figure A-2 shows a relatively stable deep sound channel at approximately 1800 meters extending across the Gulf of Aden and northern Arabian Basin. Axial velocities less than 1495 m/sec probably represent regions lacking substantial RSIW flows (Figure C-5). Figure A-3 shows

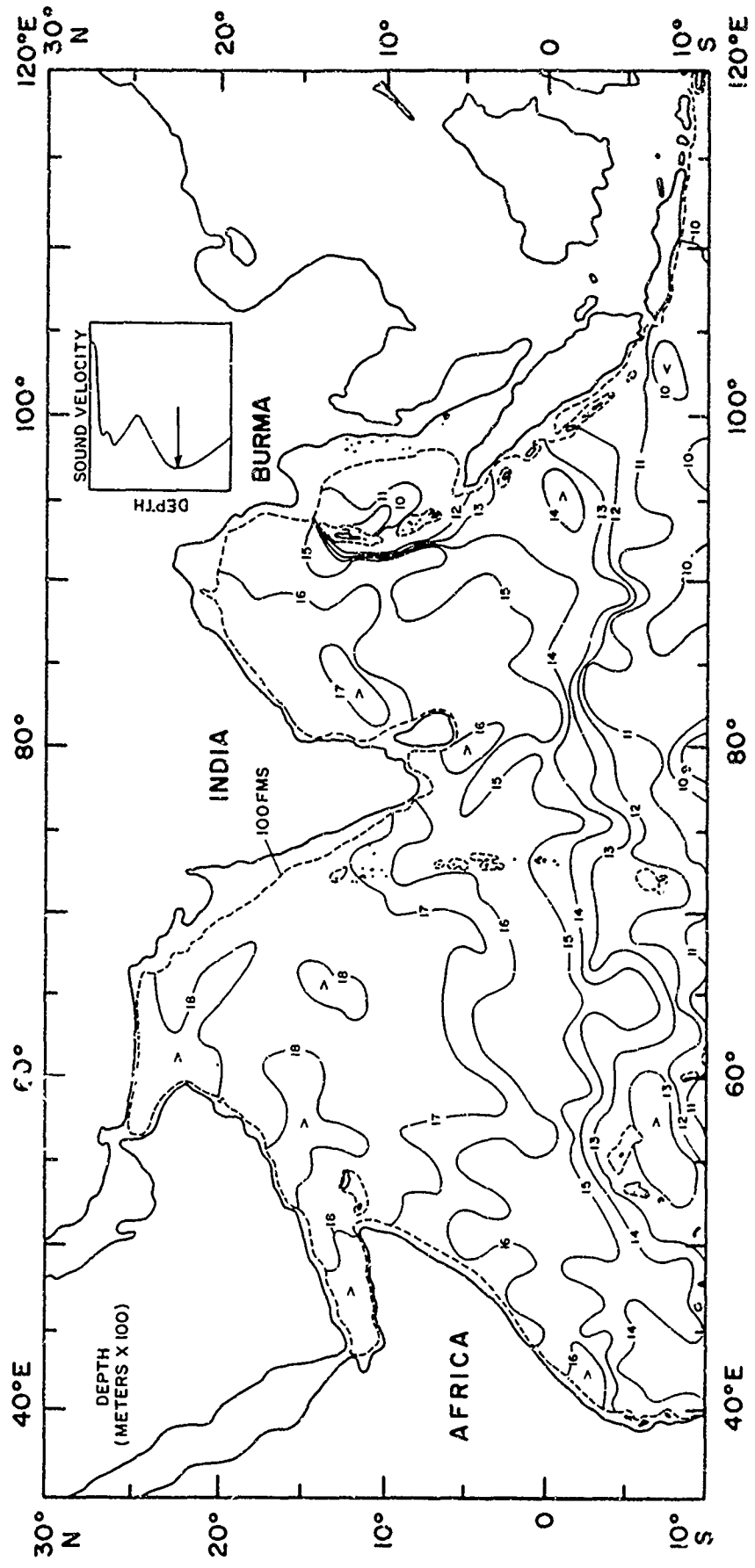


FIGURE 5. ANNUAL AVERAGE DEPTH OF DEEP SOUND CHANNEL AXIS

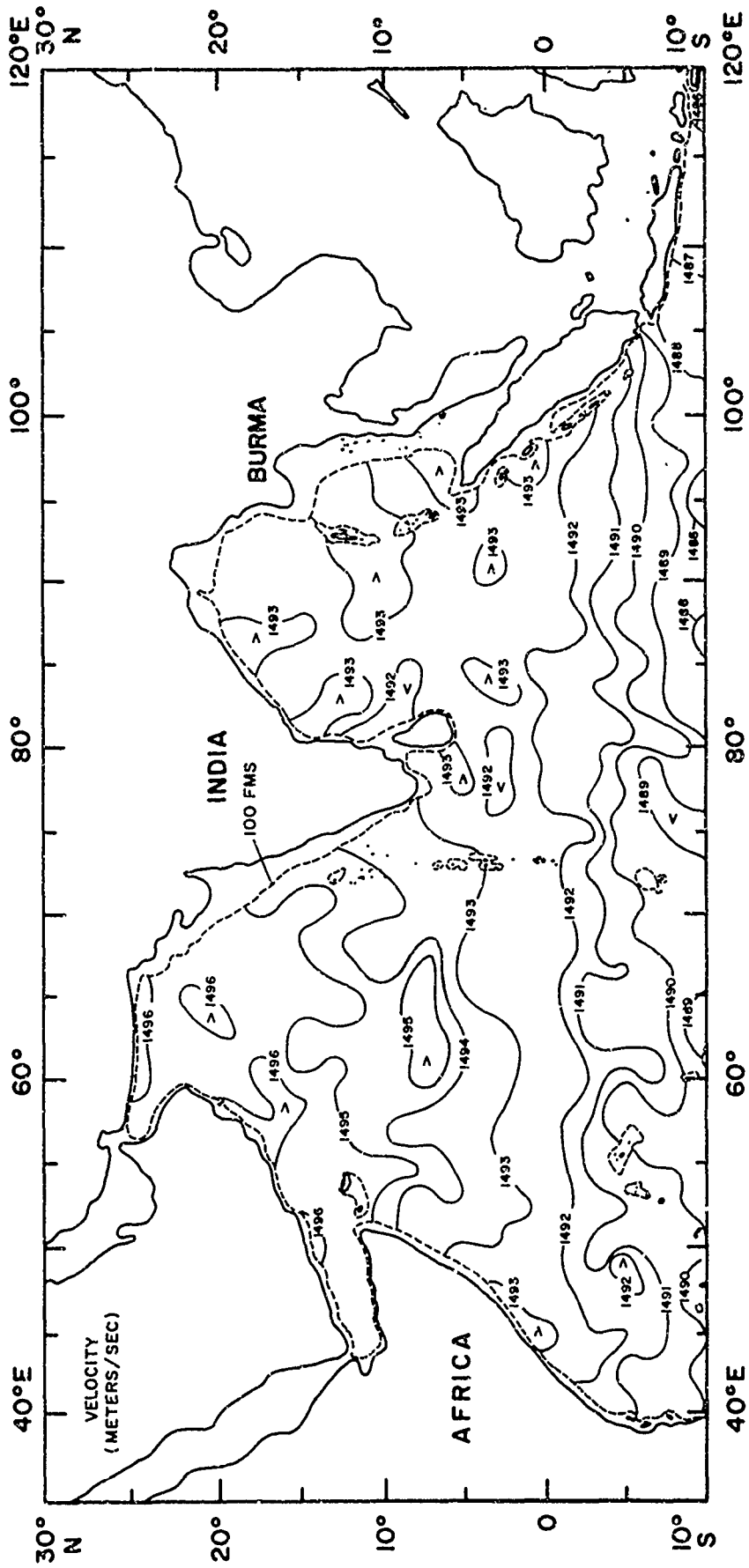


FIGURE 6. ANNUAL AVERAGE DEEP AXIAL VELOCITY

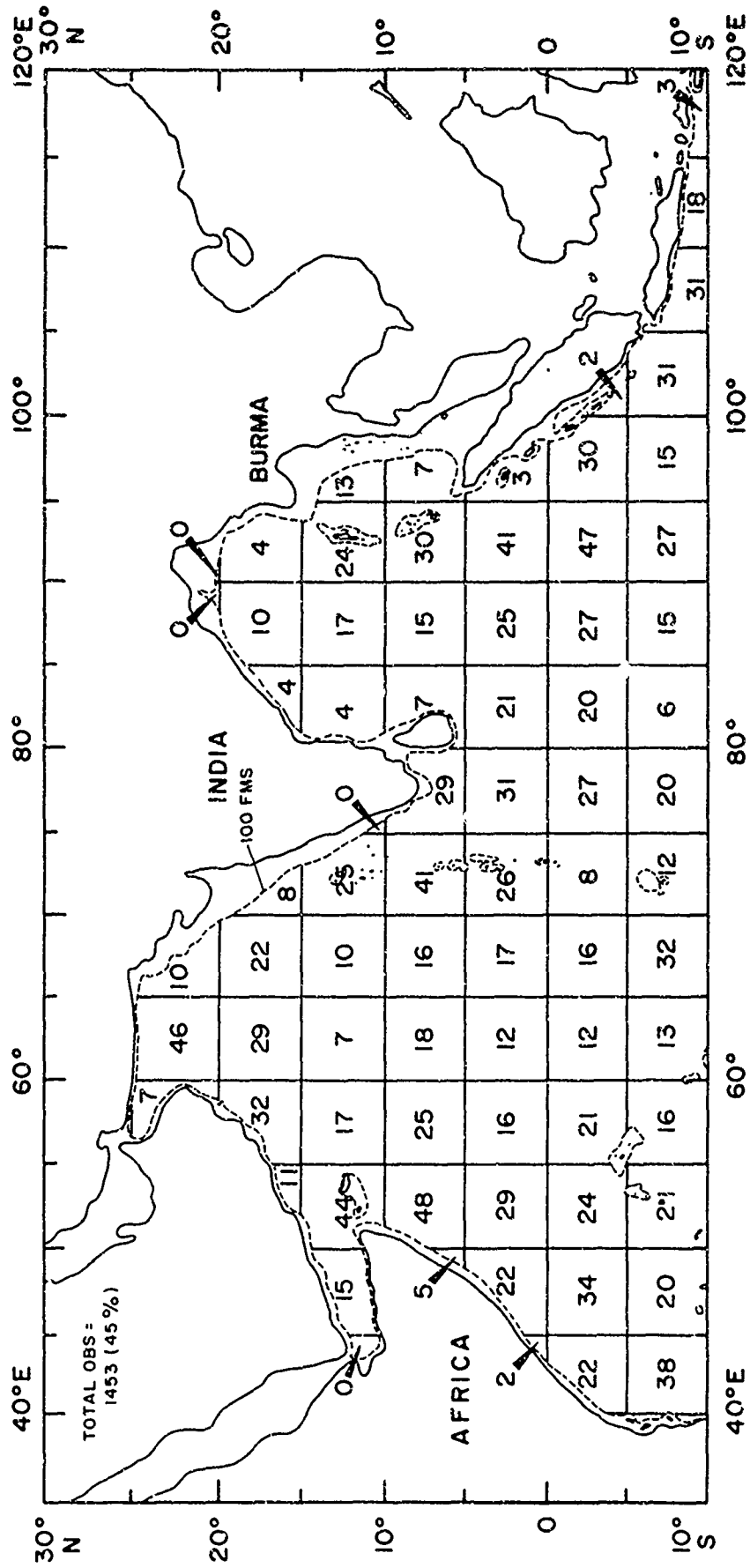


FIGURE 7. NUMBER OF OBSERVATIONS DEEPER THAN DEEP SOUND CHANNEL AXIS (ALL MONTHS)

the extremely broad deep channel at depths less than 1800 meters and velocities less than 1495 m/sec in the Bay of Bengal (much diluted RSIW). Figure A-5 shows a deep axis that shoals from 1600 to less than 1000 meters over the Andaman-Nicobar Ridge and then deepens to approximately 1100 meters inside the Andaman Basin. Axial velocities are less than 1495 m/sec throughout, but closely approach 1495 m/sec in the passage over the Andaman-Nicobar Ridge. Figure A-6 shows a relatively stable deep sound channel that extends from the Somali Republic to the northern tip of Sumatra at depths of 1500 to 1800 meters and velocities less than 1495 m/sec (somewhat diluted RSIW). The channel is considerably broader in the east (lesser concentrations of RSIW). In the Mentawai Trough, axial depths are approximately 1100 meters (similar to Andaman Basin). Farther south, Figure A-7 shows a relatively stable deep channel over the Somali Basin at depths between 1400 and 1600 meters and velocities less than 1495 m/sec (much diluted RSIW). However, east of the Seychelles Islands, the deep channel fluctuates between depths and velocities less than 1100 meters and 1490 m/sec (BIW) and depths and velocities greater than 1500 meters and less than 1495 m/sec (much diluted RSIW). The lack of substantial concentrations of unmixed RSIW results in an extremely broad channel across the area. Rapid changes in deep axial depth and velocity over the Carlsberg Ridge correspond to intensive mixing of RSIW and BIW. In the Mentawai Trough, axial depths are less than 1000 meters and axial velocities greater than 1500 m/sec (local modification of IEW).

In the north-south direction, Figure A-8 shows a channel that deepens to the north over the Somali Basin from about 1200 meters to greater than 1600 meters. Deep axial velocities vary from less than 1490 m/sec in the south (BIW) to less than 1495 m/sec off Mogadiscio (somewhat diluted RSIW). Higher RSIW concentrations in the north result in a much narrower deep channel. Farther east, Figure A-10 shows a similar deepening of the channel to the north, accompanied by an increase in deep axial velocity and a northward constriction in the vertical extent of the channel. Deep axial velocities greater than 1495 m/sec over the Arabian Basin are associated with an east-west flow of RSIW (Figure C-5). At about 6° S. latitude, sound velocity perturbations above and below deep axial depth merge with the deep sound channel (mixing of RSIW and BIW). Over the Mid-Indian Basin and in the Bay of Bengal, Figure A-12 shows a channel that deepens to the north (from less than 1000 to about 1700 meters) at velocities ranging from less than 1490 to less than 1495 m/sec. However, the deep sound channel is only slightly wider in the south than in the north (much diluted RSIW along entire cross-section). Over the North Wharton Basin, Figure A-13 shows a relatively stable deep axis at 1000 to 1200 meters (BIW) that deepens rapidly to 1500 meters at about 3° S. latitude (preferential RSIW flow), shoals to 1000 meters

over the Andaman-Nicobar Ridge, and then deepens slightly inside the Andaman Basin. Axial velocities vary from less than 1490 m/sec over the North Wharton Basin to nearly 1495 m/sec in the Andaman Basin. The very narrow deep sound channel north of the Andaman-Nicobar Ridge is caused by a combination of relatively large RSIW concentrations and local modification of IEW. At about 2° S. latitude, sound velocity perturbations above and below deep axial depth merge with the deep sound channel (mixing of RSIW and BIW).

In summary, unmixed RSIW is the main factor controlling deep sound channel structure in the North Indian Ocean. In the southern Arabian Basin, Bay of Bengal, and throughout most of the Somali, Mid-Indian, and North Wharton Basins, the deep sound channel is very broad with an axis between 1200 and 1600 meters at velocities less than 1495 m/sec (Figures B-13, B-16, B-19, B-22 and B-24, respectively). In these same regions, concentrations of unmixed RSIW are less than 15%. However, in the Gulf of Aden, northern Arabian Basin, and Arabian Sea, the deep sound channel has a narrower structure with an axis deeper than 1700 meters at velocities greater than 1495 m/sec (Figures B-7, B-8, and B-9, respectively). In the Gulf of Aden and northern Arabian Basin, RSIW concentrations vary between 15% and 35%. In the Arabian Sea, salinities above 1500 meters are greater than that for 15% RSIW (due to mixing of RSIW with PGIW and high salinity ArSW). Therefore, relatively high salinities below 1000 meters (often associated with high RSIW concentrations) result in a deeper and narrower sound channel, while relatively low salinities below 1000 meters (often associated with low RSIW concentrations) result in a somewhat shallower and broader sound channel. An analogous situation occurs in the North Atlantic Ocean in the presence of varying concentrations of high salinity MIW (Fenner and Bucca, Nov 1971). Very low salinities below 1000 meters (associated with BIW) result in a shallower and narrower deep sound channel (Figure B-36).

DEEP SOUND VELOCITY PROFILES

Figure 8 shows the location of the six physiographic basins in the North Indian Ocean that have somewhat different velocity structures below 2000 meters. Typical sound velocities for each of these basins are given at 500-meter intervals on Table I. The concept of typical velocity curves for physiographic basins was initially shown for the North Atlantic Ocean by Moore, November 1965. Deep temperature and salinity profiles for major ocean basins (including the Somali, Madagascar-Mascarene, Mid-Indian, and Wharton Basins) have been discussed by Olson, June 1968. These profiles can be used with the equation of Wilson, 1960 to obtain deep sound velocity profiles.

Table I shows deep velocity variations of less than 3.0 m/sec below 2000 meters between the five major North Indian basins. However, in the Andaman

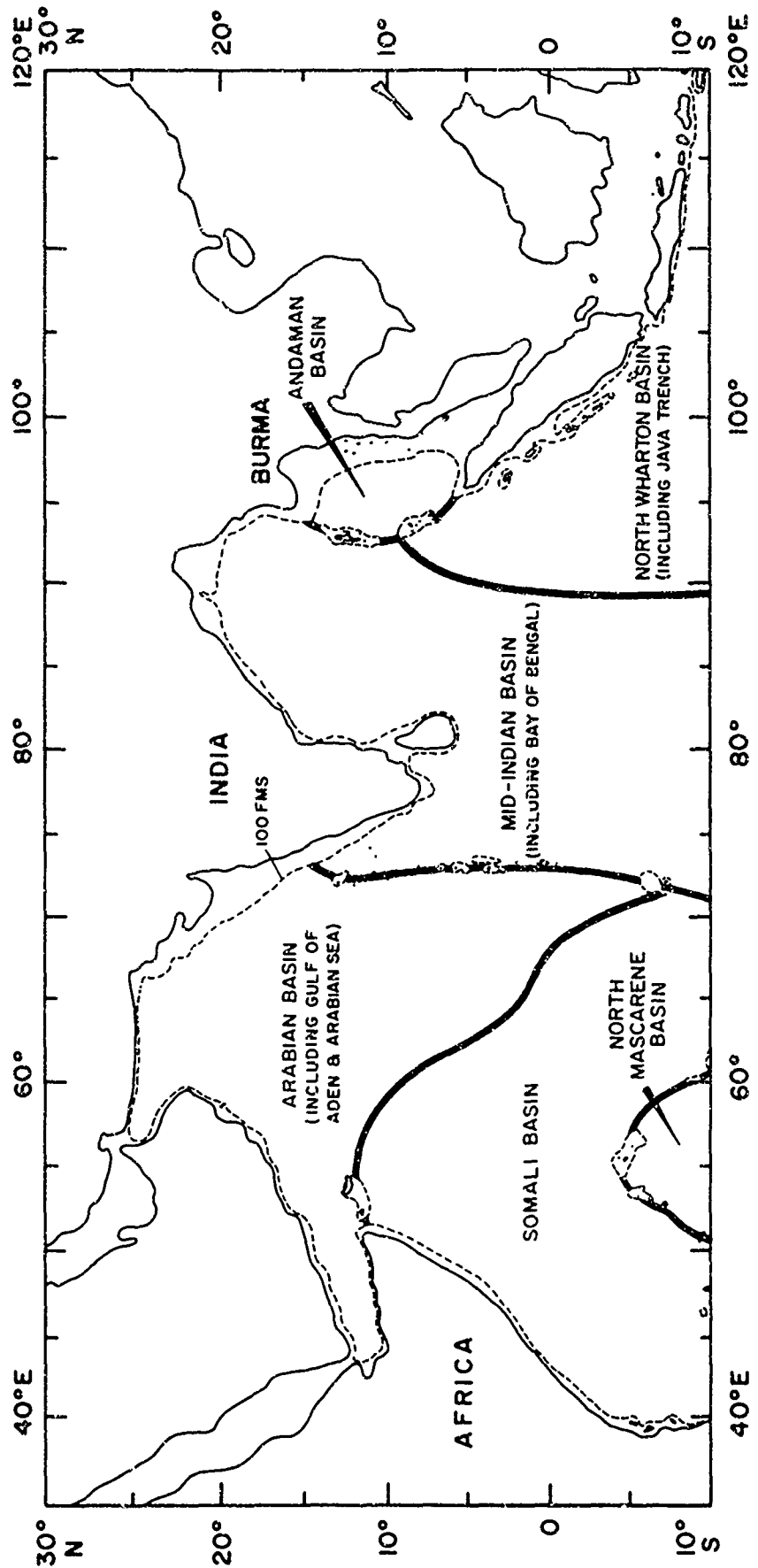


FIGURE 8. BASINS WITH DIFFERENT SOUND VELOCITY STRUCTURE BELOW 2000 METERS

TABLE 1. TYPICAL SOUND VELOCITIES FOR MAJOR NORTH INDIAN BASINS

DEPTH (M)	TYPICAL SOUND VELOCITIES(m/sec)					
	Arabian Basin	Somali Basin	North Mascas- Basin	Mid- Indian Basin	North Wharton Basin	Andaman Basin
2000	1495.1	1494.1	1493.5	1492.4	1494.4	1503.8
2500	1500.4	1500.0	1500.0	1499.7	1500.0	1512.3
3000	1507.7	1506.9	1507.3	1506.9	1507.0	1521.1
3500	1515.9	1514.9	1514.9	1514.7	1514.2	1530.3
4000	1524.7	1523.3	1522.7	1523.2	1522.3	1539.6
4500	1534.0	1531.9	1531.2	1532.1	1531.0	-----
5000	-----	1540.8	-----	1541.3	1540.2	-----
5500	-----	1549.9	-----	1550.8	1549.6	-----
6000	-----	-----	-----	1560.7	1559.3	-----
6500	-----	-----	-----	-----	1569.3	-----

Basin, deep velocities are 10- to 17-m/sec greater than those in the North Indian Ocean proper. This is due to the higher temperatures and salinities of Andaman Sea Deep and Bottom Water (Figure B-1) which is formed by local modification of RSIW and IEW. The deep profile in the Arabian Basin has consistently higher sound velocities than those in the other four major basins due to the higher T-S values found below 2000 meters in both the Arabian Basin and the Arabian Sea (influence of ArSW, PGIW, and RSIW). The deep profile in the North Wharton Basin has consistently lower sound velocities due to lower T-S values found below 2000 meters. The Wharton Basin extends to about 35° S. latitude and is a primary route for deep water flow between the Antarctic and the North Indian Ocean (Zaklinskii, 1963). The deep velocity profiles for the Somali, North Mascarene, and Mid-Indian Basins are intermediate between those for the Arabian and North Wharton Basins.

SEASONAL CRITICAL DEPTHS

Figures 9 and 11 show critical depths for the northeast and southwest monsoon. The data bases for these figures are given on Figures 10 and 12. Overall, 47% of the existing critical depth data represents northeast monsoon conditions, 53% southwest monsoon conditions. During the southwest monsoon, data are inadequate to evaluate in a large region north and east of Ceylon. Critical depths were derived using the deep sound velocity profiles shown on Table I. Critical depth contours for both seasons are accurate to ± 50 meters throughout the area.

During the northeast (winter) monsoon, critical depths range from greater than 5200 meters in the southern Somali Basin to less than 4700 meters off Pakistan. In the Andaman Sea, critical depths are approximately 4100 meters due to the anomalous deep sound velocity profile for the Andaman Basin (Table I). The marked differences in deep velocity structures on either side of the Andaman-Nicobar Ridge result in an apparent 900-meter change in critical depth in the various passages into the Andaman Sea. Critical depths less than 4800 meters in the northern end of the Arabian Sea correspond well with sea surface temperature minima shown for December through February by La Violette and Frontenac, August 1967. Critical depths less than 4900 meters in the northern Bay of Bengal correspond to similar sea surface temperature minima shown by La Violette, August 1967. Critical depths less than 4800 meters off the Kenya and east India coasts represent local regions of northeast monsoon upwelling (Figure C-1). In the western Somali Basin, the northeast to southwest tendency of the 4900- and 5000-meter isolines is caused by the Northeast Monsoon Current which carries warmer, more saline ArSW into the region north of the Seychelles Islands. This mechanism combined with surface insolation leads to deeper critical depths throughout the southern Somali Basin. Warmer, more saline waters carried

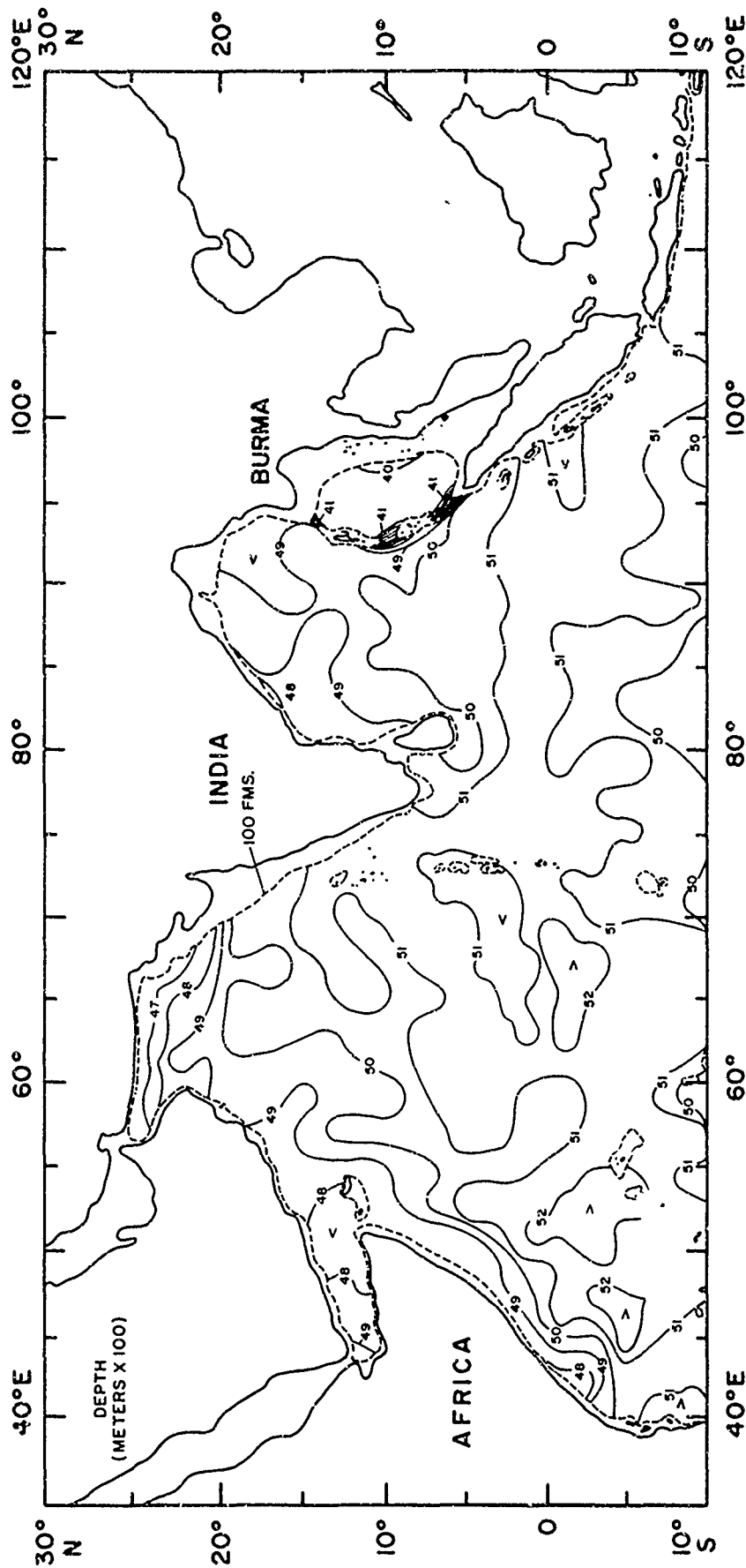


FIGURE 9. AVERAGE CRITICAL DEPTH FOR NORTHEAST MONSOON (NOV-APR)

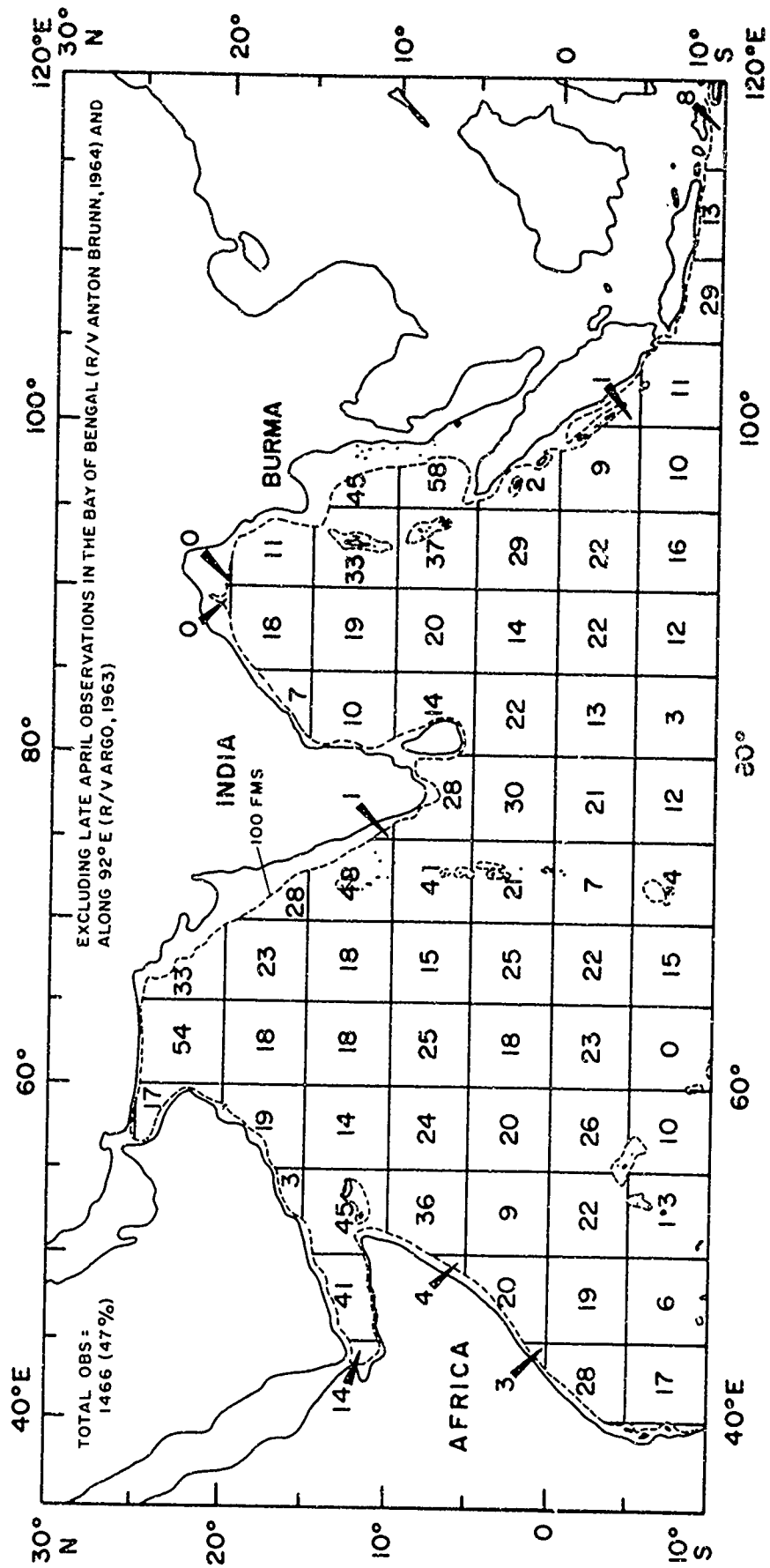


FIGURE 10. TOTAL NUMBER OF OBSERVATIONS FOR NORTHEAST MONSOON (NOV-APR)

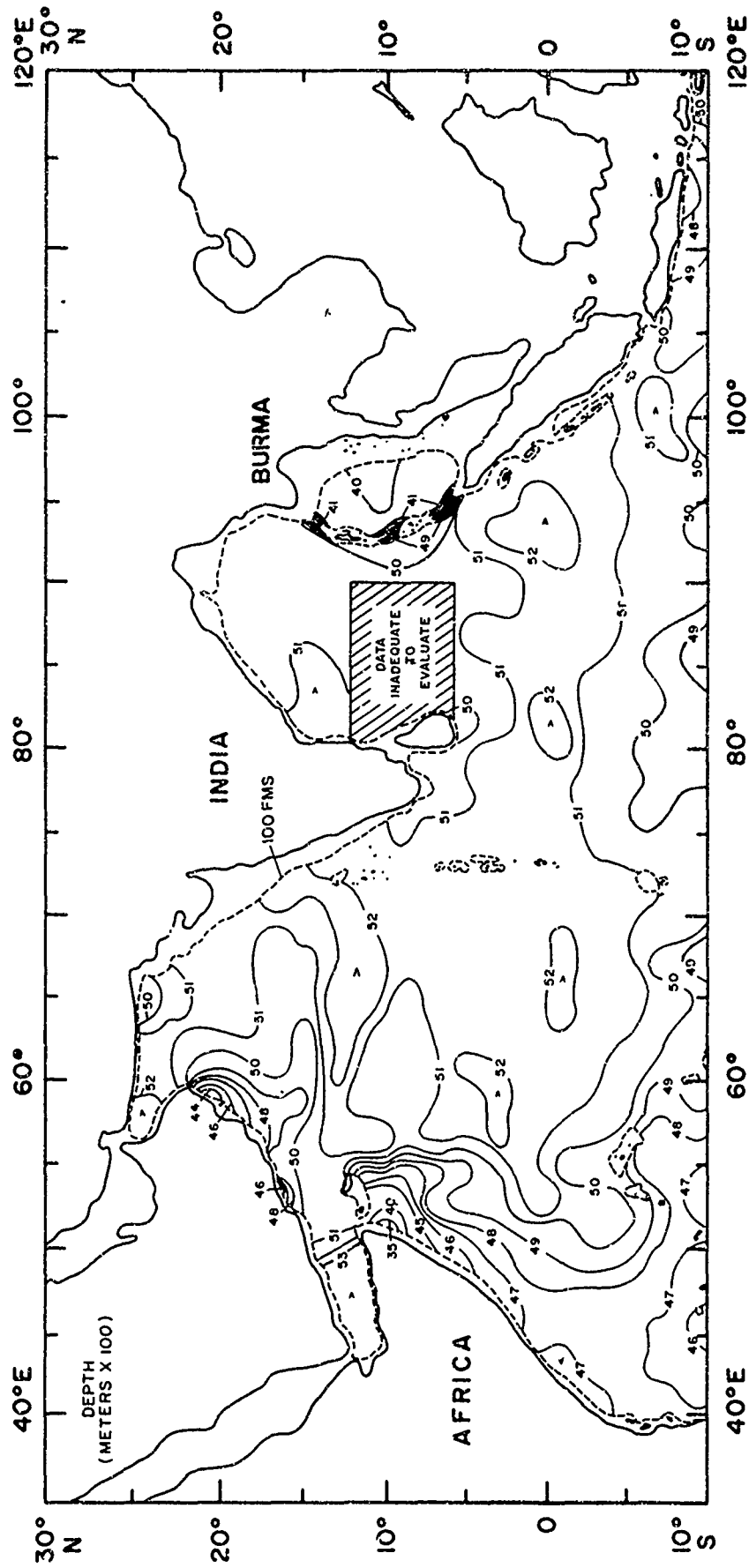


FIGURE 11. AVERAGE CRITICAL DEPTH FOR SOUTHWEST MONSOON (MAY-OCT)

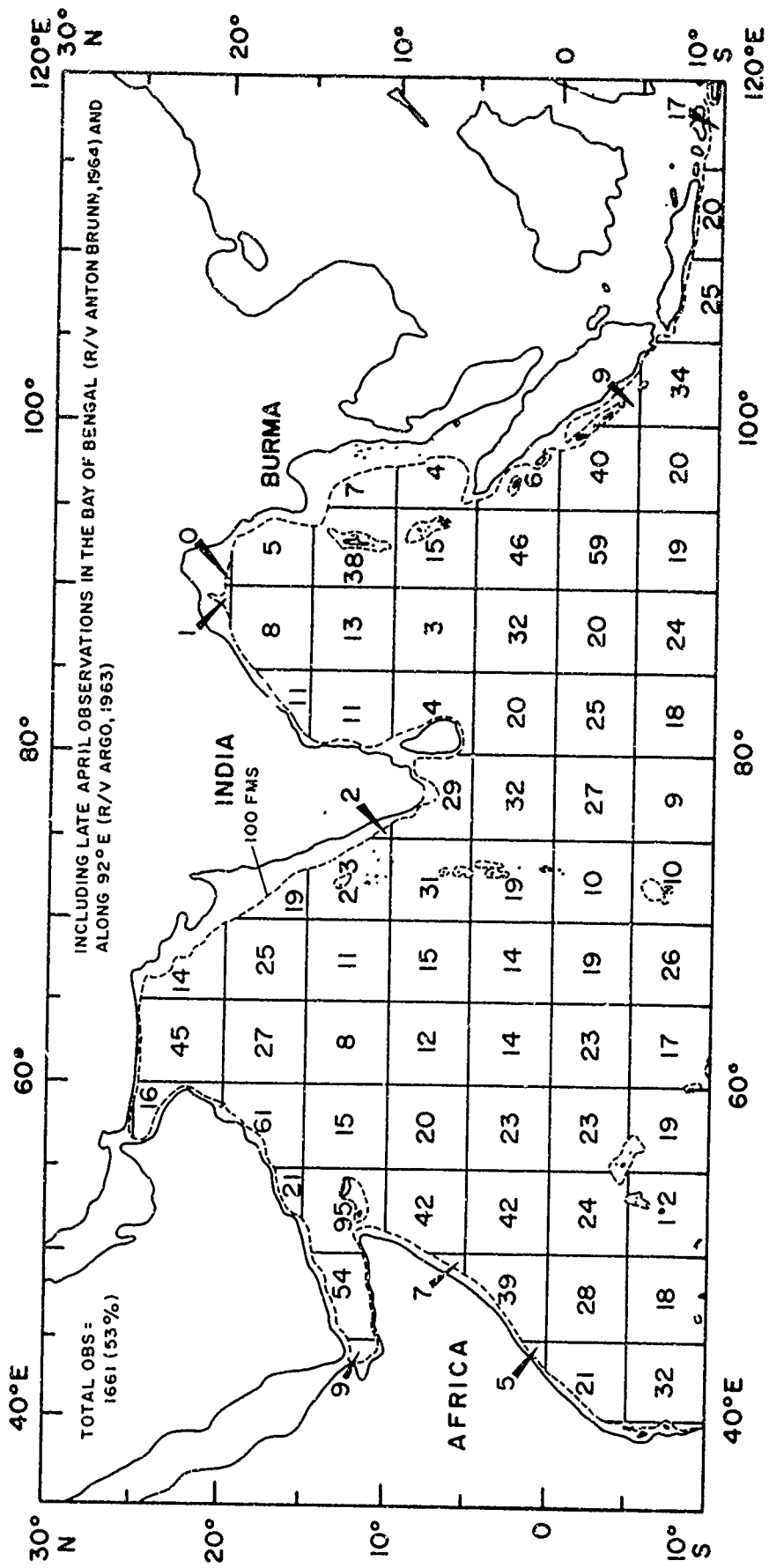


FIGURE 12. TOTAL NUMBER OF OBSERVATIONS FOR SOUTHWEST MONSOON (MAY-OCT)

east by the Equatorial Countercurrent result in the greater than 5100-meter critical depths along the Equator in the Mid-Indian and North Wharton Basins. Critical depths less than 5100 meters north of the Equator on either side of the Maldive Islands are caused by less saline IEW carried by the North Equatorial Current. Critical depths less than 5000 meters along the southern boundary of the area are related to the flow of the South Equatorial Current.

During the southwest (summer) monsoon, critical depths vary from greater than 5200 meters along the Equator and west of the Laccadive Islands to less than 3500 meters in the strong upwelling center off the Somali Republic (Figure C-2). Upwelling off the Somali Republic causes the shoalest annual critical depths found in the North Indian Ocean (also see Figures A-4 and B-11). Southwest monsoon upwelling also causes critical depths less than 4700 meters off the east Africa coast, less than 4400 meters off Muscat and Oman, and less than 4800 meters south of Java. Despite the effects of upwelling, critical depths in the Arabian Sea are 100 to 300 meters deeper during the southwest monsoon due to increased surface insolation. Critical depths in the Bay of Bengal are about 200 meters deeper during the southwest than during the northeast monsoon. The clockwise circulation of the South Equatorial, Somali, and Southwest Monsoon Currents causes a similar pattern in the critical depth isolines south of about 5° N. latitude and west of about 70° E. longitude (4800- through 5100-meter isolines). The intense packing of isolines in the northwestern Somali Basin is a result of both upwelling and an oceanic front associated with the eastern wall of the Somali Current. Critical depths greater than 5100 meters between about 5° N. and 5° S. latitude are related to surface insolation and the Southwest Monsoon Current which carries warmer, more saline ArSW to the south. Critical depths less than 5000 meters along the southern boundary of the area are related to the colder, more dilute flow of the South Equatorial Current (IEW). Critical depths in the Andaman Sea are similar to those for the northeast monsoon.

South of about 10° N. latitude, critical depths are similar during both monsoons in the region between the Seychelles Islands and Sumatra. This indicates that critical depths are independent of monsoonal effects in this truly equatorial area. However, in the Arabian Sea, Bay of Bengal, western Somali Basin and in the region south of Java, critical depths vary by at least 200 meters between the northeast and southwest monsoons. In the Arabian Sea and Bay of Bengal, this variance is attributable to increased surface insolation during the southwest monsoon (except off the coast of Muscat and Oman). In the western Somali Basin, the region south of Java, and off Muscat and Oman this variance is related to upwelling caused by monsoonal reversal in surface circulation.

SUMMARY

Interaction of high salinity Red Sea Intermediate Water (RSIW) and Persian Gulf Intermediate Water (PGIW) with low salinity Subtropical Subsurface Water (SSW), Antarctic Intermediate Water (AAIW), and Banda Intermediate Water (BIW) results in anomalous sound velocity structures throughout much of the North Indian Ocean. Interaction of PGIW and SSW causes an extremely strong negative velocity gradient between the surface mixed layer and about 200 meters. Mixing of RSIW with SSW and/or AAIW results in either sporadic sound velocity perturbations or an essentially isovelocity layer directly above deep axial depth. Relatively unmixed RSIW results in anomalously large deep axial depth values, whereas relatively well mixed RSIW causes a broader and somewhat shoaler deep sound channel. Relatively unmixed BIW results in the formation of a somewhat shoaler and narrower deep sound channel. Intensive mixing of RSIW and BIW can cause sound velocity perturbations below deep axial depth.

Sound velocity perturbations (Figures 2 and 3) occur greater than 80% of the time in the Gulf of Aden and much of the Somali Basin; 20-80% of the time throughout the Arabian Basin, southern Somali Basin, and in a band between about 5° N. and 5° S. latitude east of India and Ceylon; but are effectively absent in the northeast Arabian Sea, Bay of Bengal and southern Mid-Indian Basins. The lack of high unmixed RSIW concentrations throughout most of the area precludes the formation of a well defined upper sound channel and subsurface sound velocity maximum such as found in the Northeast Atlantic Ocean in the presence of high salinity Mediterranean Intermediate Water (Fenner and Bucca, Dec 1969).

RSIW is the major factor affecting deep sound channel structure in the North Indian Ocean (Figures 5 and 6). In the Gulf of Aden, northern Arabian Basin and Arabian Sea, the sound channel is relatively narrow, deep (greater than 1700 meters), and high velocity (greater than 1493 m/sec) in the presence of 15-35% unmixed RSIW. In the southern Arabian and Somali Basins, in the Bay of Bengal, and in most of the Mid-Indian and North Wharton Basins the sound channel is relatively wide, somewhat shoaler (1200 to 1600 meters), and somewhat lower velocity (1490 to 1493 m/sec) in the presence of less than 15% unmixed RSIW. In the southeast corner of the area, the channel is narrow, shallow (less than 1100 meters), and low velocity (less than 1490 m/sec) due to low salinity BIW. In the Andaman Sea, the channel is very narrow, shallow (less than 1100 meters) and relatively high velocity (about 1493 m/sec) due to RSIW and local modification of Indian Equatorial Water. An analogous situation occurs in the North Atlantic Ocean in the presence of varying concentrations of Mediterranean Intermediate Water (Fenner and Bucca, Nov 1971).

Seasonal critical depths (Figures 10 and 12 for northeast and southwest monsoons, respectively) are quite similar (5000 to 5200 meters) except in the Arabian Sea, Bay of Bengal, western Somali Basin, and south of Java. In the Arabian Sea and Bay of Bengal, critical depths are 100-300 meters deeper during the southwest monsoon due to increased surface insolation. However, in the western Somali Basin, off Muscat and Oman, and south of Java, critical depths are substantially less during the southwest monsoon due to upwelling induced by reversing monsoon circulation. During the southwest monsoon, critical depths less than 3500 meters are found in the Somali Basin, less than 4400 meters off Muscat and Oman, and less than 4800 meters south of Java. These values are approximately 1400, 500 and 300 meters less than northeast monsoon critical depths, respectively. In the Andaman Sea, critical depths during both monsoons are about 900 meters less than those found in the Mid-Indian Basin due to the anomalous deep velocity profile for the Andaman Basin. Below 2000 meters, variances of less than 3.0 m/sec were found between the five major basins (Table I). However, deep velocities were 10 to 17 m/sec higher in the semi-enclosed Andaman Basin due to local modification of higher temperature and salinity RSIW and Indian Equatorial Water.

The 12 sound velocity cross-sections shown in Appendix A and the 36 sound velocity/T-S comparisons given in Appendix B (including 13 seasonal comparisons) illustrate the anomalous characteristics of North Indian Ocean sound velocity structure. They also indicate that reversing monsoon circulation does not markedly effect sound velocities below 200 to 300 meters (strong negative velocity gradient) except in areas of upwelling. This finding is in agreement with that of Duing, 1970 concerning vertical extent of monsoonal effects. However, in the major upwelling center off the Somali Republic, seasonal variability was found to depths greater than 1000 meters (see Figures A-4 and B-11).

In addition, Appendix C contains figures showing generalized surface circulation during the northeast and southwest monsoons; generalized subsurface circulation of PGIW and SSW; and generalized intermediate circulation of RSIW, AAIW, and BIW. Water mass flow diagrams were derived from core salinity depth data in order to determine the causes of various anomalous sound velocity features, but include original work of Rochford, 1964 and 1966a.

CONCLUSIONS

- Interaction of subsurface and intermediate water masses and variations resulting from the reversing northeast and southwest monsoons cause anomalous sound velocity conditions in the North Indian Ocean.

Seasonal critical depths (Figures 10 and 12 for northeast and southwest monsoons, respectively) are quite similar (5000 to 5200 meters) except in the Arabian Sea, Bay of Bengal, western Somali Basin, and south of Java. In the Arabian Sea and Bay of Bengal, critical depths are 100-300 meters deeper during the southwest monsoon due to increased surface insolation. However, in the western Somali Basin, off Muscat and Oman, and south of Java, critical depths are substantially less during the southwest monsoon due to upwelling induced by reversing monsoon circulation. During the southwest monsoon, critical depths less than 3500 meters are found in the Somali basin, less than 4400 meters off Muscat and Oman, and less than 4800 meters south of Java. These values are approximately 1400, 500 and 300 meters less than northeast monsoon critical depths, respectively. In the Andaman Sea, critical depths during both monsoons are about 900 meters less than those found in the Mid-Indian Basin due to the anomalous deep velocity profile for the Andaman Basin. Below 2000 meters, variances of less than 3.0 m/sec were found between the five major basins (Table I). However, deep velocities were 10 to 17 m/sec higher in the semi-enclosed Andaman Basin due to local modification of higher temperature and salinity RSIW and Indian Equatorial Water.

The 12 sound velocity cross-sections shown in Appendix A and the 36 sound velocity/T-S comparisons given in Appendix B (including 13 seasonal comparisons) illustrate the anomalous characteristics of North Indian Ocean sound velocity structure. They also indicate that reversing monsoon circulation does not markedly effect sound velocities below 200 to 300 meters (strong negative velocity gradient) except in areas of upwelling. This finding is in agreement with that of Duing, 1970 concerning vertical extent of monsoonal effects. However, in the major upwelling center off the Somali Republic, seasonal variability was found to depths greater than 1000 meters (see Figures A-4 and B-11).

In addition, Appendix C contains figures showing generalized surface circulation during the northeast and southwest monsoons; generalized subsurface circulation of PGIW and SSW; and generalized intermediate circulation of RSIW, AAIW, and BIW. Water mass flow diagrams were derived from core salinity depth data in order to determine the causes of various anomalous sound velocity features, but include original work of Rochford, 1964 and 1966a.

CONCLUSIONS

- Interaction of subsurface and intermediate water masses and variations resulting from the reversing northeast and southwest monsoons cause anomalous sound velocity conditions in the North Indian Ocean.

- An extremely strong negative velocity gradient is present between the surface and about 200 meters.

- Sound velocity perturbations are present just above the deep sound channel with the following temporal and spatial distributions:

- present greater than 80% of the time in the Gulf of Aden and much of the Somali Basin

- present 20-80% of the time in the Arabian Basin, southern Somali Basin, and between 5° N. and 5° S. latitude east of India

- present less than 20% of the time in the northeast Arabian Sea, Bay of Bengal, and southern Mid-Indian Basin.

- No well defined upper sound channel or subsurface sound velocity maximum is present except in the Gulf of Aden and along the coast of Africa.

- The deep sound channel has the following characteristics:

- relatively deep, narrow, and high velocity north of about 10° N. latitude

- relatively wide, shoaler, and lower velocity south of about 10° N. latitude

- narrow, shoal, and low velocity in the southeast corner of the area

- very narrow, shoal, and relatively high velocity in the Andaman Sea.

- High salinity intrusive water masses cause a relatively narrow, anomalously deep, and high velocity sound channel in large unmixed concentrations; but result in a relatively broad, shoaler, and lower velocity channel after substantial mixing.

- Critical depths are similar during both monsoons with the following exceptions:

- deeper during the southwest monsoon north of about 10° N. latitude

- shoaler during the southwest monsoon off the Somali Republic, Muscat and Oman, and south of Java.

- Anomalous critical depths in the Andaman Sea are caused by greater sound velocities at depth.

- Reversing monsoon circulation does not effect sound velocity structures below 200-300 meters except in regions of upwelling.

- The overall data distribution in the North Indian Ocean is better than that found in most major oceanic areas.

APPENDIX A

SELECTED SOUND VELOCITY CROSS-SECTIONS

APPENDIX A

SELECTED SOUND VELOCITY CROSS-SECTIONS

Figure 1 gives the location of the 12 sound velocity cross-sections shown as Figures A-2 through A-13. The basic contour interval used is 10 m/sec (shown by solid line). A subsidiary 1495-m/sec contour (dashed line) has been added on all figures for better definition of the deep sound channel. When present, the following sound velocity features are shown on each cross-section:

- deep sound channel axis (primary minimum)
- secondary subsurface minima (including the upper sound velocity minimum, minima associated with other perturbations above deep axial depth, and minima associated with perturbations below deep axial depth)
- subsurface maxima (including sonic layer depth, the intermediate sound velocity maximum, maxima associated with other perturbations above deep axial depth, and maxima associated with perturbations below deep axial depth)
- critical (limiting) depth.

The locations of individual sound velocity profiles are shown by ticks inside the bottom margin on each cross-section. These profiles were plotted at NODC standard depths and analyzed at 5- and 10-m/sec intervals to either the bottom or a maximum depth of 5000 meters.

The bathymetric profiles shown on each cross-section were drawn from a large number of sources, including:

- Five 1:2,000,000 charts for the southern Somali, southern Arabian, Mid-Indian, and North Wharton Basins and the Bay of Bengal provided by R. L. Fisher, Scripps Institution of Oceanography (personal communication)
- The chart of Fisher, et al., 1968 (northern Somali and southern Arabian Basins)
- The chart of Curray and Moore, 1971 (Mid-Indian Basin and Bay of Bengal)

- The chart of Rodolfo, 1969 (Andaman Sea)
- Charts contoured by NAVOCEANO prior to 1960.

These profiles are highly generalized and only show large-scale bathymetric features that influence sound velocity structures.

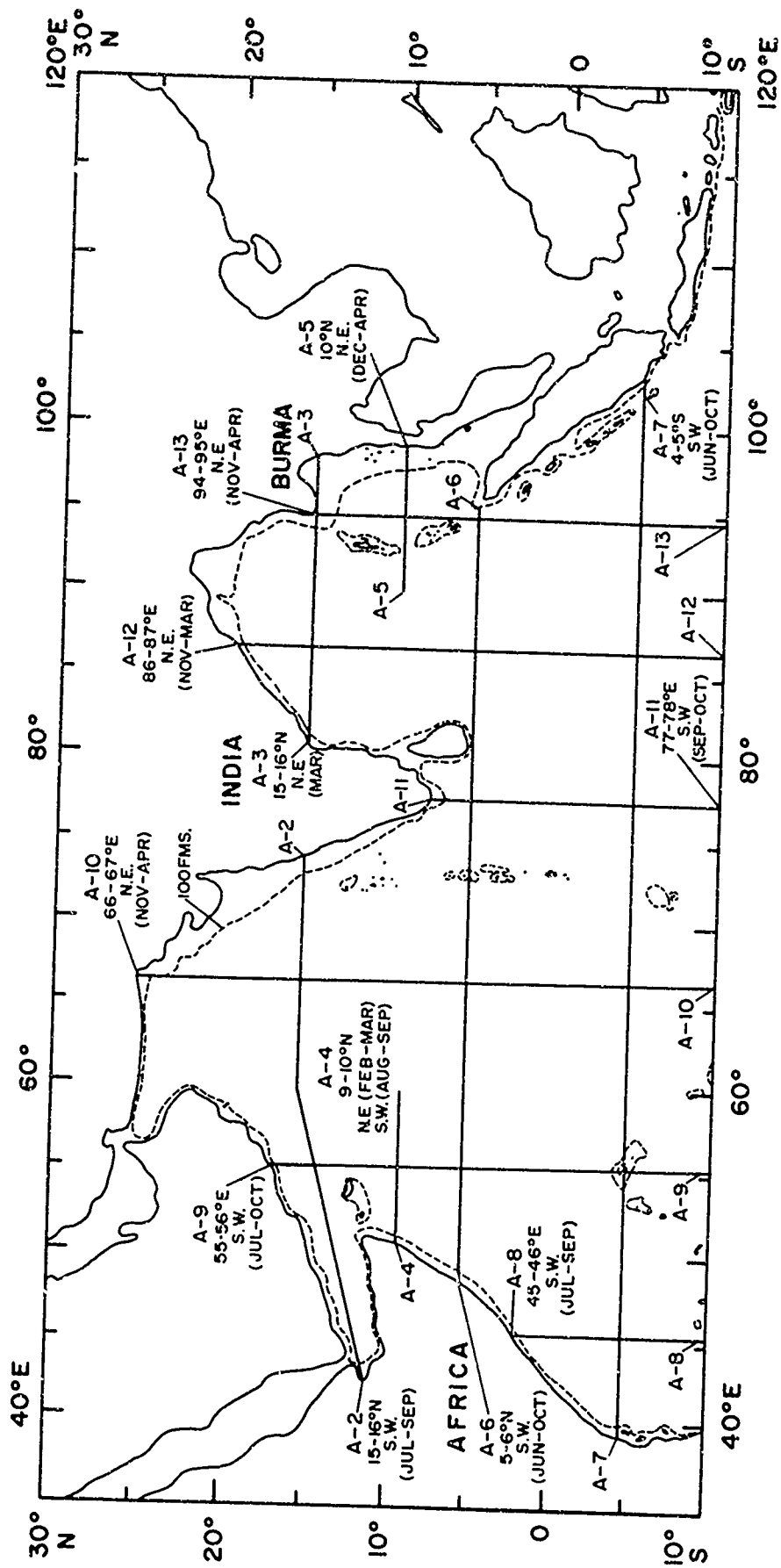
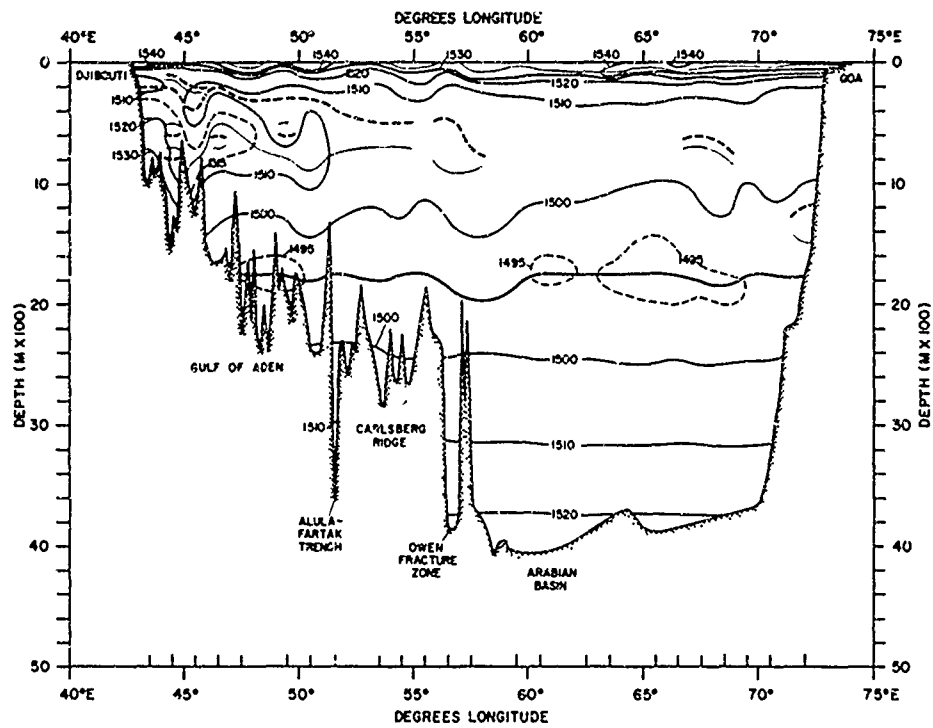


FIGURE A-1. LOCATION OF SELECTED SOUND VELOCITY CROSS-SECTIONS (FIGURES A-2 THROUGH A-13)



LEGEND

— DEEP SOUND CHANNEL (PRIMARY MINIMUM)	--- SECONDARY SUBSURFACE MINIMA
- - - SUBSURFACE MAXIMA	- - - LIMITING (CRITICAL) DEPTH

NOTES:

- INSIDE TICKS ARE PROFILE LOCATIONS
- SOUND VELOCITY IN METERS/SECOND

FIGURE A-2. SOUND VELOCITY CROSS-SECTION BETWEEN 15° AND 16° N. LATITUDE AND INTO THE GULF OF ADEN FOR SOUTHWEST MONSOON (JUL-SEP)

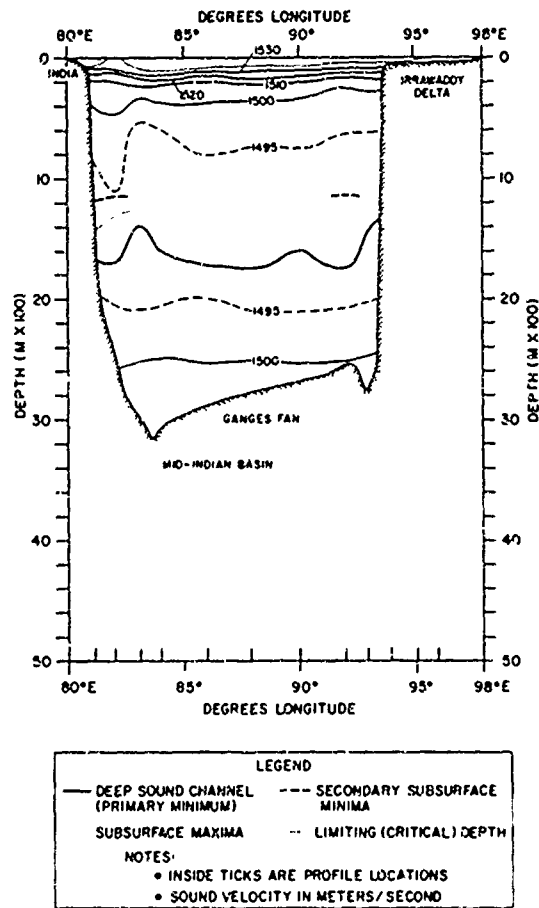


FIGURE A-3. SOUND VELOCITY CROSS-SECTION BETWEEN 15° AND 16° N. LATITUDE (BAY OF BENGAL) FOR NORTHEAST MONSOON (MAR)

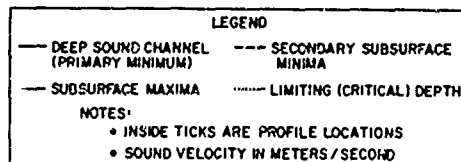
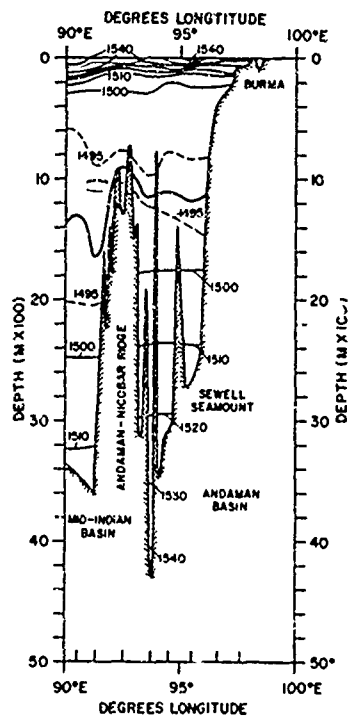


FIGURE A-5. SOUND VELOCITY CROSS-SECTION ALONG 10° N. LATITUDE (ANDAMAN SEA) FOR NORTHEAST MONSOON (DEC-APR)

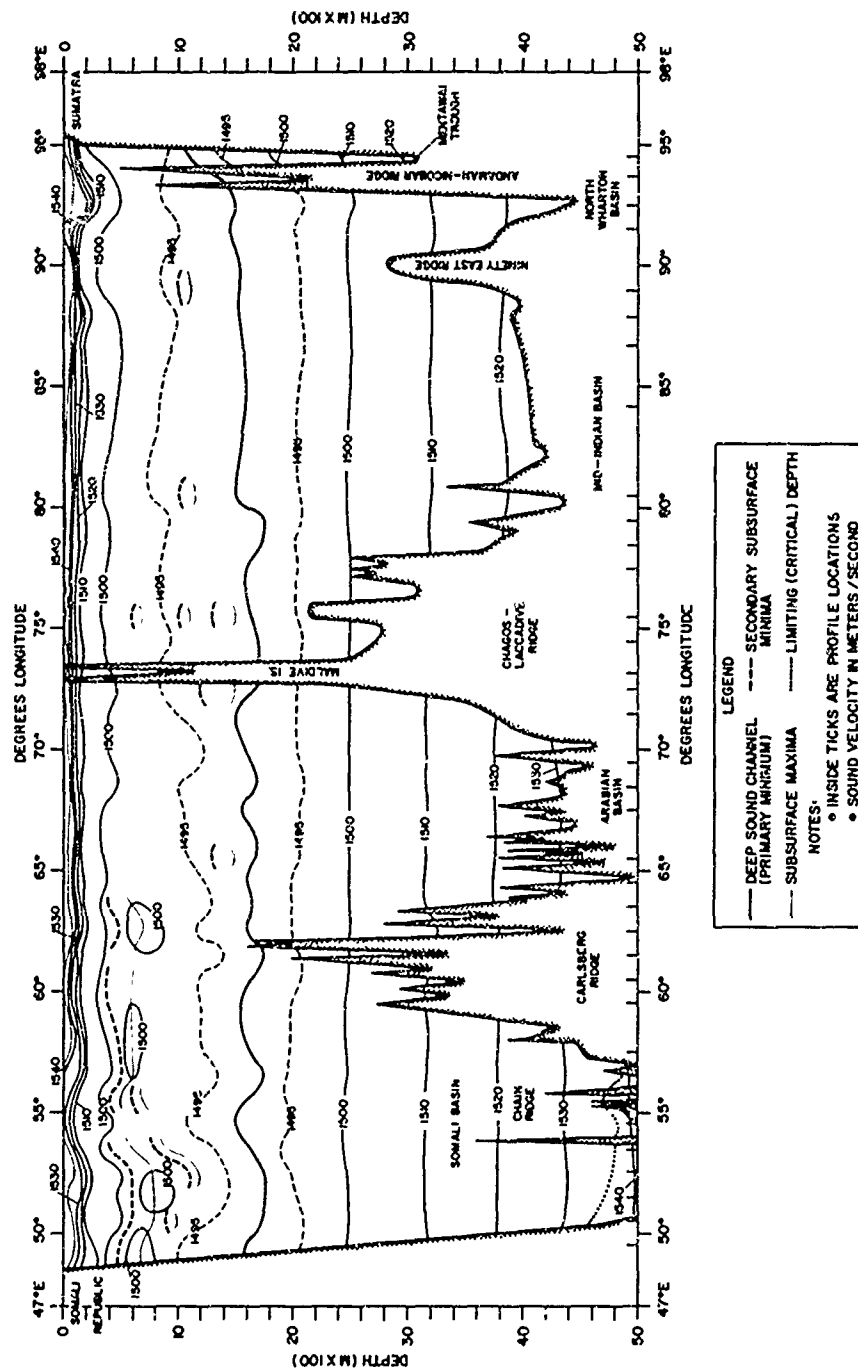


FIGURE A-6. SOUND VELOCITY CROSS-SECTION BETWEEN 5° AND 6° N. LATITUDE FOR SOUTHWEST MONSOON (JUN-OCT)

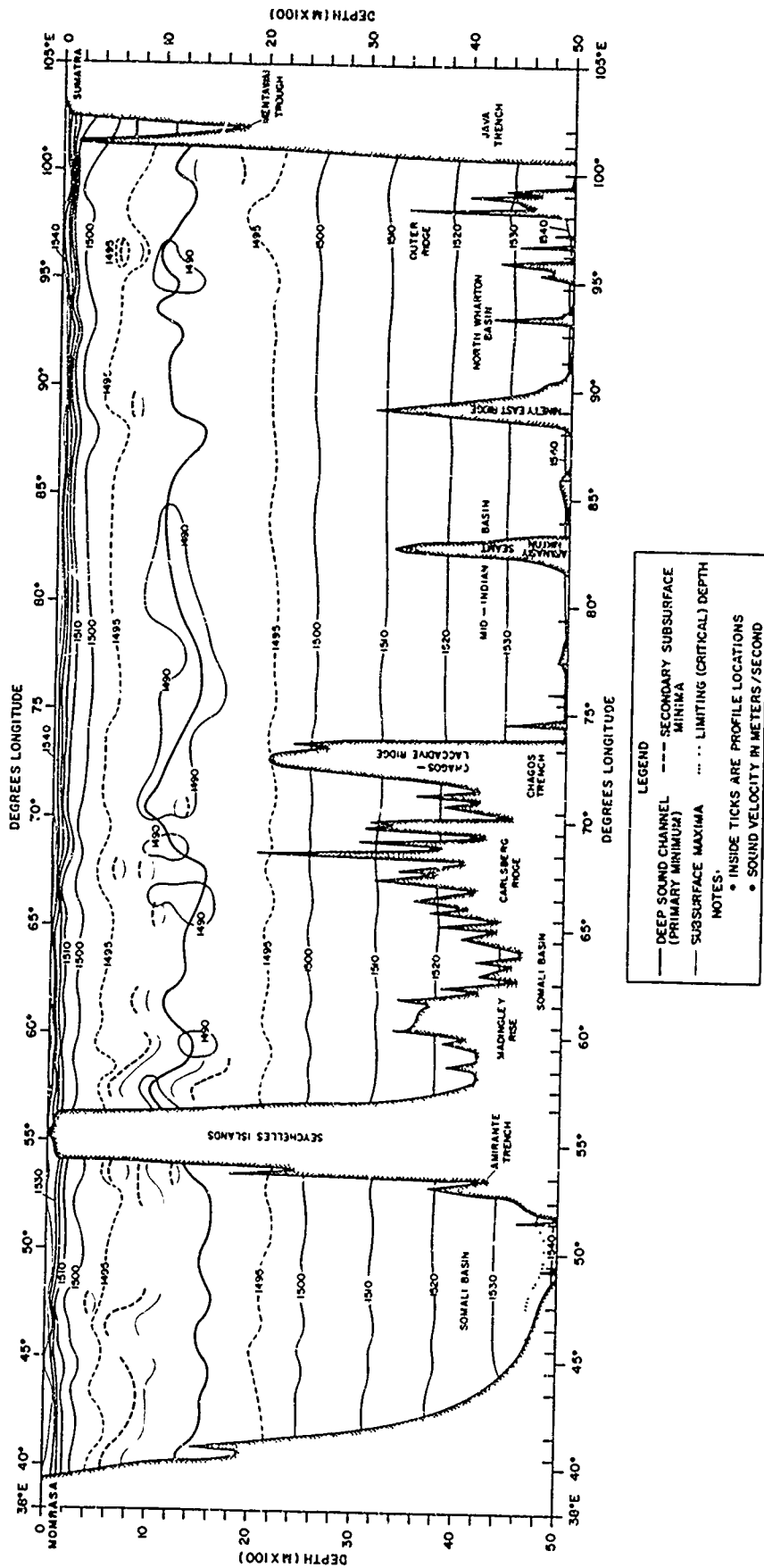


FIGURE A-7. SOUND VELOCITY CROSS-SECTION BETWEEN 4° AND 5° S. LATITUDE FOR SOUTHWEST MONSOON (JUN-OCT)

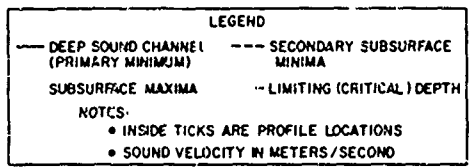
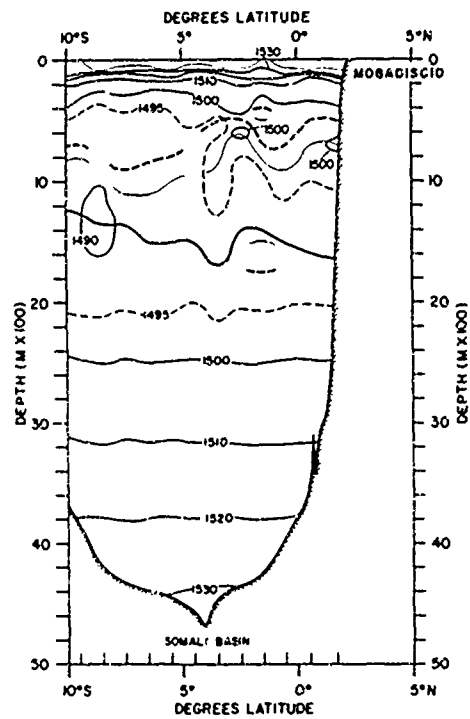


FIGURE A-8. SOUND VELOCITY CROSS-SECTION BETWEEN 45° AND 46° E. LONGITUDE FOR SOUTHWEST MONSOON (JUL-SEP)

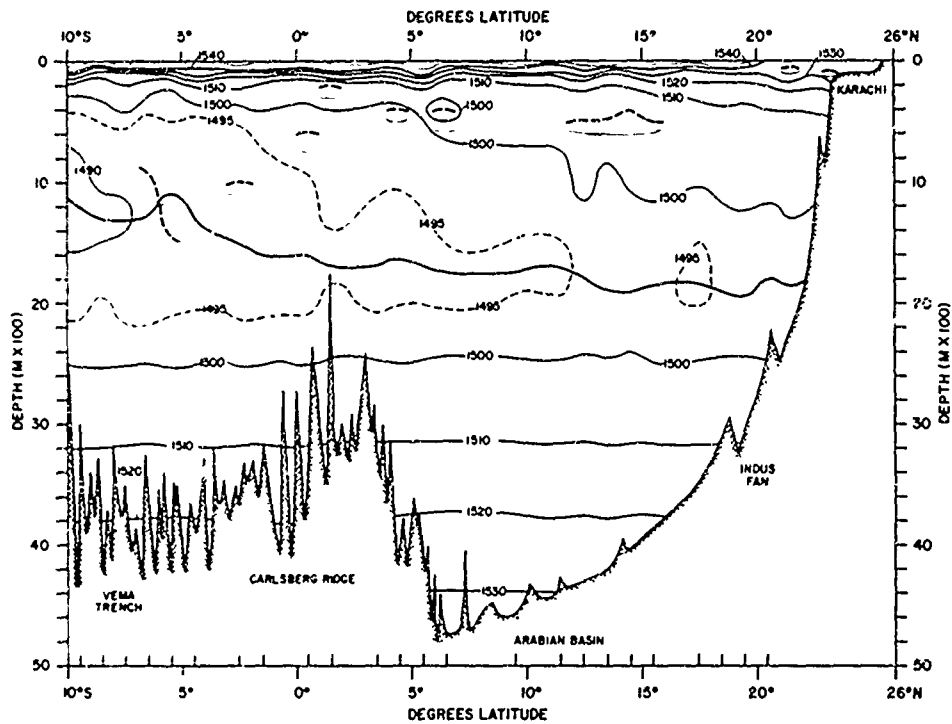


FIGURE A-10. SOUND VELOCITY CROSS-SECTION BETWEEN 66° AND 67° E. LONGITUDE FOR NORTHEAST MONSOON (NOV-APR)

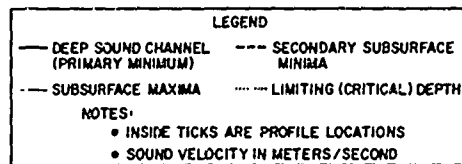
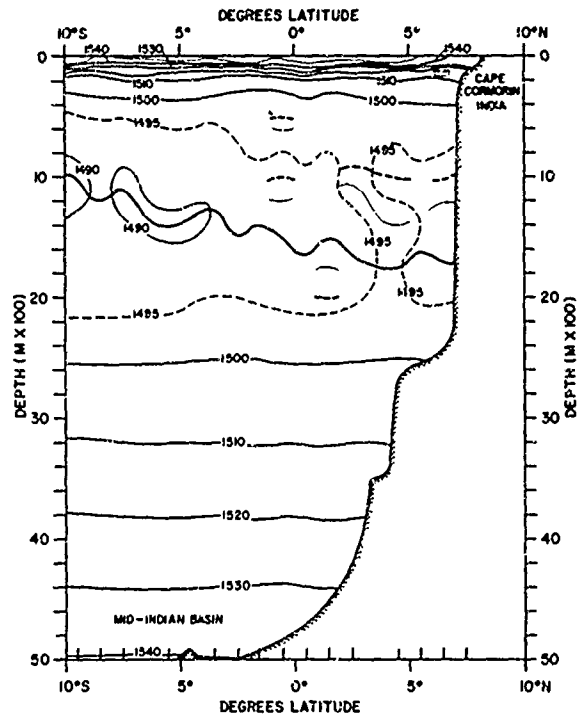


FIGURE A-11. SOUND VELOCITY CROSS-SECTION BETWEEN 77° AND 78° E, LONGITUDE FOR SOUTHWEST MONSOON (SEP-OCT)

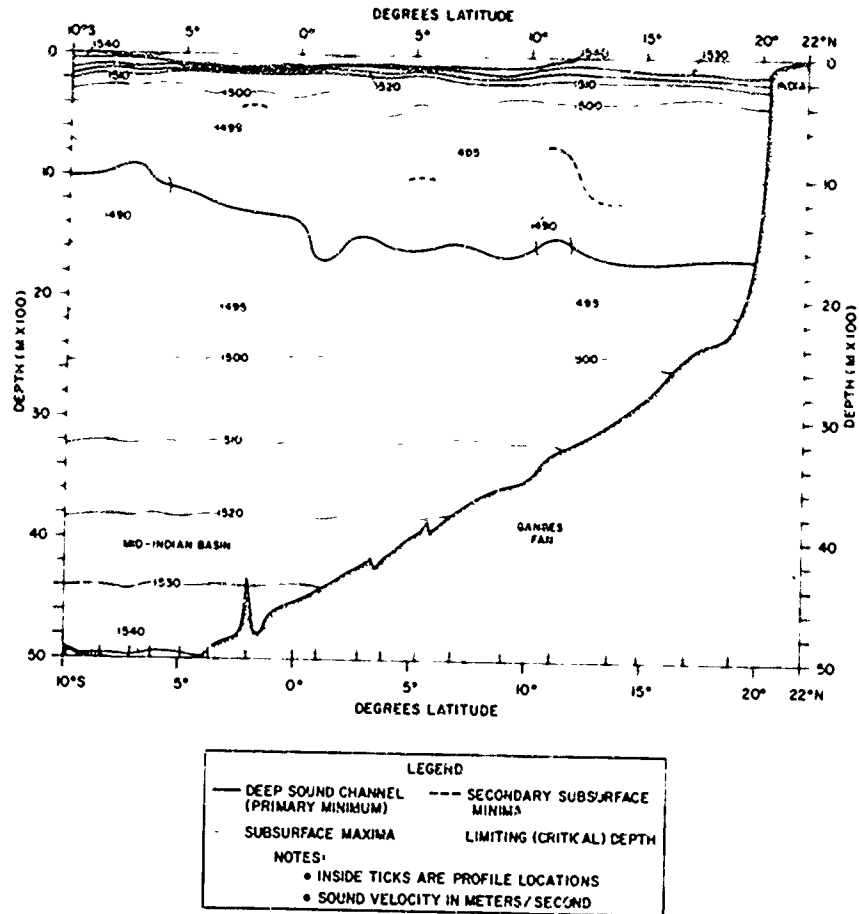
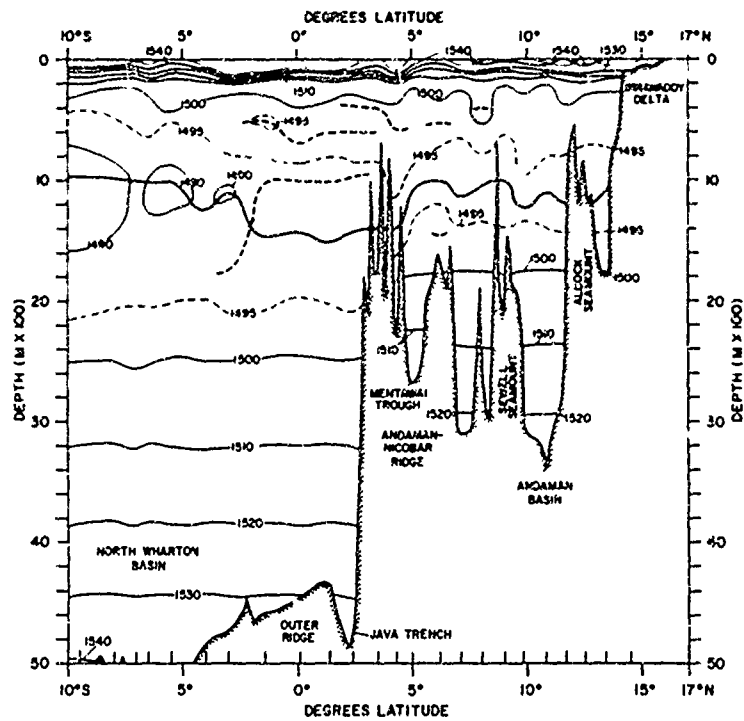


FIGURE A-12. SOUND VELOCITY CROSS-SECTION BETWEEN 86° AND 87° E, LONGITUDE FOR NORTHEAST MONSOON (NOV-MAR)



LEGEND

— DEEP SOUND CHANNEL (PRIMARY MINIMUM) --- SECONDARY SUBSURFACE MINIMA
 SUBSURFACE MAXIMA — LIMITING (CRITICAL) DEPTH

NOTES:
 • INSIDE TICKS ARE PROFILE LOCATIONS
 • SOUND VELOCITY IN METERS/SECOND

FIGURE A-13. SOUND VELOCITY CROSS-SECTION BETWEEN 94° AND 95° E. LONGITUDE FOR NORTHEAST MONSOON (DEC-APR)

APPENDIX B

SELECTED SOUND VELOCITY AND T-S PROFILES

Preceding page blank

APPENDIX B

SELECTED SOUND VELOCITY AND T-S PROFILES

T-S RELATIONS IN THE NORTH INDIAN OCEAN

Figure B-1 shows general T-S relations for the North Indian Ocean. The T-S indices for IEW were taken directly from Sverdrup, et al., 1942. The indices for ArSW and BBW were derived from extensive historical data in the Arabian Sea and Bay of Bengal. BBW closely resembles Bay of Bengal Tropospheric Water (Mamayev, 1969). The indices for Andaman Sea Deep and Bottom Water, NIDW, and North Indian Bottom Water also were derived from extensive historical data. NIDW closely resembles that of Shcherbinin, 1969b. North Indian Bottom Water has salinity characteristics similar to those of Indian Antarctic Deep and Bottom Water (Mamayev, 1969) but lies at somewhat warmer temperatures.

The T-S curves for PGIW and RSIW are modified after those of Rochford, 1964. Percentages of unmixed RSIW were derived assuming a T-S value of $23^{\circ}\text{C}-40\text{‰}$ for 100% RSIW (Mamayev, 1969) and values of $8^{\circ}\text{C}-34.8\text{‰}$ and $4^{\circ}\text{C}-34.6\text{‰}$ for 0% RSIW (upper and lower lobes, respectively). A RSIW concentration of approximately 20% marks the maximum observed limit of interfingering with AAIW and/or BIW. The curves for SSW and BIW were derived using historical data. The curve for AAIW was taken directly from Sverdrup, et al., 1942.

GENERAL COMMENTS

Figure B-2 gives the locations of the 36 sound velocity/T-S comparisons shown as Figures B-3 through B-38. Figures B-4, B-7, B-9, B-11, B-13, B-14, B-21, B-23, B-25, B-26, B-28, B-35, and B-36 show a sound velocity and T-S profile for both northeast (N.E.) and southwest (S.W.) monsoon conditions. The remainder of the comparisons show a sound velocity and T-S profile representative of either northeast or southwest monsoon conditions. The maximum depth of each sound velocity profile approximates the corrected bottom depth. The depth limits of actual sound velocity data are indicated on the various figures by two parallel horizontal lines (=). Sound velocity profiles that have been extended below the depth of actual data (based on nearby historical data) are indicated by a dotted line. T-S profiles have not been extended below the depth of actual data. The percentages of unmixed RSIW shown on the various figures were derived using the curve shown on Figure B-1.

To facilitate water mass identification and comparison between sound velocity and T-S profiles, the following legend has been used:

A or a: depth of PGIW salinity maximum for northeast or southwest monsoon, respectively

B or b: depth of SSW salinity minimum

C or c: depth of upper RSIW salinity maximum (upper lobe)

C' or c': depth of lower RSIW salinity maximum (lower lobe after interfingering with AAIW and/or BIW)

C" or c'': depth of NIDW salinity maximum (generally below BIW salinity minimum)

D or d: depth of AAIW salinity minimum

E or e: depth of BIW salinity minimum

A/C or a/c: depth of salinity maximum caused by mixing of PGIW and RSIW

B/D or b/d: depth of salinity minimum caused by mixing of SSW and AAIW

D/E or d/e: depth of salinity minimum caused by mixing of AAIW and BIW.

The "B" or "b" notations above are used only in the presence of RSIW.

TREATMENT OF DATA

All sound velocity profiles (Figures B-3 through B-38) were derived according to the equation of Wilson, 1960. All T-S profiles were drawn from either Nansen cast or salinity-temperature-depth recorder (STD) observations. Sound velocity and T-S profiles for any given season and location represent the same single observation in all cases. No averaging processes were used in the construction of the profiles. Although the given profiles are not typical of any large region, they show general trends encountered throughout the area.

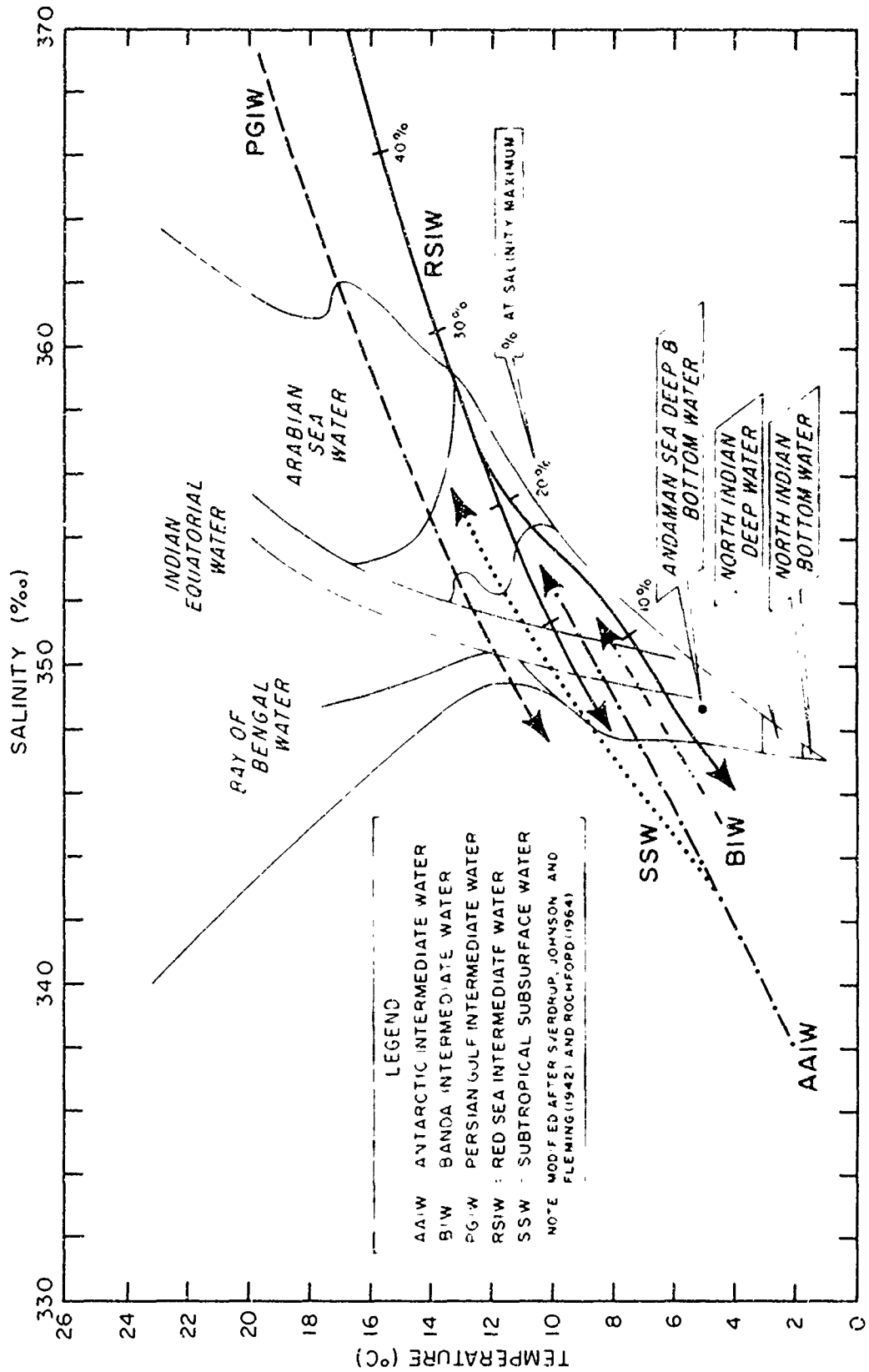


FIGURE B-1. T-S RELATIONS IN THE NORTH INDIAN OCEAN

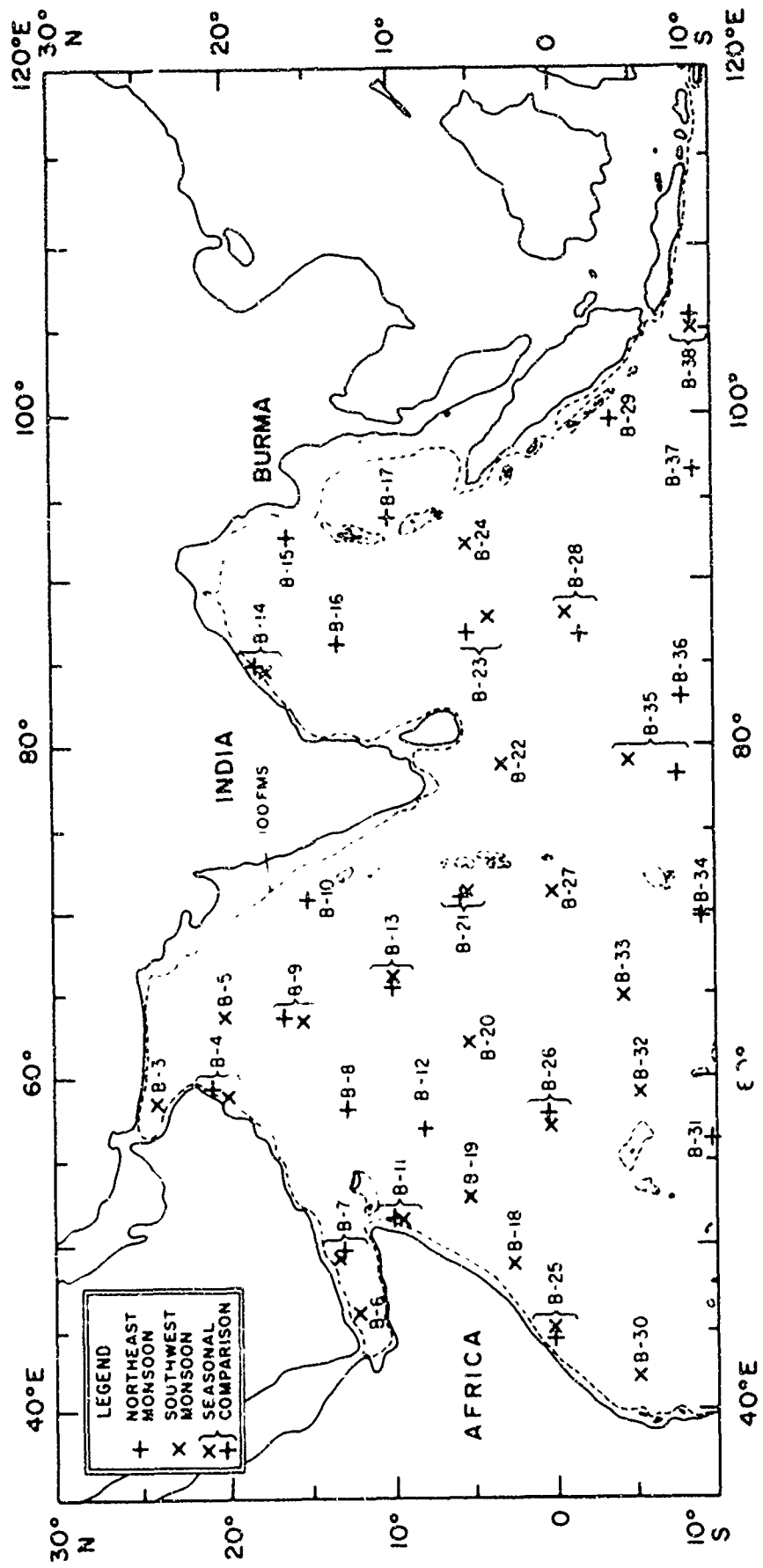


FIGURE B-2. LOCATION OF SELECTED SOUND VELOCITY/T-S COMPARISONS (FIGURES B-3 THROUGH B-38)

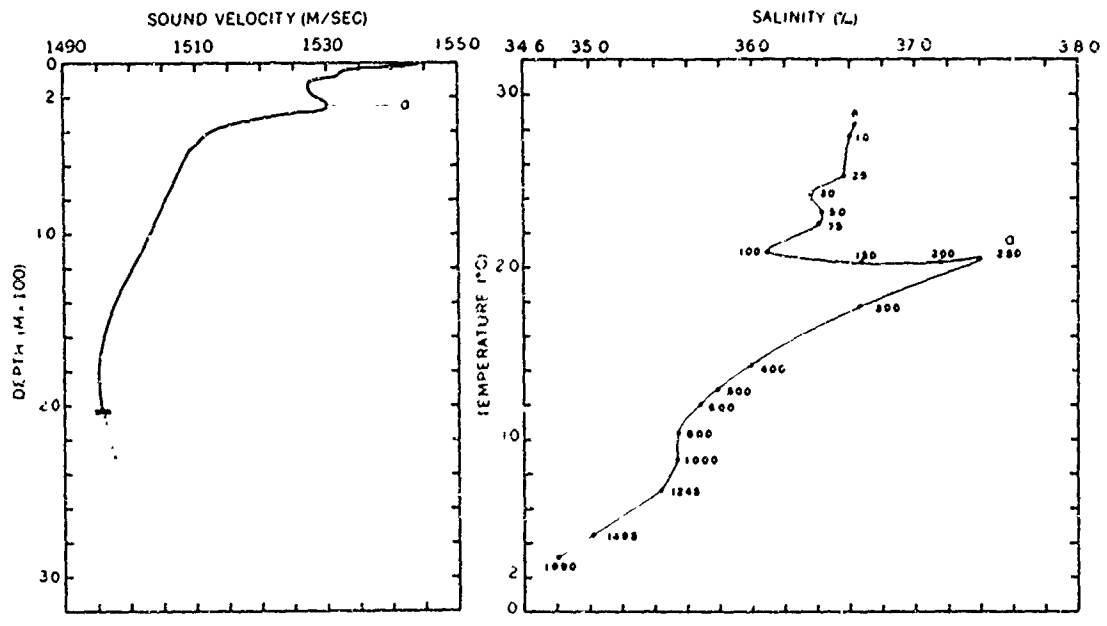


FIGURE B-3. SOUND VELOCITY/T-S COMPARISON FOR SOUTHWEST MONSOON

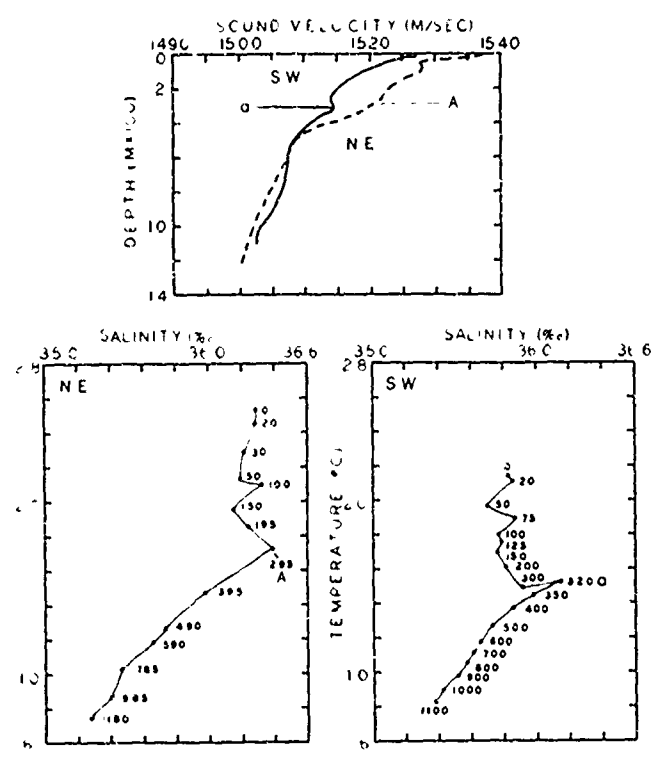


FIGURE B-4. SEASONAL SOUND VELOCITY/T-S COMPARISON

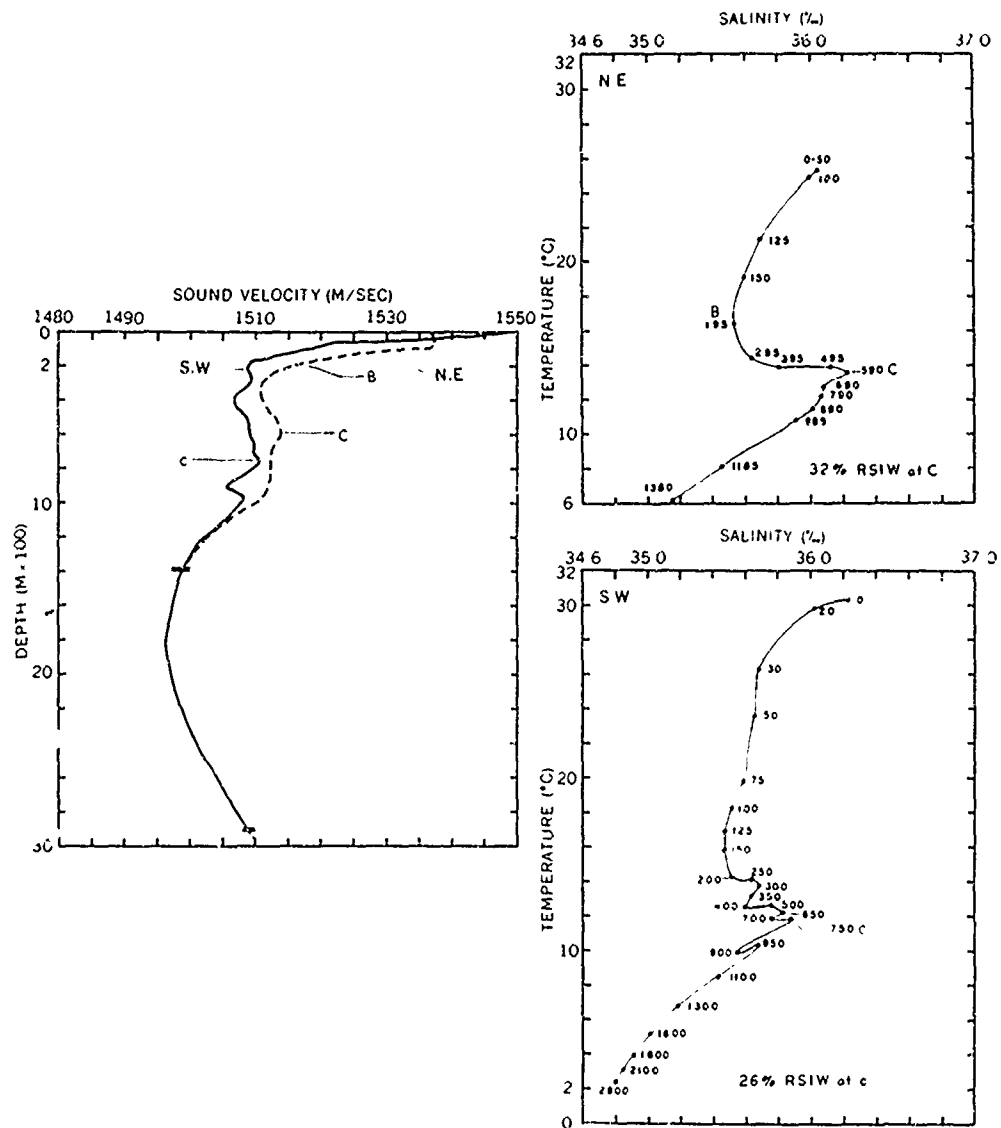


FIGURE B-7. SEASONAL SOUND VELOCITY T-S COMPARISON

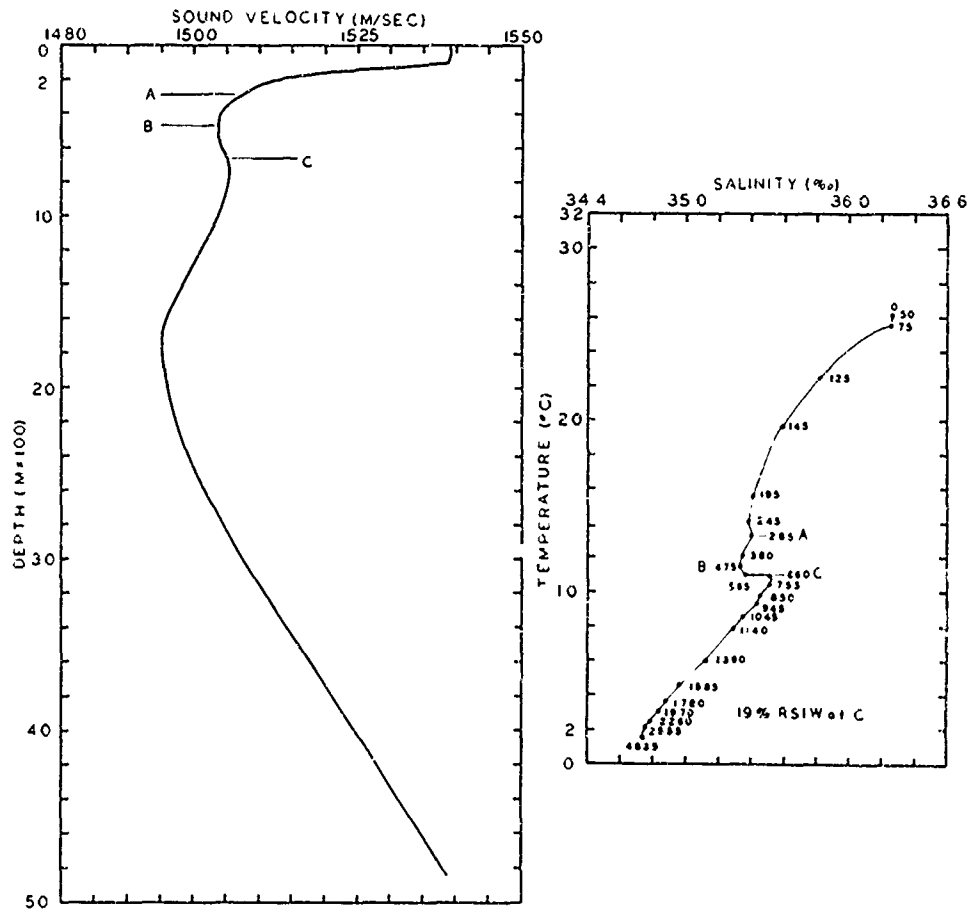


FIGURE B-8. SOUND VELOCITY/T-S COMPARISON FOR NORTHEAST MONSOON

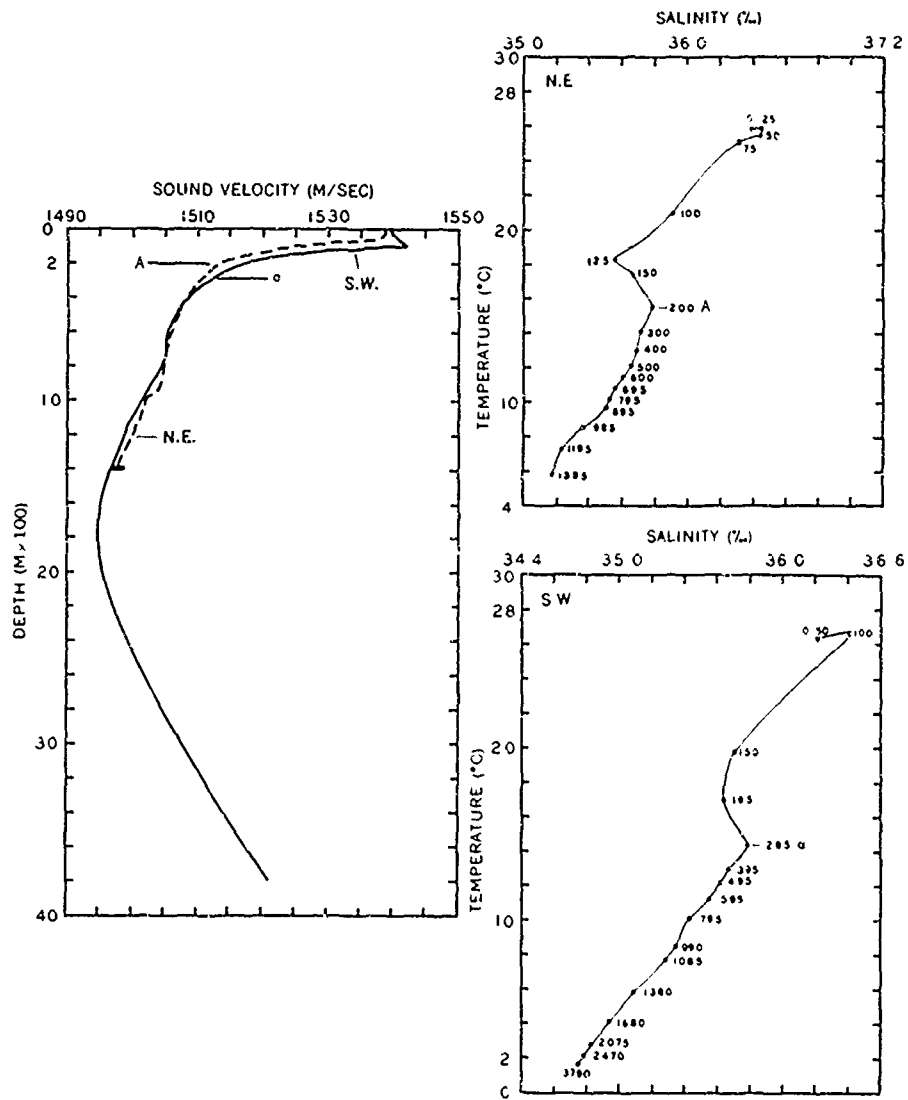


FIGURE B-9. SEASONAL SOUND VELOCITY/T-S COMPARISON

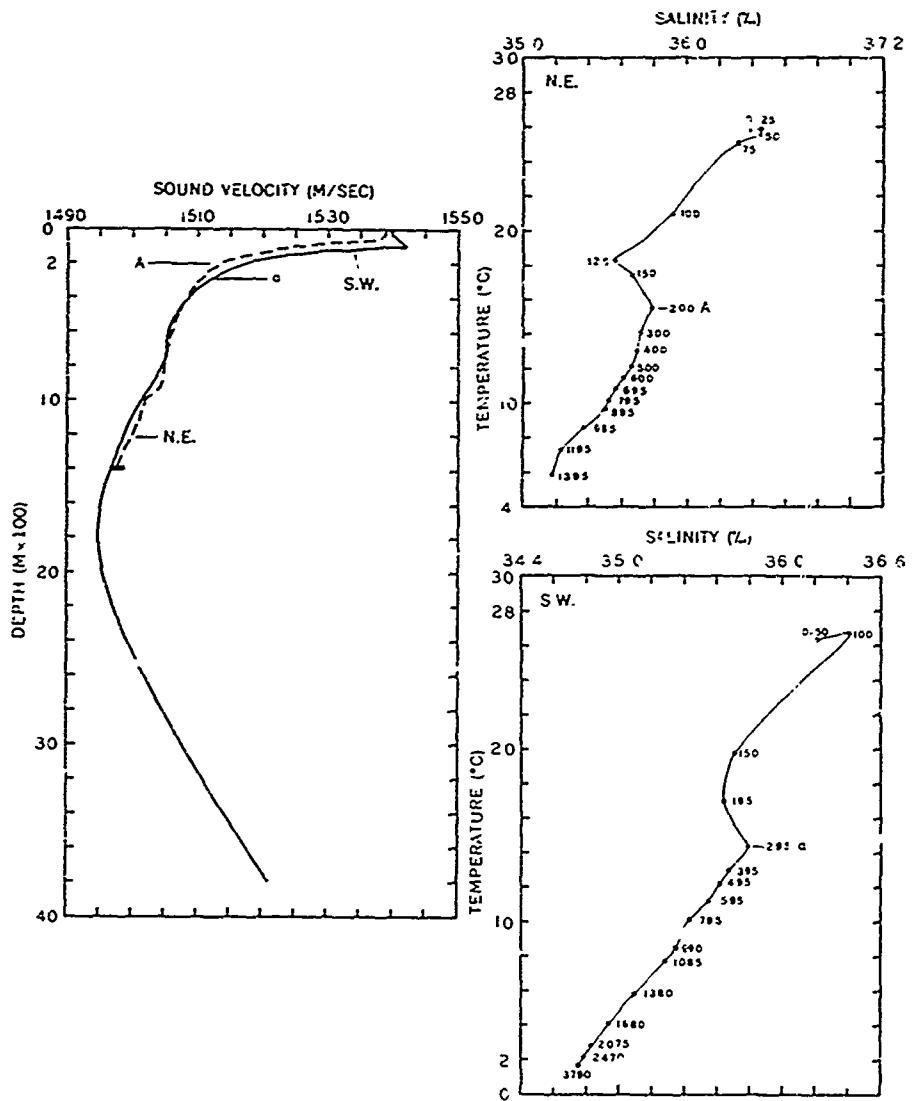


FIGURE B-9. SEASONAL SOUND VELOCITY/T-S COMPARISON

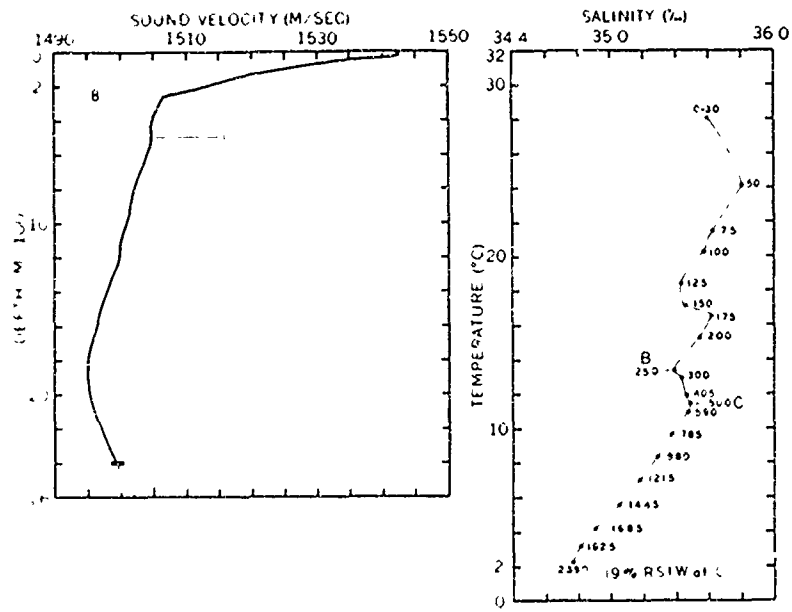


FIGURE B-10. SOUND VELOCITY/T-S COMPARISON FOR NORTHEAST MONSOON

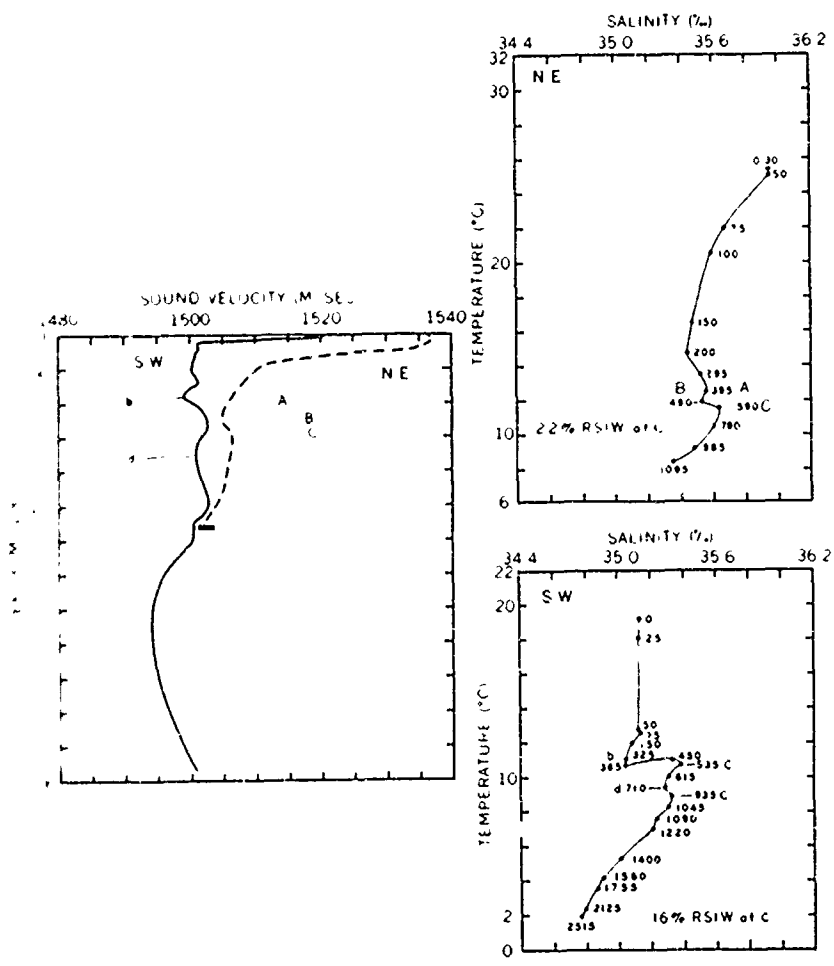


FIGURE B-11. SEASONAL SOUND VELOCITY/T-S COMPARISON

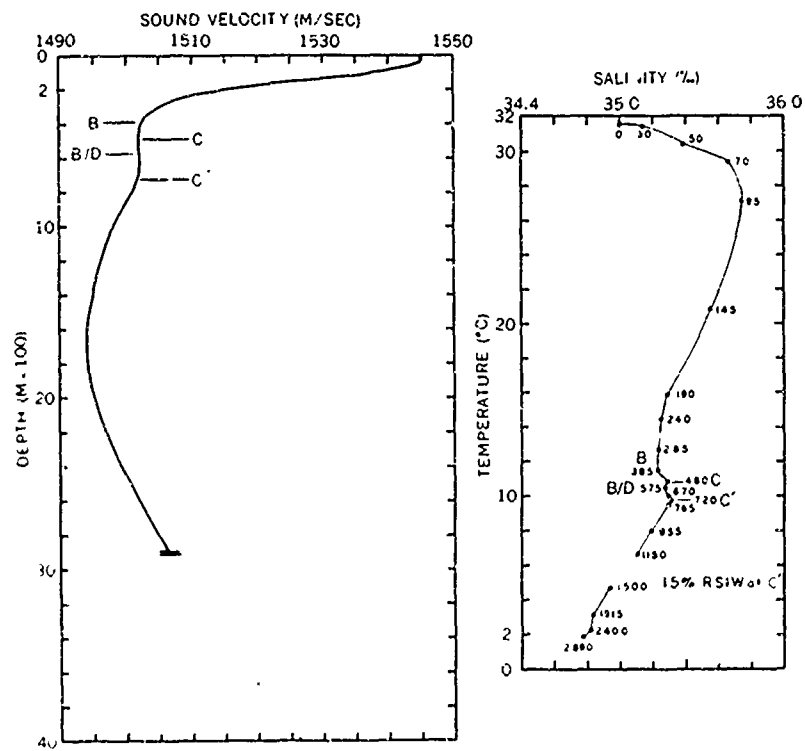


FIGURE B-12. SOUND VELOCITY/T-S COMPARISON FOR NORTHEAST MONSOON

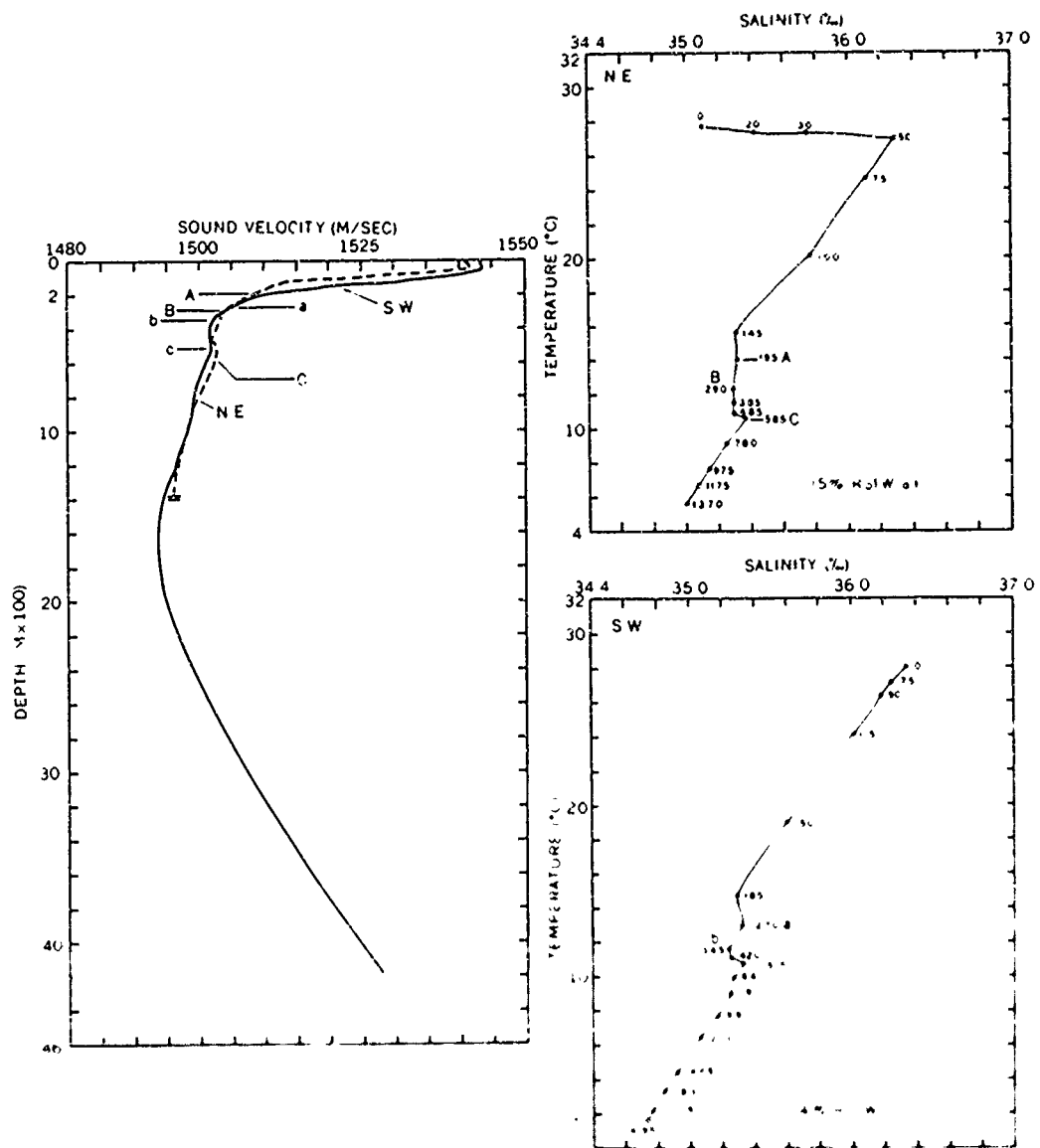


FIGURE B-13. SEASONAL SOUND VELOCITY/T-S COMPARISON

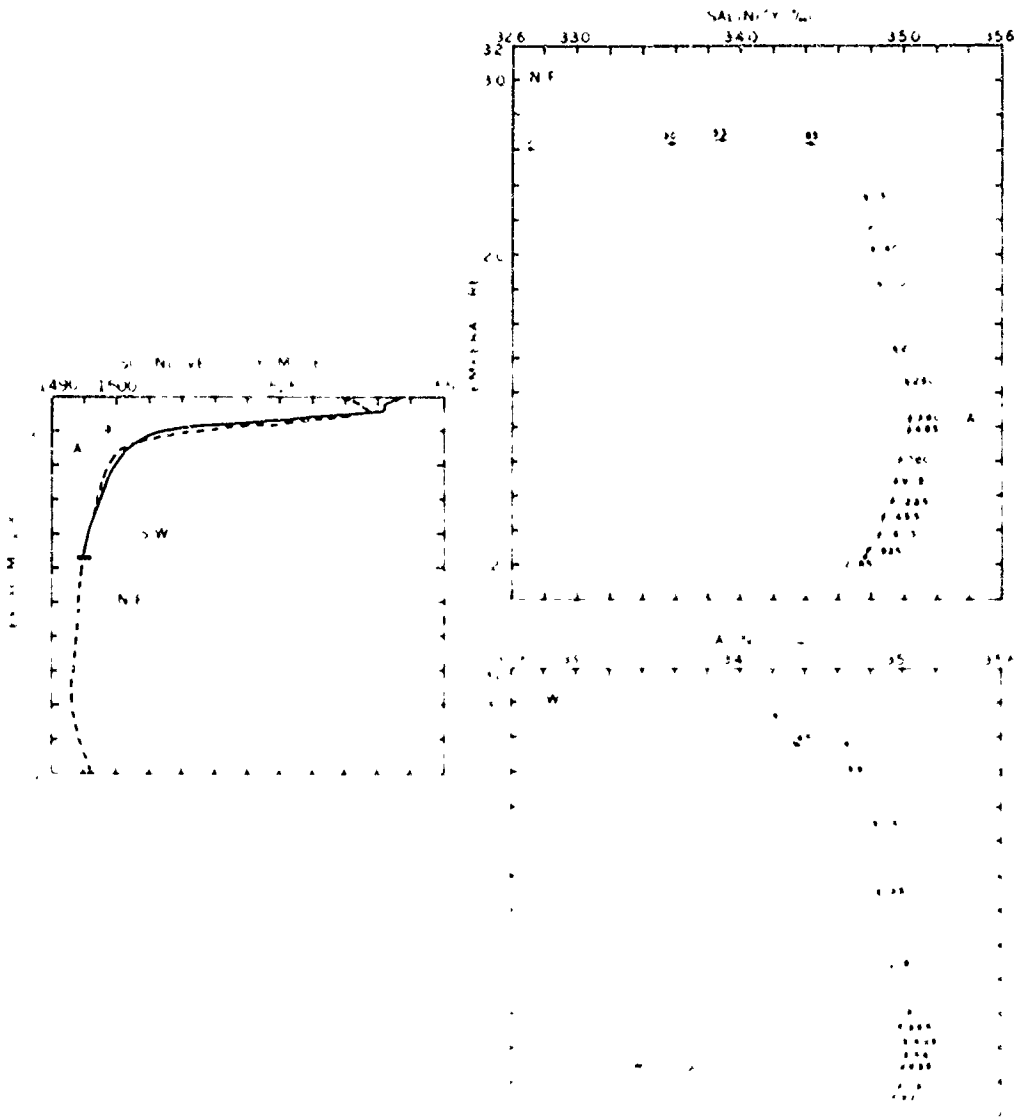


FIGURE B-14 SEASONAL CONDUCTIVITY DEPTH COMPARISON.

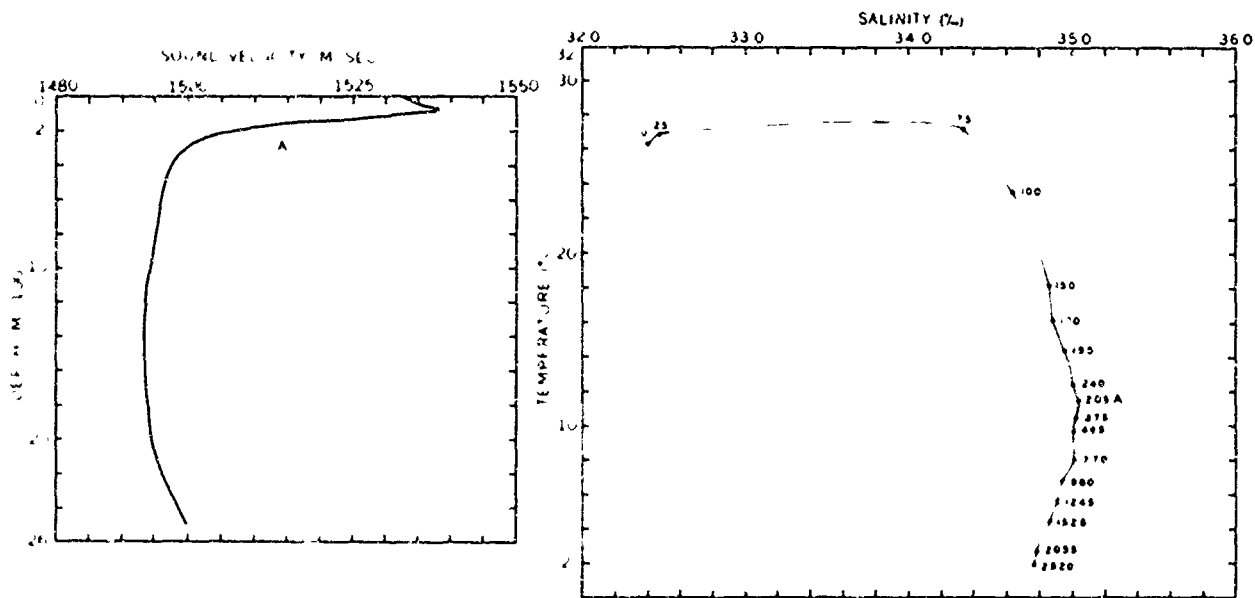


FIGURE B-15. SOUND VELOCITY/T-S COMPARISON FOR NORTHEAST MONSOON

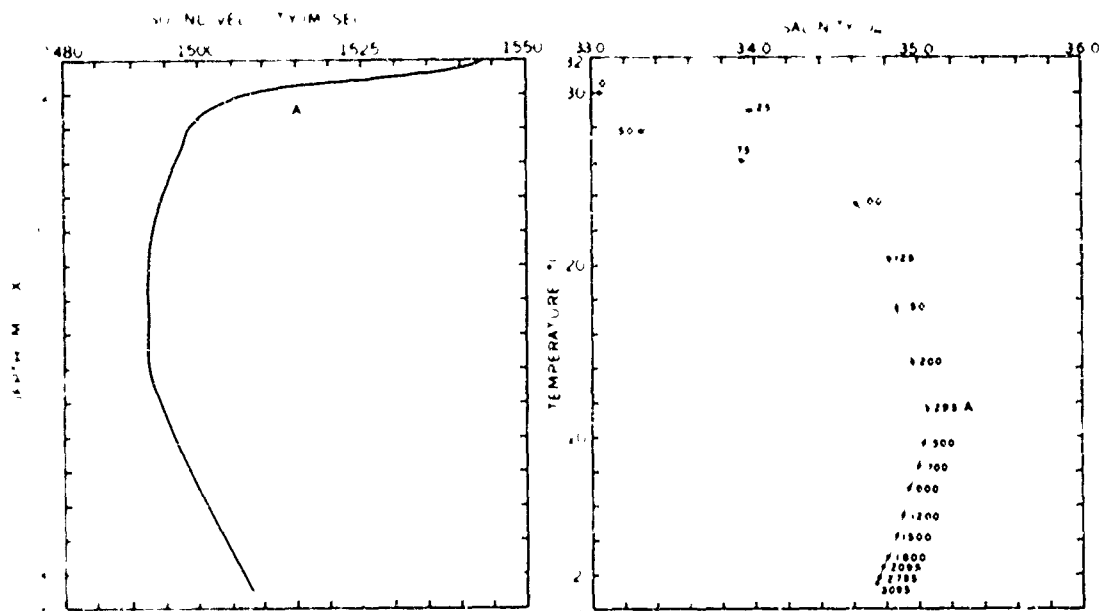


FIGURE B-16. SOUND VELOCITY/T-S COMPARISON FOR NORTHEAST MONSOON

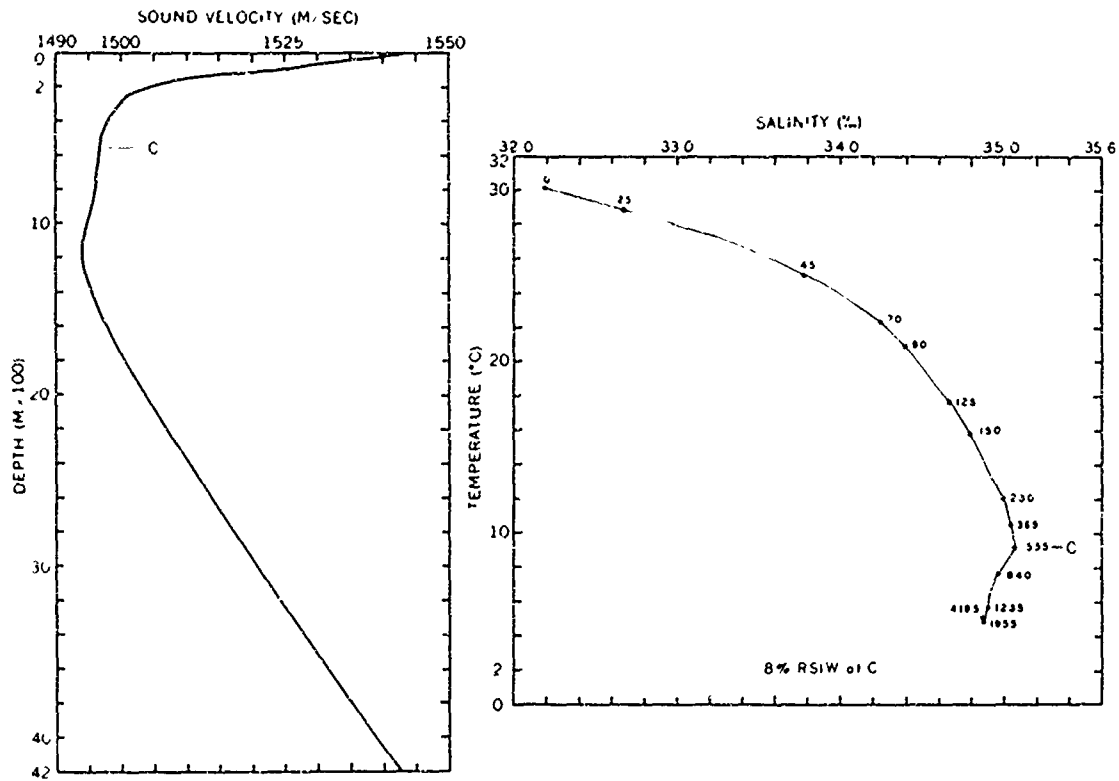


FIGURE B-17. SOUND VELOCITY/T-S COMPARISON FOR NORTHEAST MONSOON

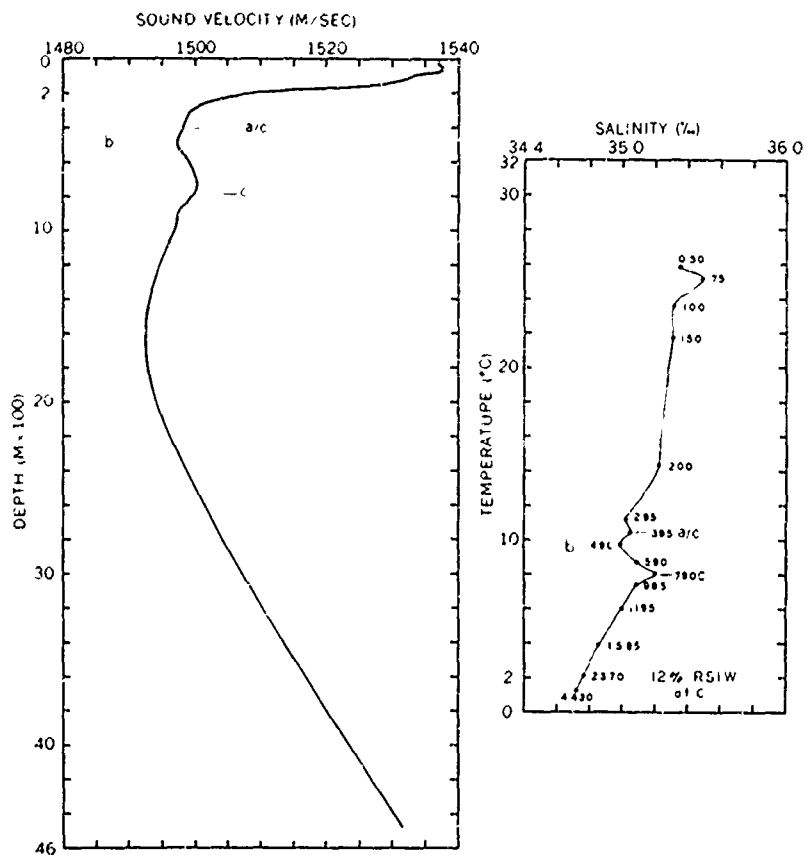


FIGURE B-18. SOUND VELOCITY/T-S COMPARISON FOR SOUTHWEST MONSOON

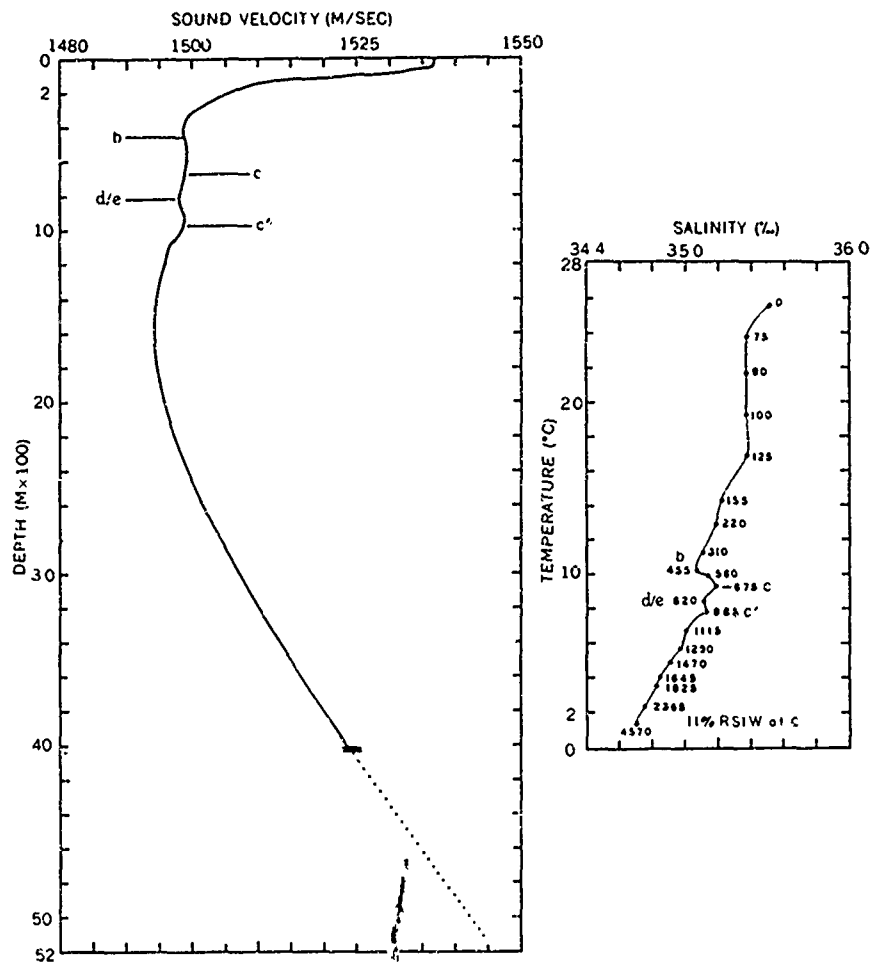


FIGURE B-19. SOUND VELOCITY/T-S COMPARISON FOR SOUTHWEST MONSOON

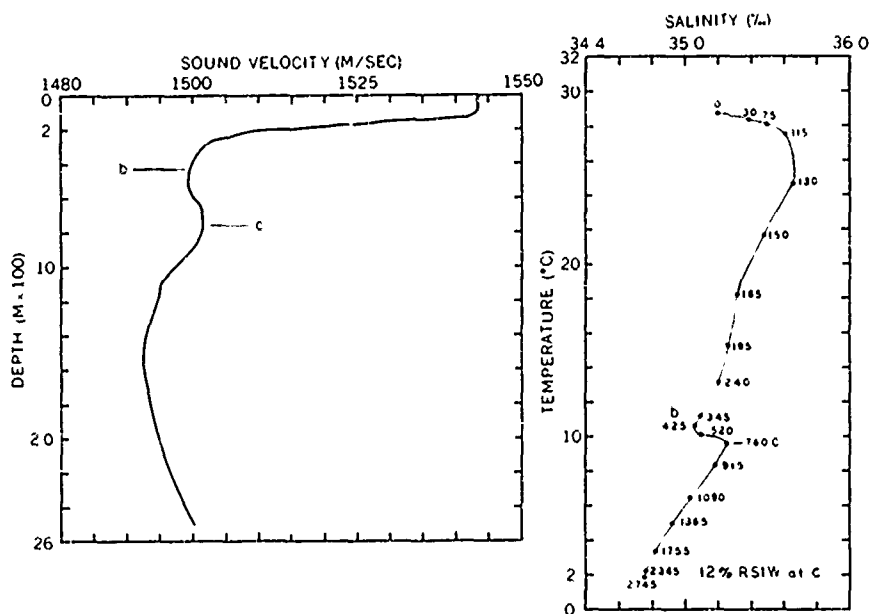


FIGURE B-20. SOUND VELOCITY/T-S COMPARISON FOR SOUTHWEST MONSOON

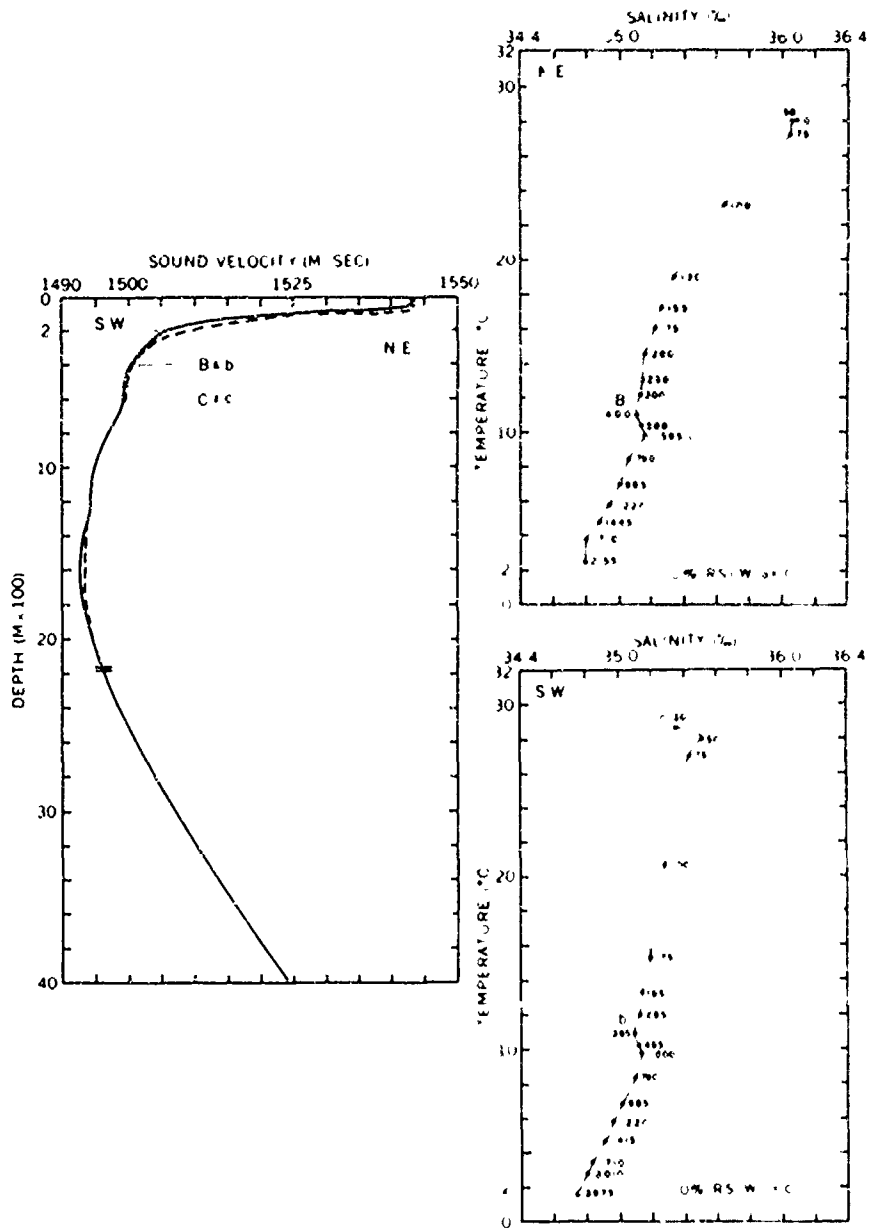


FIGURE B-21. SEASONAL SOUND VELOCITY/T-S COMPARISON

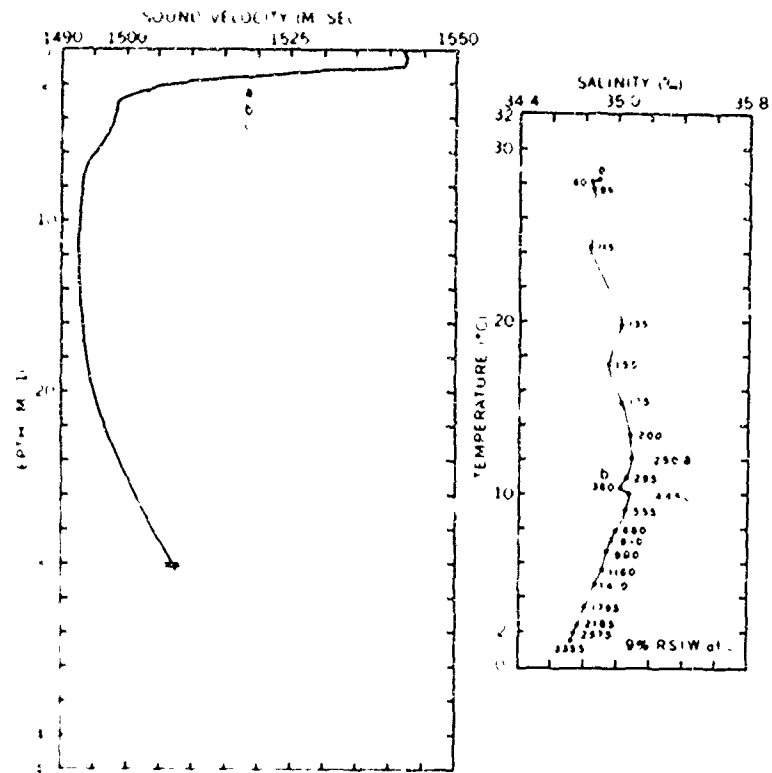


FIGURE B-22. SOUND VELOCITY/T-S COMPARISON FOR SOUTHWEST MONSOON

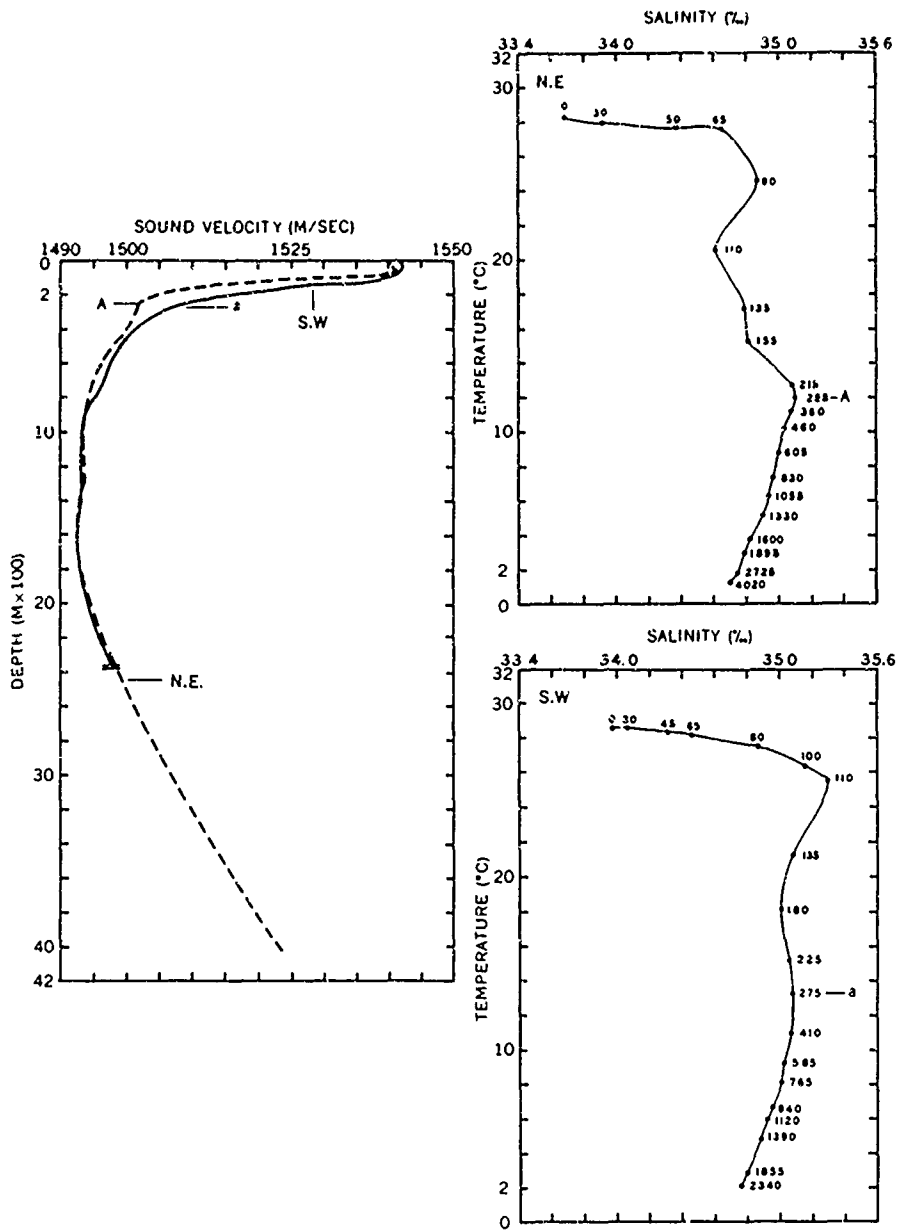


FIGURE B-23. SEASONAL SOUND VELOCITY/T-S COMPARISON

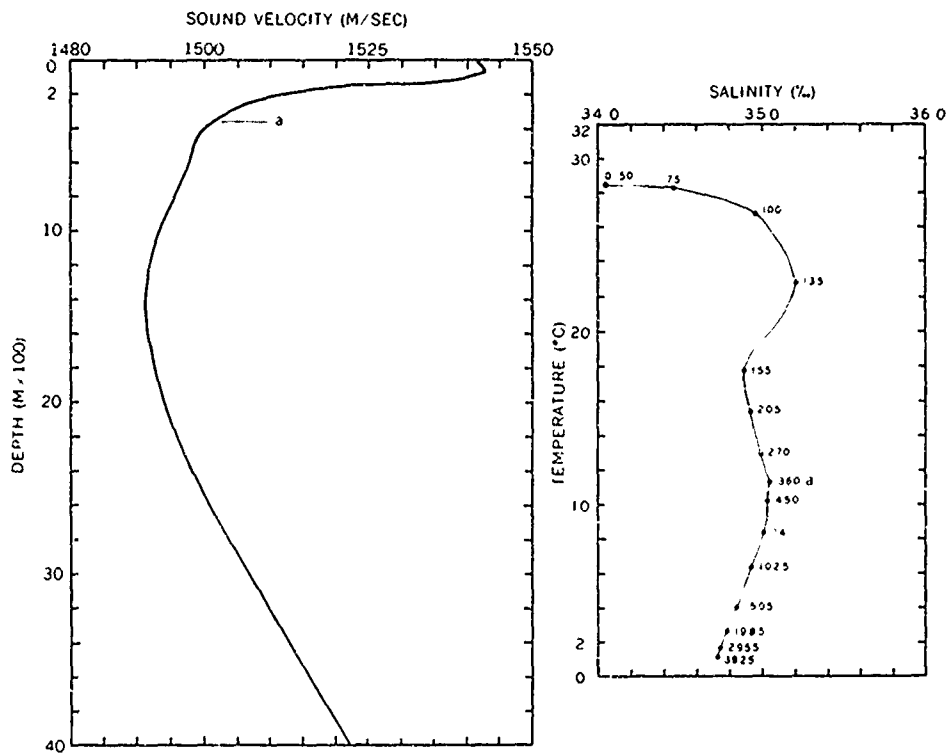


FIGURE B-24. SOUND VELOCITY/T-S COMPARISON FOR SOUTHWEST MONSOON

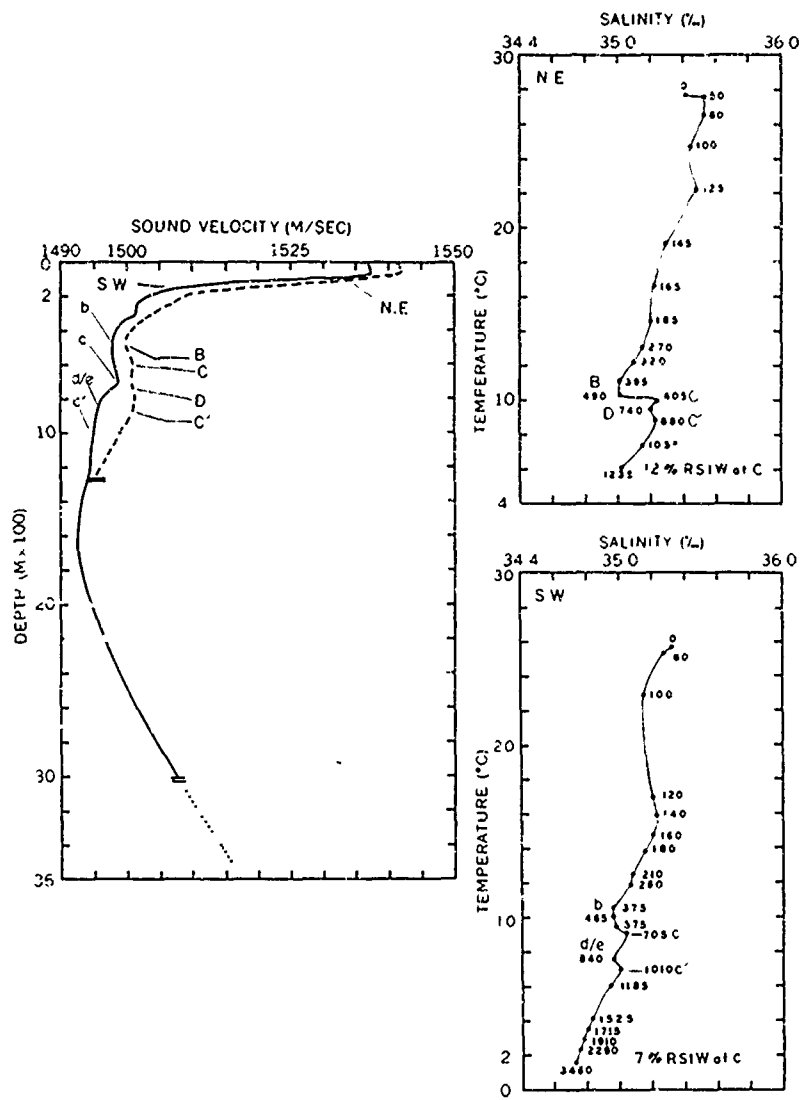


FIGURE B-25. SEASONAL SOUND VELOCITY/T-S COMPARISON

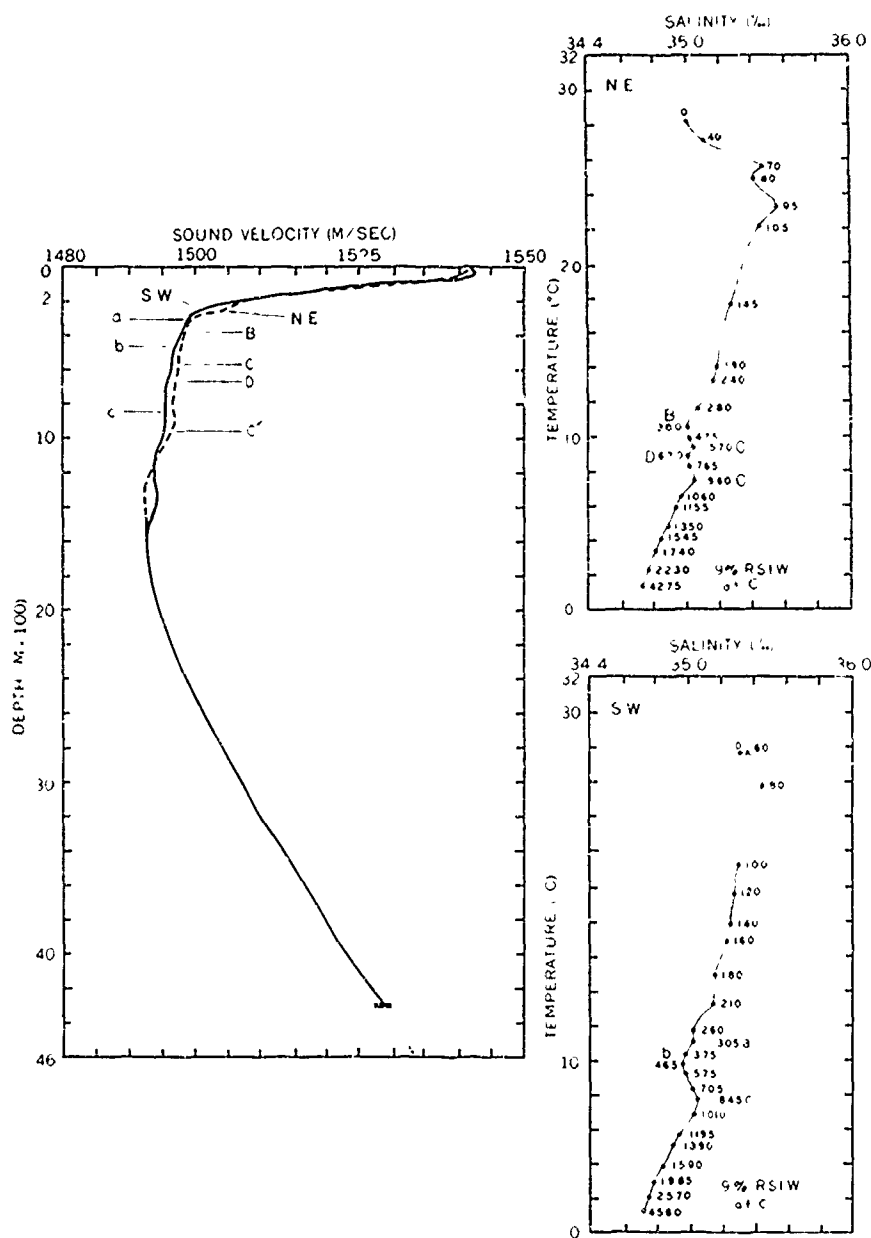


FIGURE B-26. SEASONAL SOUND VELOCITY/T-S COMPARISON

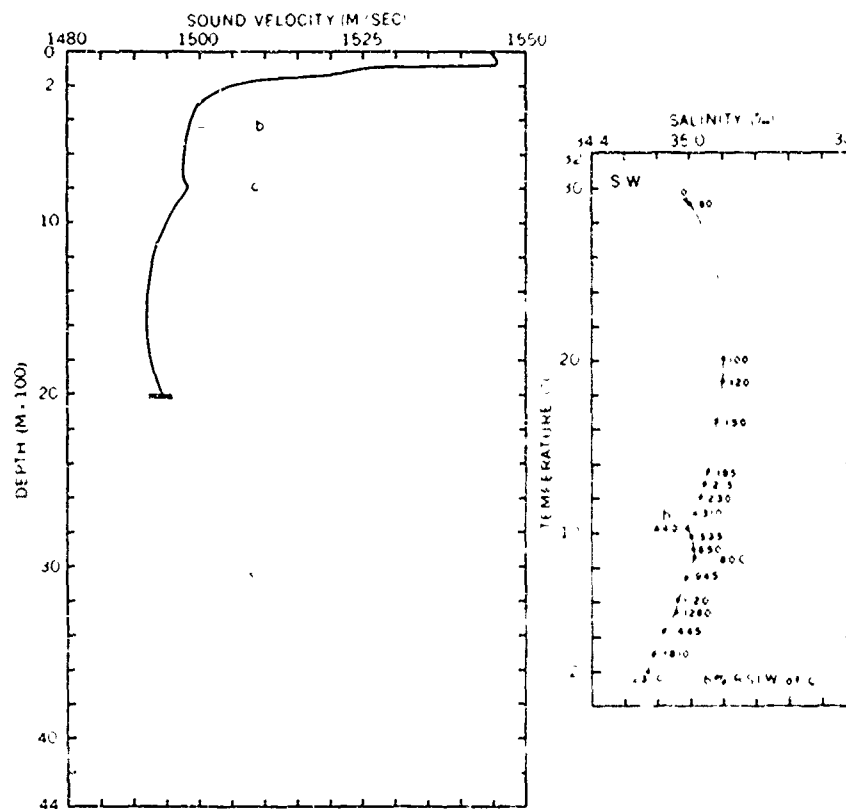


FIGURE B-27. SOUND VELOCITY/T-S COMPARISON FOR SOUTHWEST MONSOON

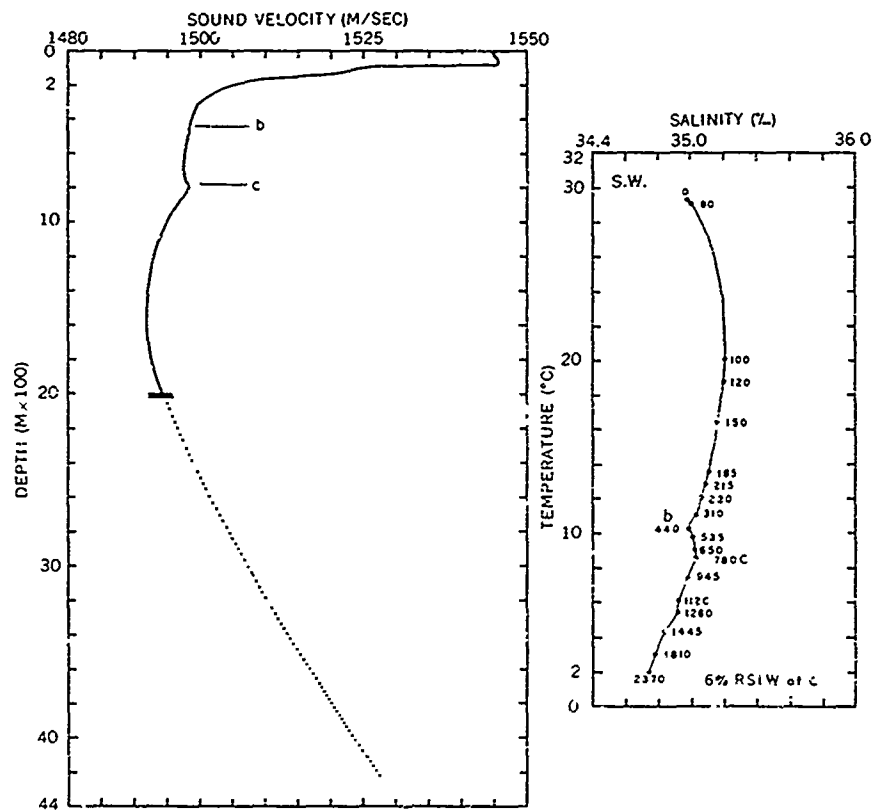


FIGURE B-27. SOUND VELOCITY/T-S COMPARISON FOR SOUTHWEST MONSOON

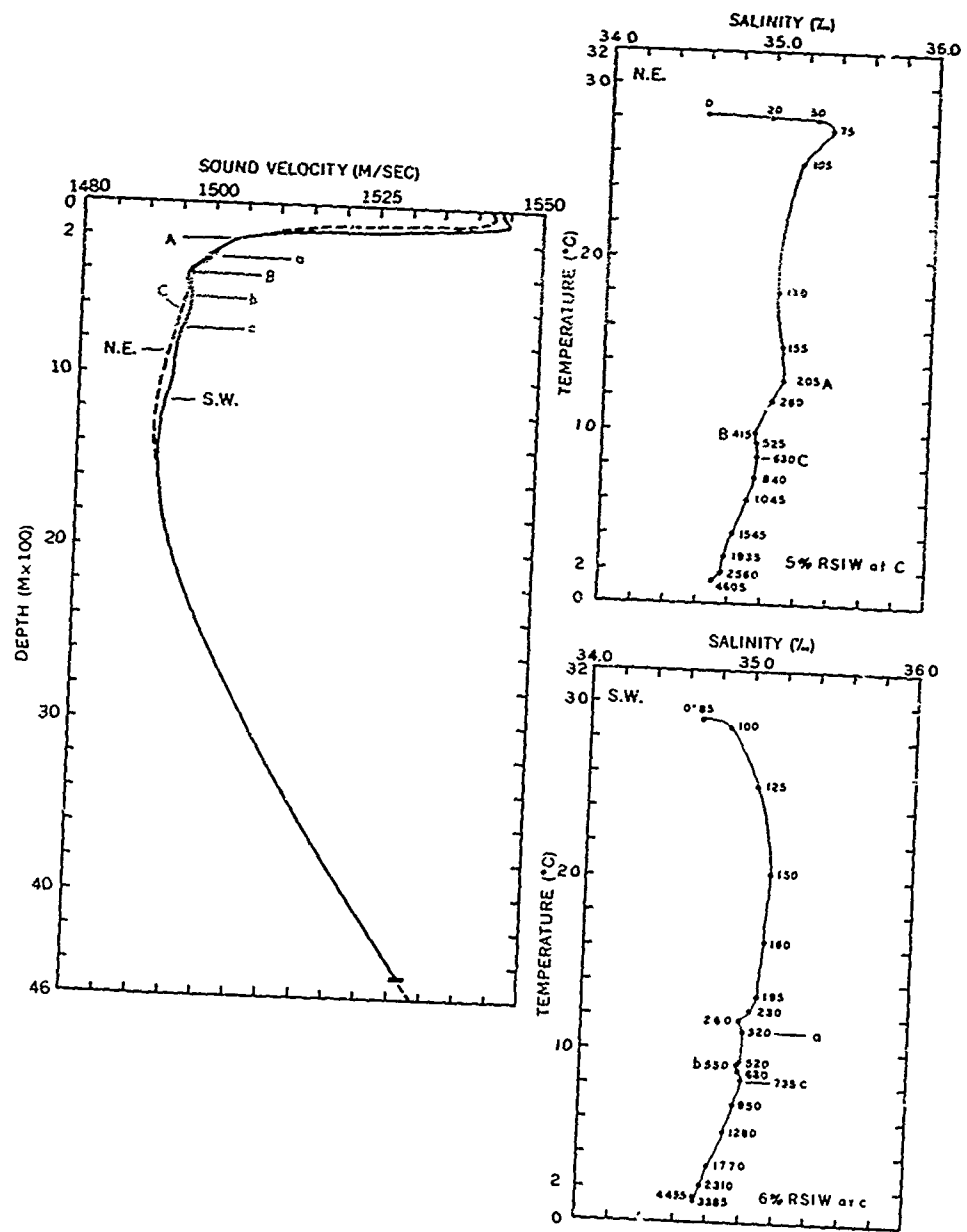


FIGURE B-28. SEASONAL SOUND VELOCITY/T-S COMPARISON

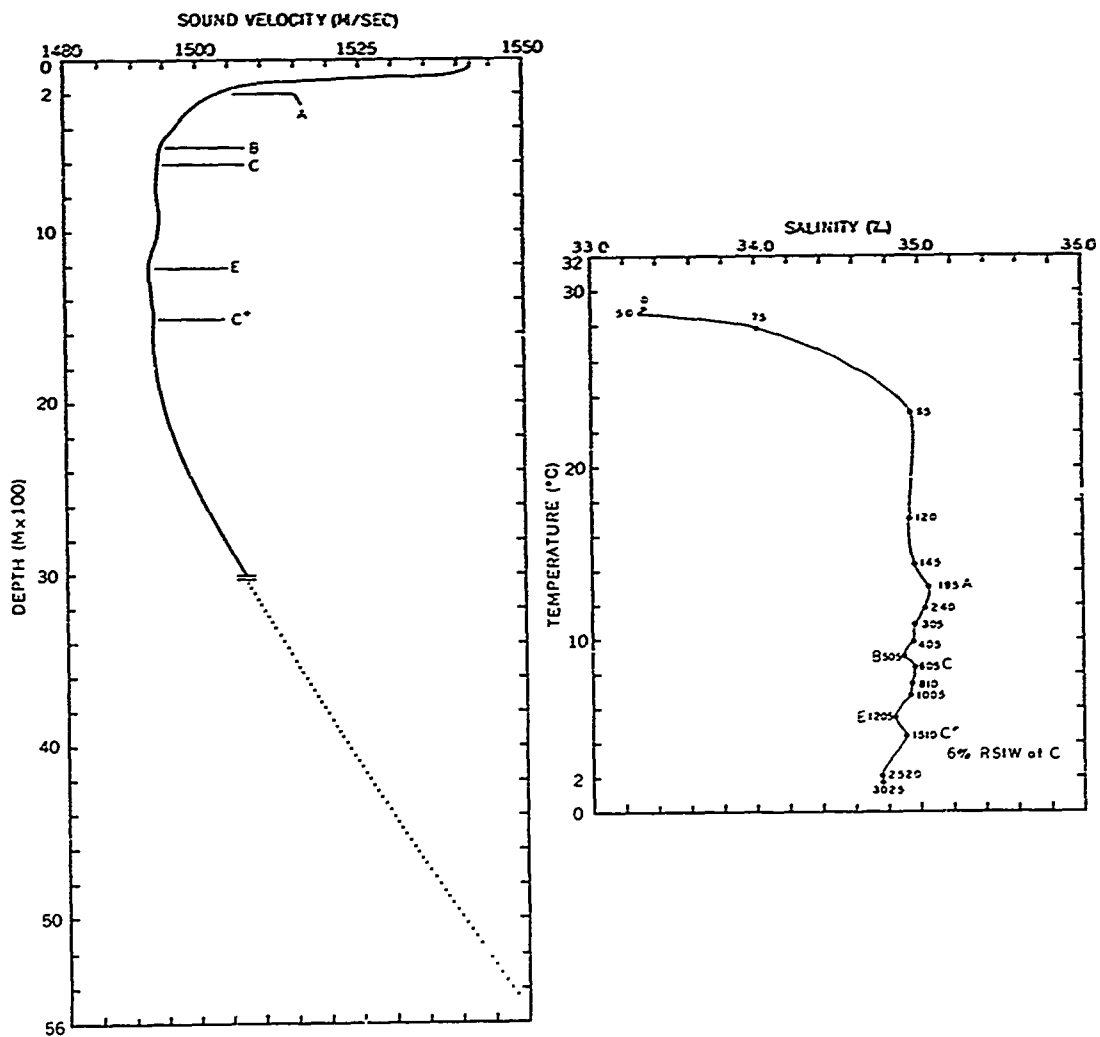


FIGURE B-29. SOUND VELOCITY/T-S COMPARISON FOR NORTHEAST MONSOON

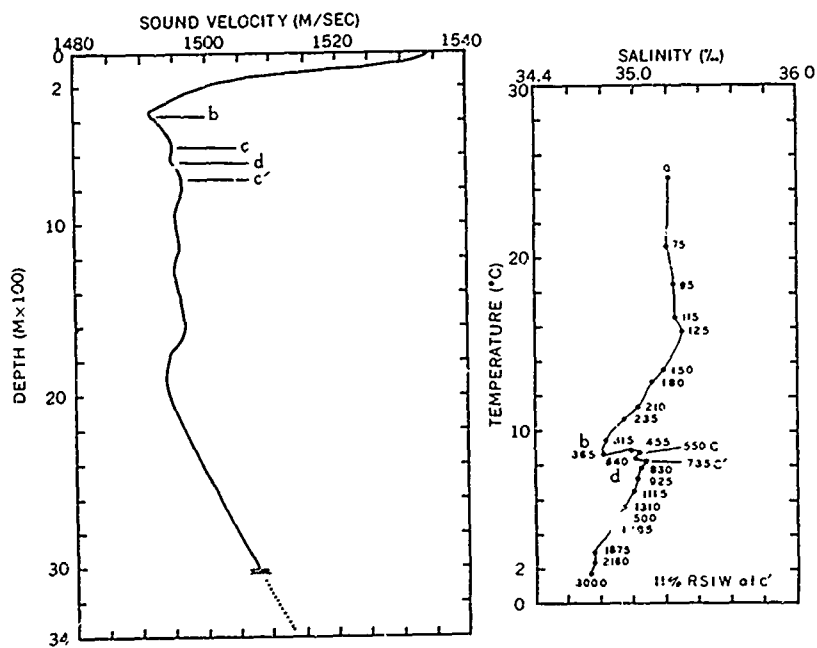


FIGURE B-30. SOUND VELOCITY/T-S COMPARISON FOR SOUTHWEST MONSOON

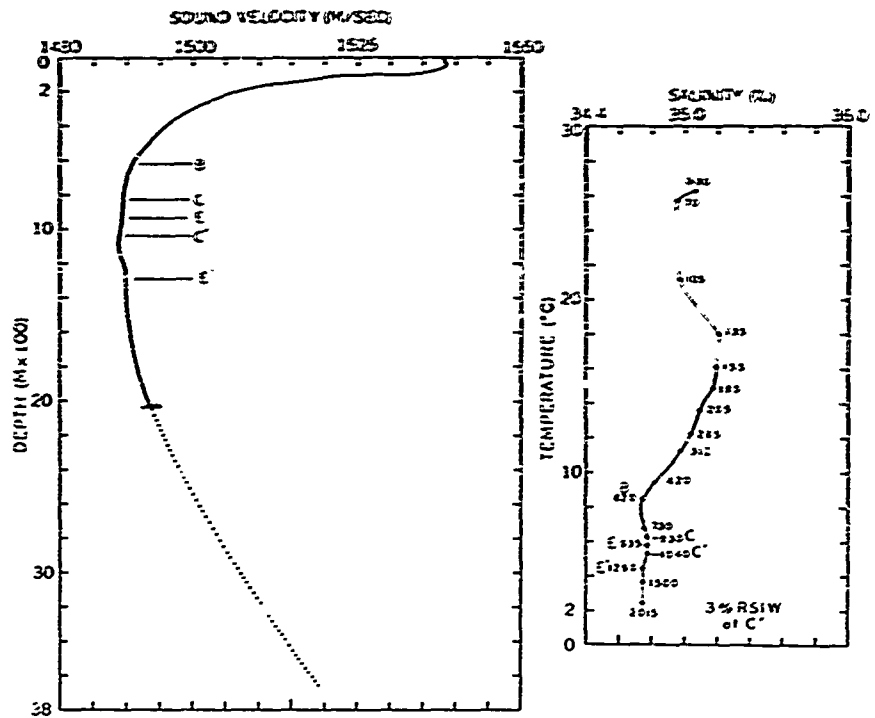


FIGURE B-31. SOUND VELOCITY/T-S COMPARISON FOR NORTHEAST MONSOON

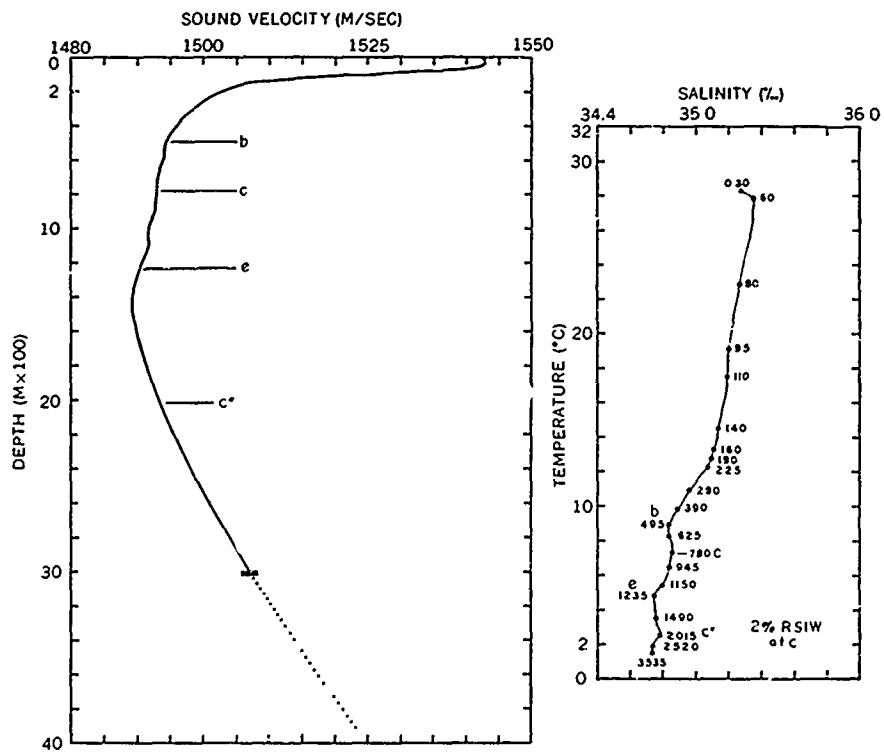


FIGURE B-32. SOUND VELOCITY/T-S COMPARISON FOR SOUTHWEST MONSOON

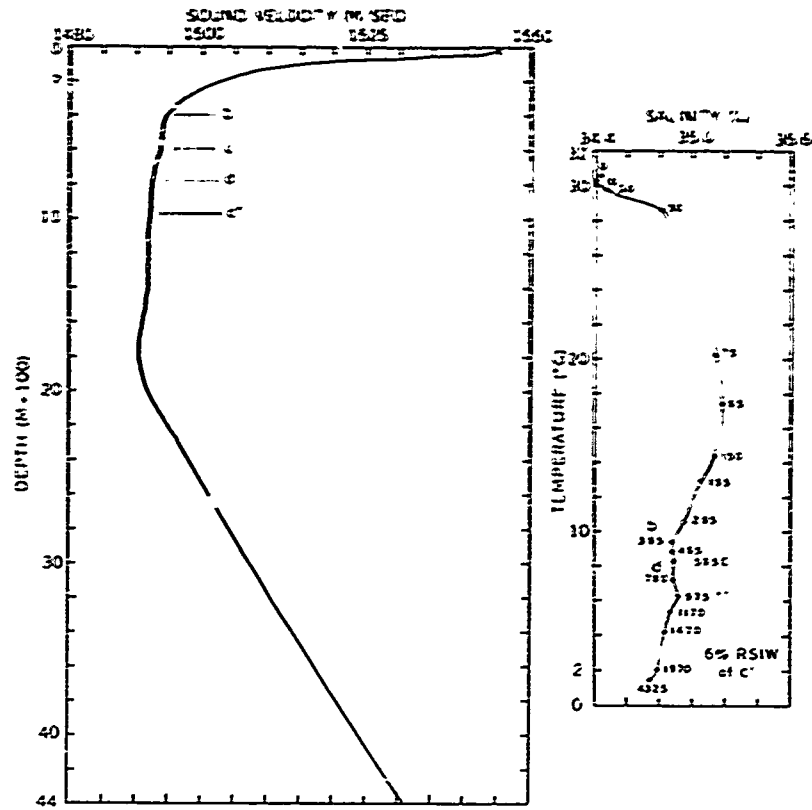


FIGURE B-33. SOUND VELOCITY/T-S COMPARISON FOR SOUTHWEST MONSOON

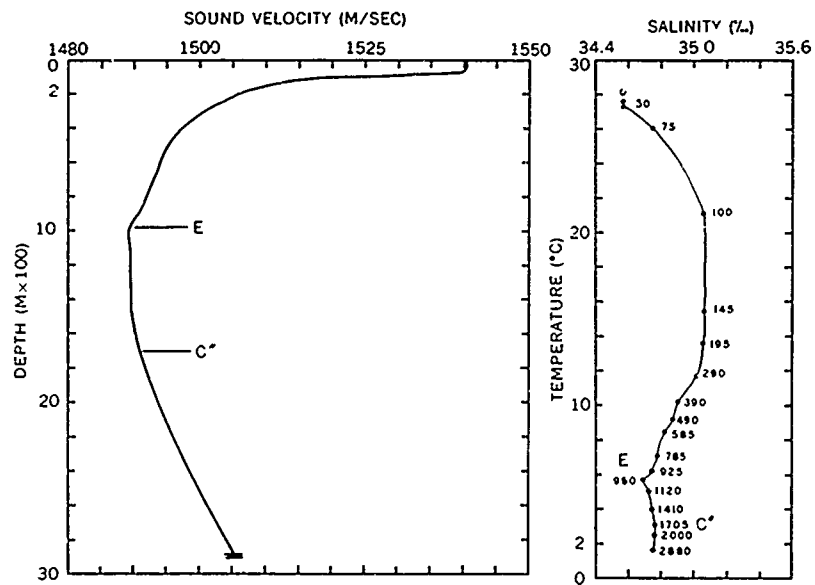


FIGURE B-34. SOUND VELOCITY/T-S COMPARISON FOR NORTHEAST MONSOON

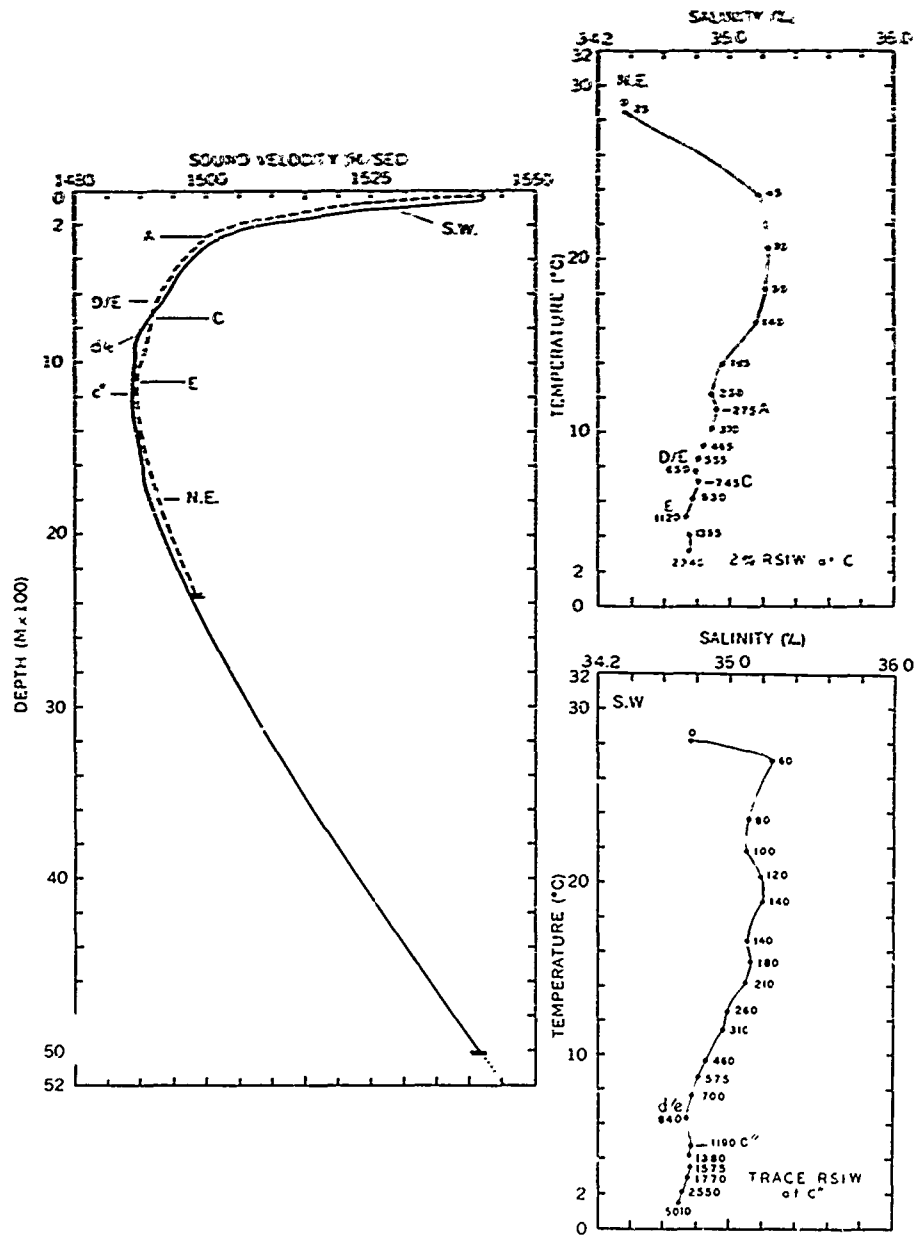


FIGURE B-35. SEASONAL SOUND VELOCITY/T-S COMPARISON

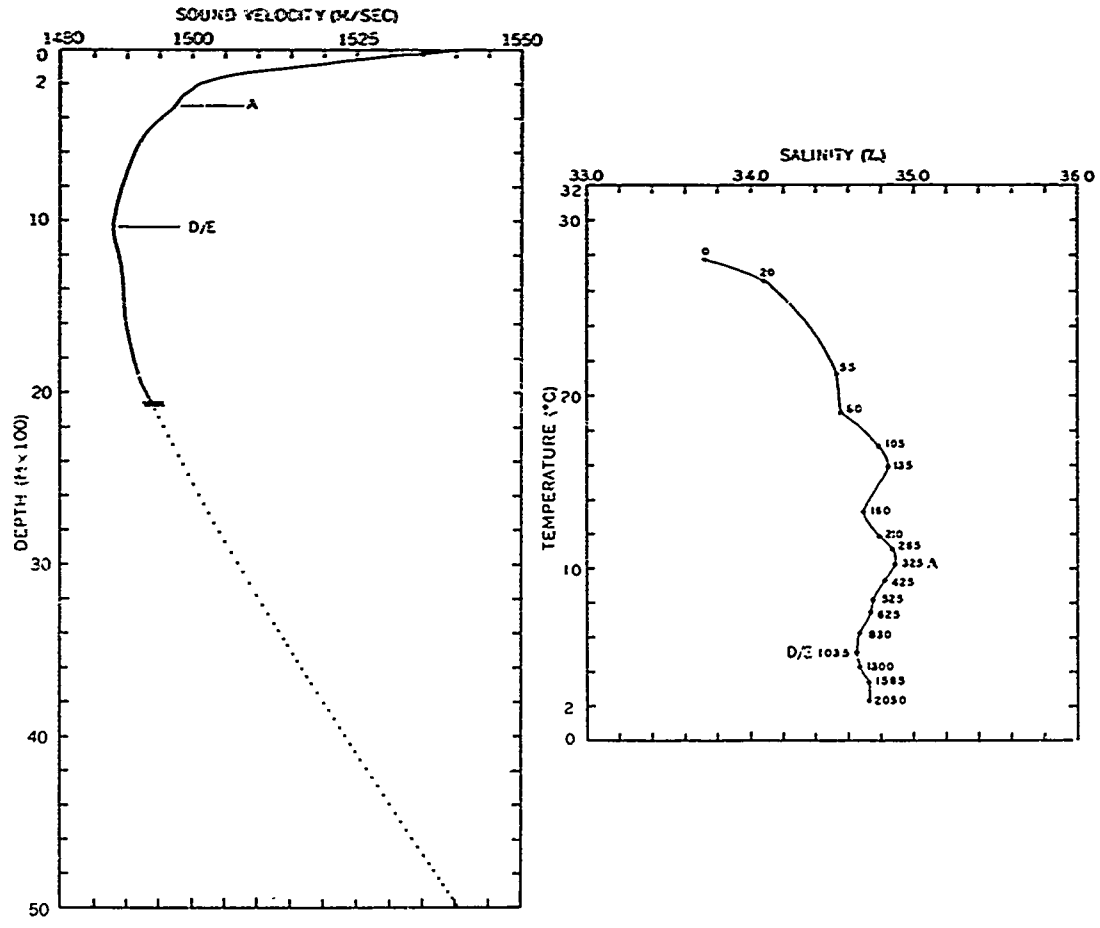


FIGURE B-36. SOUND VELOCITY/T-S COMPARISON FOR NORTHEAST MONSOON

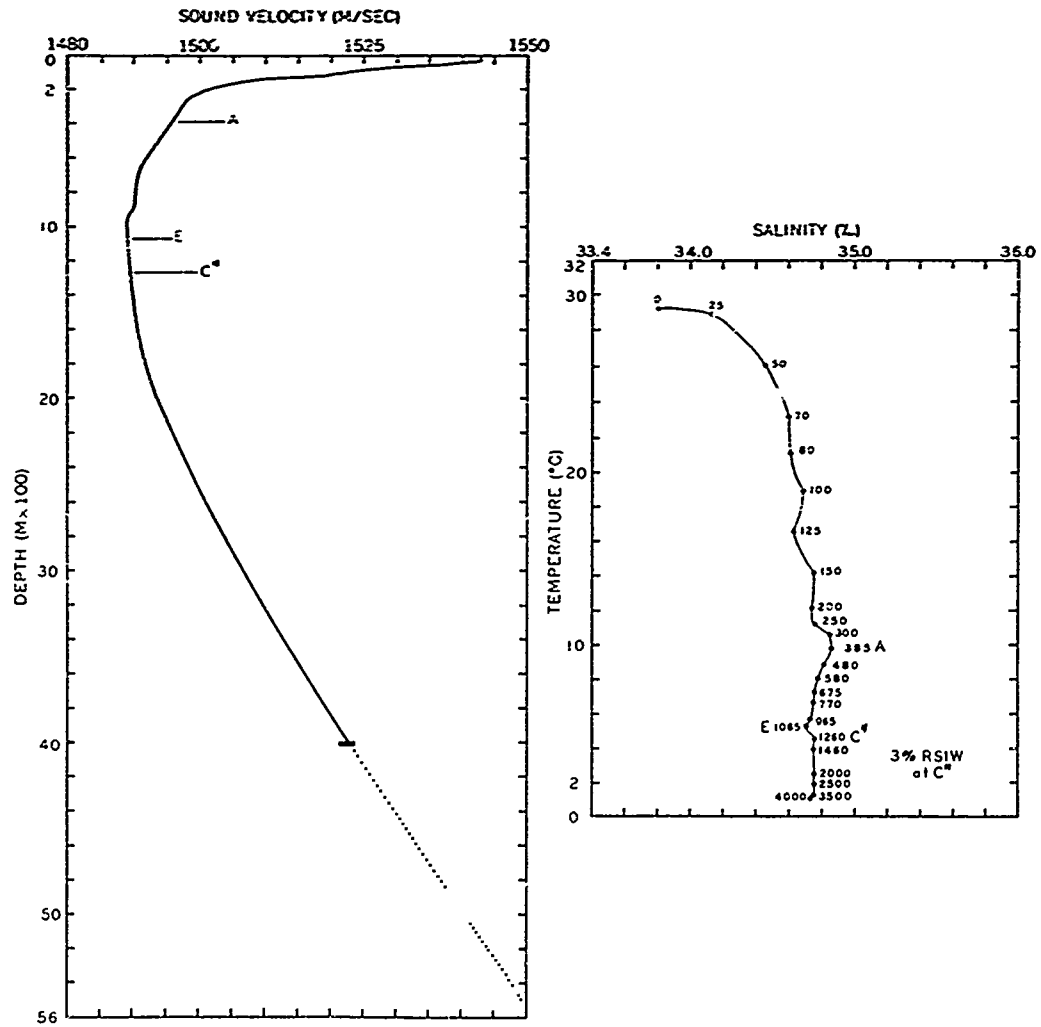


FIGURE B-37. SOUND VELOCITY/T-S COMPARISON FOR NORTHEAST MONSOON

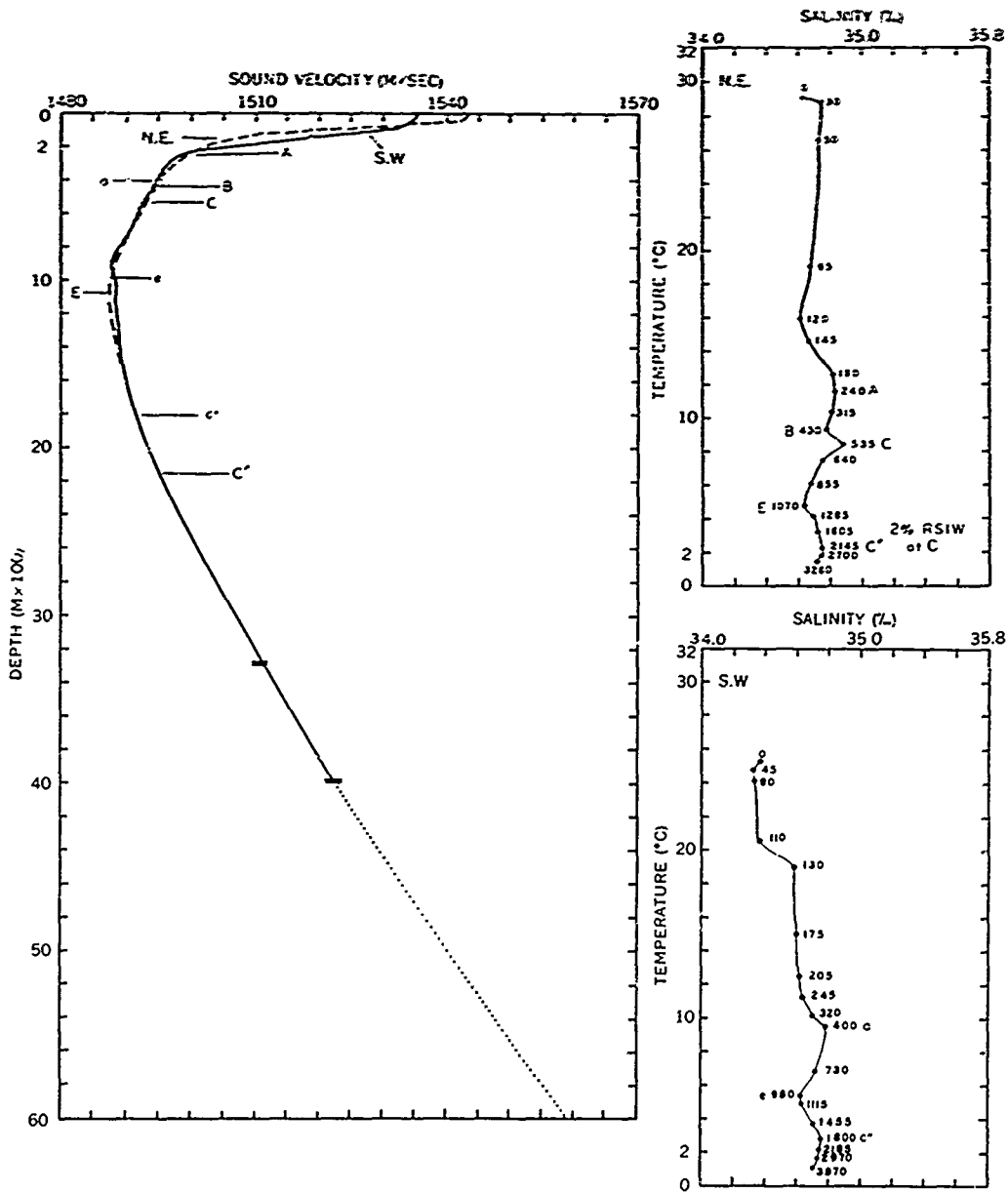


FIGURE B-38. SEASONAL SOUND VELOCITY/T-S COMPARISON

APPENDIX C

GENERALIZED FLOW AT THE SURFACE
AND AT SUBSURFACE AND INTERMEDIATE DEPTHS

APPENDIX C

GENERALIZED FLOW AT THE SURFACE AND AT SUBSURFACE AND INTERMEDIATE DEPTHS

Figures C-1 through C-7 show generalized surface circulation during the northeast and southwest monsoons, generalized flow of subsurface water masses (PGIW and SSW), and generalized flow of intermediate water masses (RSIW, AAIW, and BIW). The various figures show direction of flow only, and are not meant to indicate current magnitudes. Figures C-3 through C-7 (subsurface and intermediate flows) were derived by analyzing salinity maxima and minima core depths. The effects of circulation and water masses on sound velocity structures appears in the main body of the text. Therefore, the following comments are supplementary and not necessarily related to any previous discussion.

Figures C-1 and C-2 (surface circulation during northeast and southwest monsoons, respectively) are highly generalized and closely resemble those of Matthews, Oct 1967. Since the two figures represent composite seasons (Nov-Apr and May-Oct, respectively), they only generally resemble dynamic topography charts for winter (Dec-Feb) and late summer (Jul-Sep) shown by Duing, 1970. However, Figures C-1 and C-2 are adequate for use in explaining sound velocity variations at the surface and in the near-surface layer.

Figure C-3 (PGIW flow) shows substantial modification from that of Rochford, 1964 and is based on much more data. This figure indicates a lesser, seasonal flow in the Somali Basin; a preferential, aseasonal flow along the west coast of India; and a larger, aseasonal flow into the Bay of Bengal and Andaman Sea. A lesser occurrence of PGIW in the Somali Basin is in agreement with the findings of Hamon, 1967 and the occurrence off the west coast of India with the findings of Duing and Koske, 1967. Available data indicate that PGIW flow is aseasonal off the west coast of India and in the region north of the Equator between Ceylon and the northern tip of Sumatra.

Figure C-4 (SSW flow) is highly schematic, particularly south of the Equator in regions where RSIW is substantially diluted and/or occurs only sporadically. In the region south of the Equator between about 80° and 100° E. longitude, SSW flow could not be determined by T-S analysis because RSIW is most often absent. The sporadic flow of SSW into the Gulf of Aden is questionable.

Figure C-5 (RSIW flow) is similar to that of Rochford, 1964 in the Somali Basin, but substantially different throughout the rest of the area. More extensive data now available indicate a preferential flow across the southern Arabian

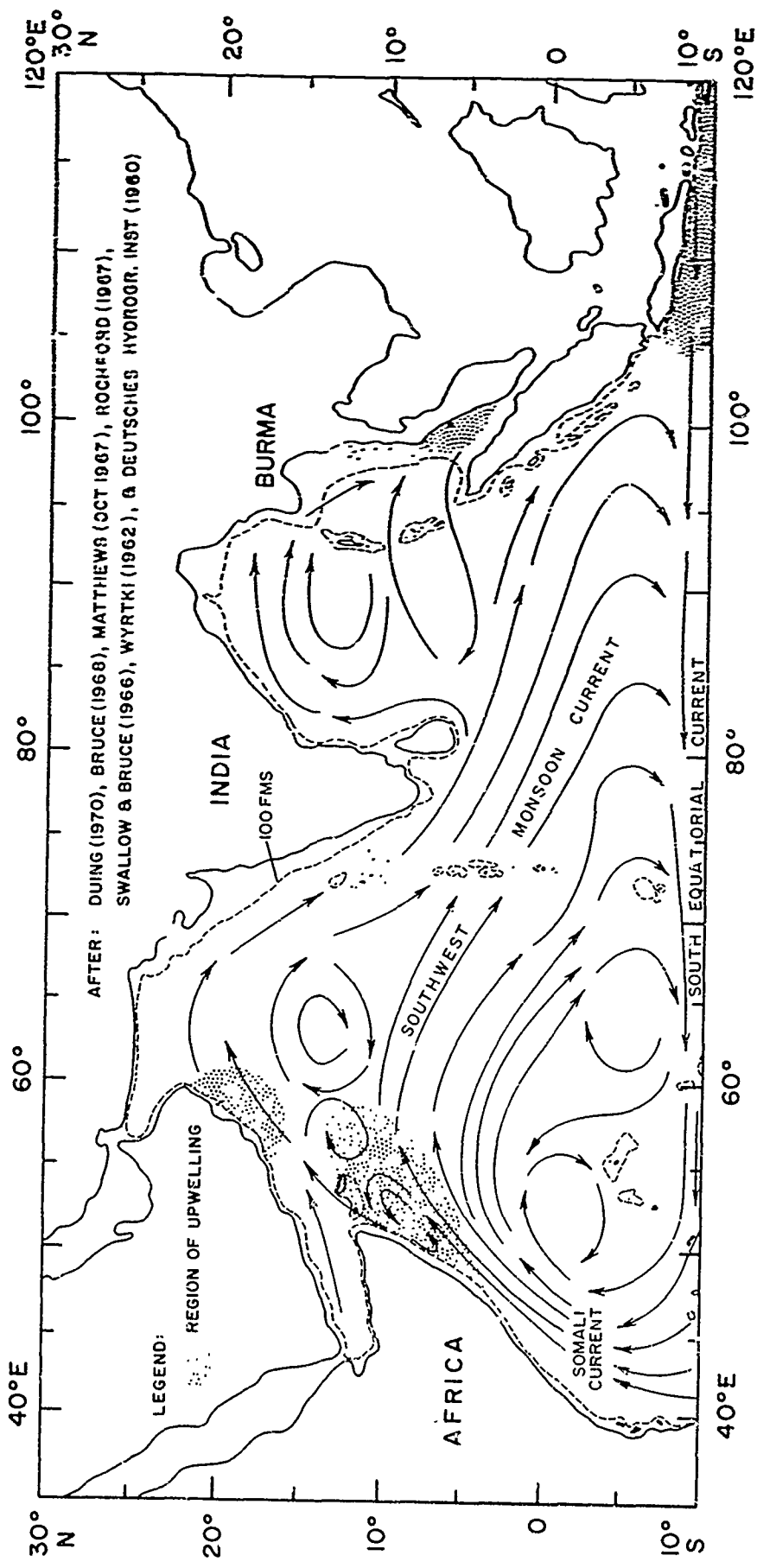


FIGURE C-2. GENERALIZED SURFACE CIRCULATION FOR SOUTHWEST MONSOON (MAY-OCT)

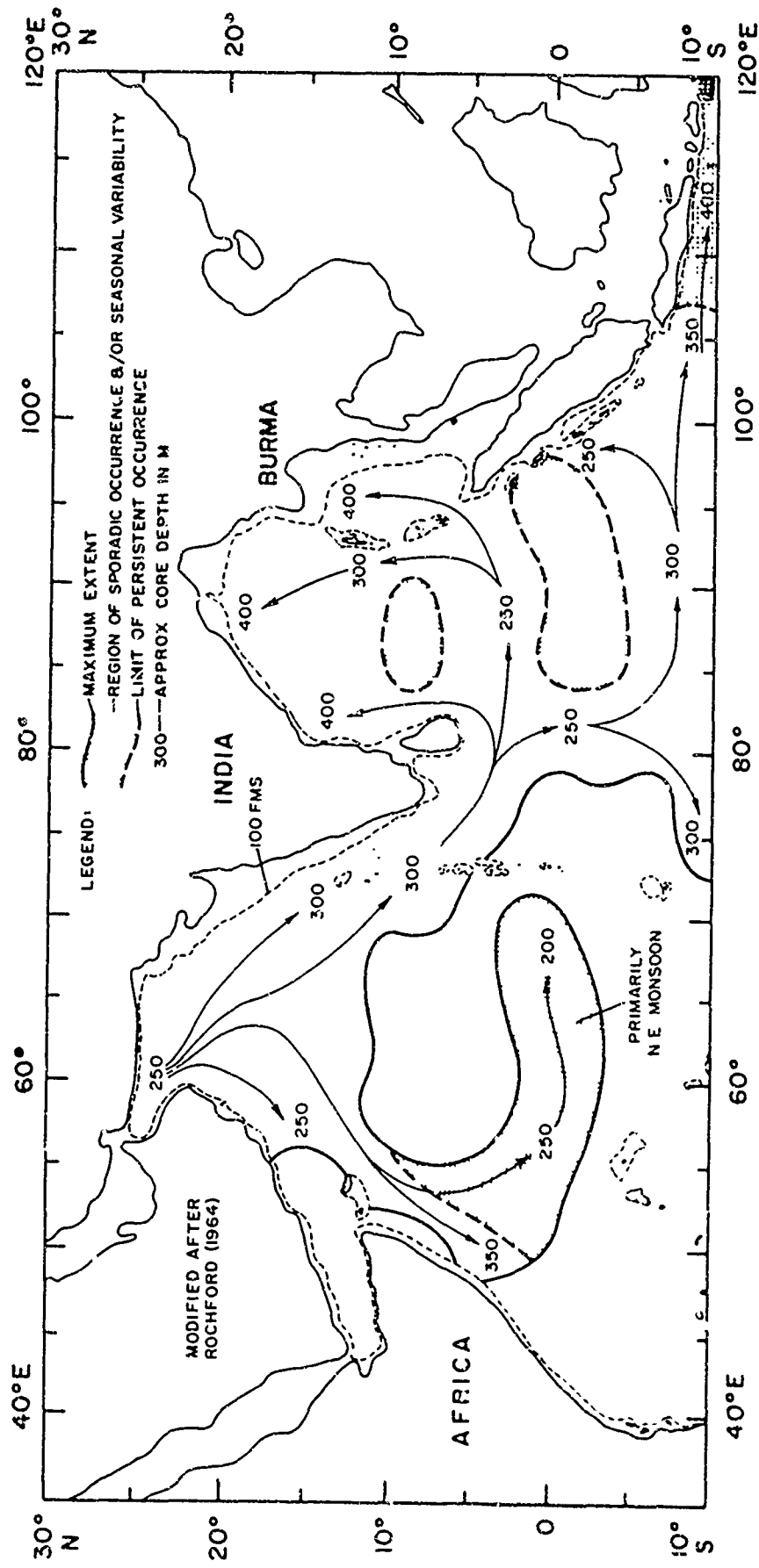


FIGURE C-3 GENERALIZED FLOW OF PERSIAN GULF INTERMEDIATE WATER (PGIW) HIGH SALINITY CORE

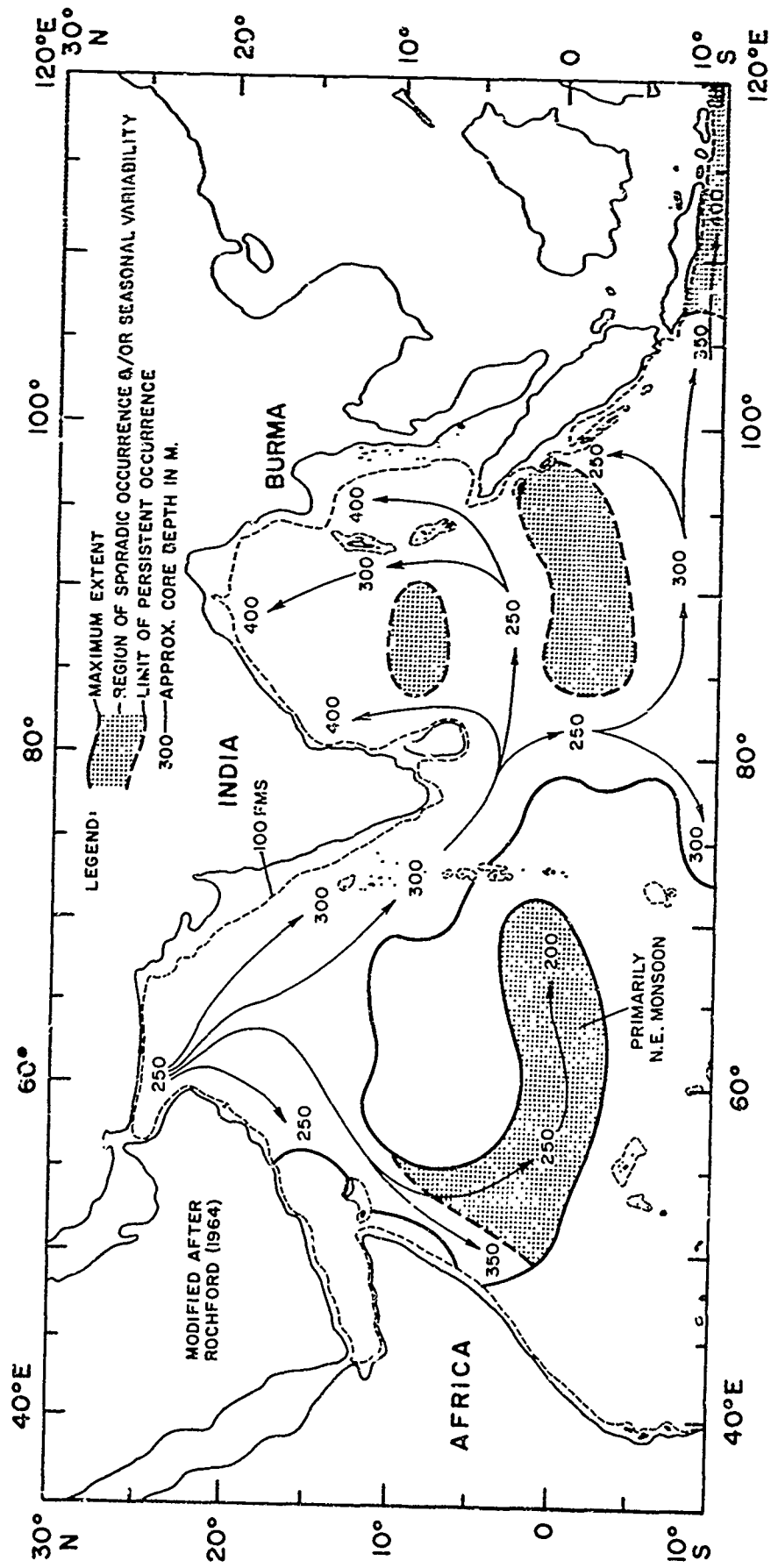


FIGURE C-3. GENERALIZED FLOW OF PERSIAN GULF INTERMEDIATE WATER (PGIW) HIGH SALINITY CORE

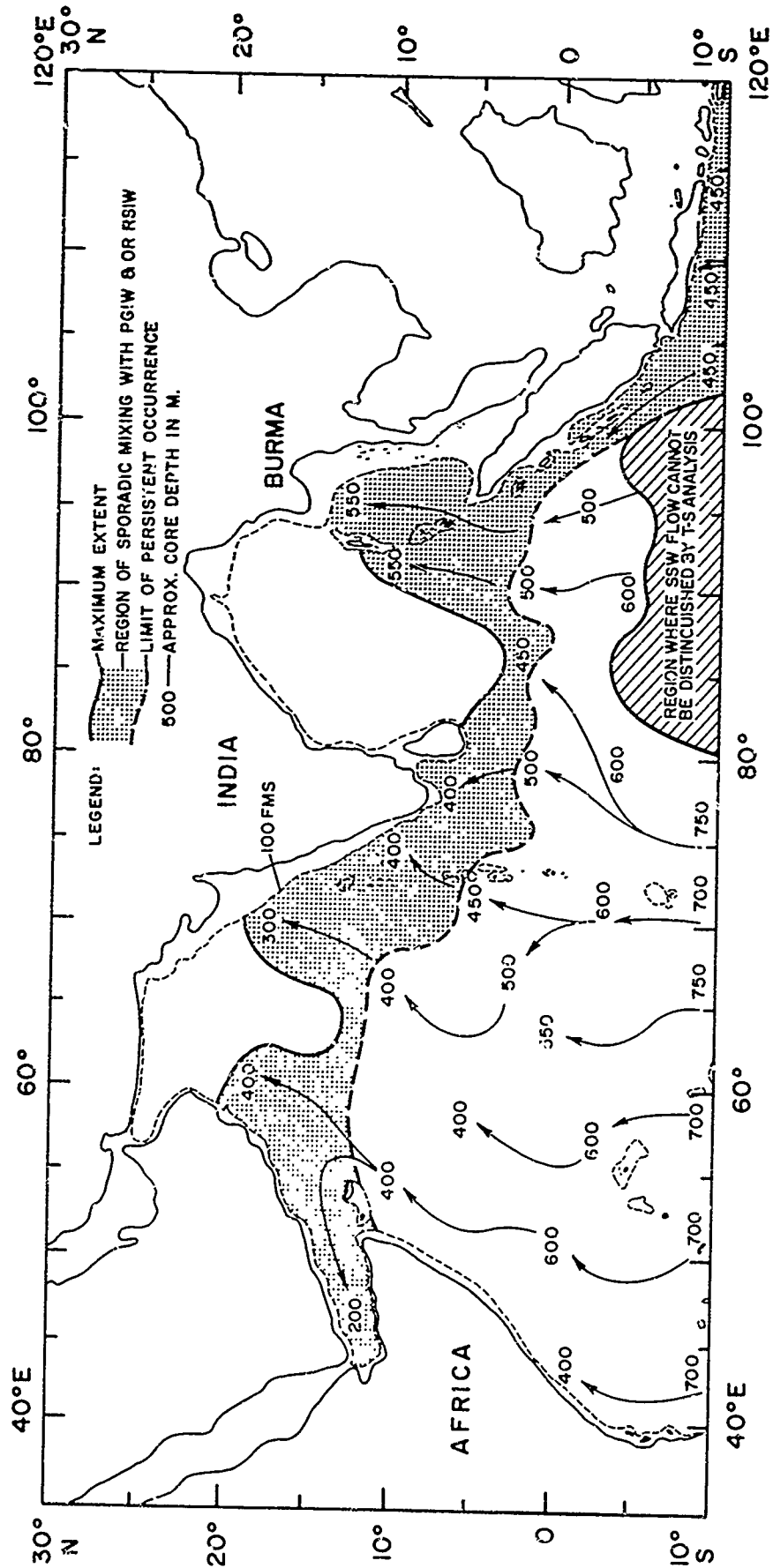


FIGURE C-4. GENERALIZED FLOW OF SUBTROPICAL SUBSURFACE WATER (SSW) LOW SALINITY CORE

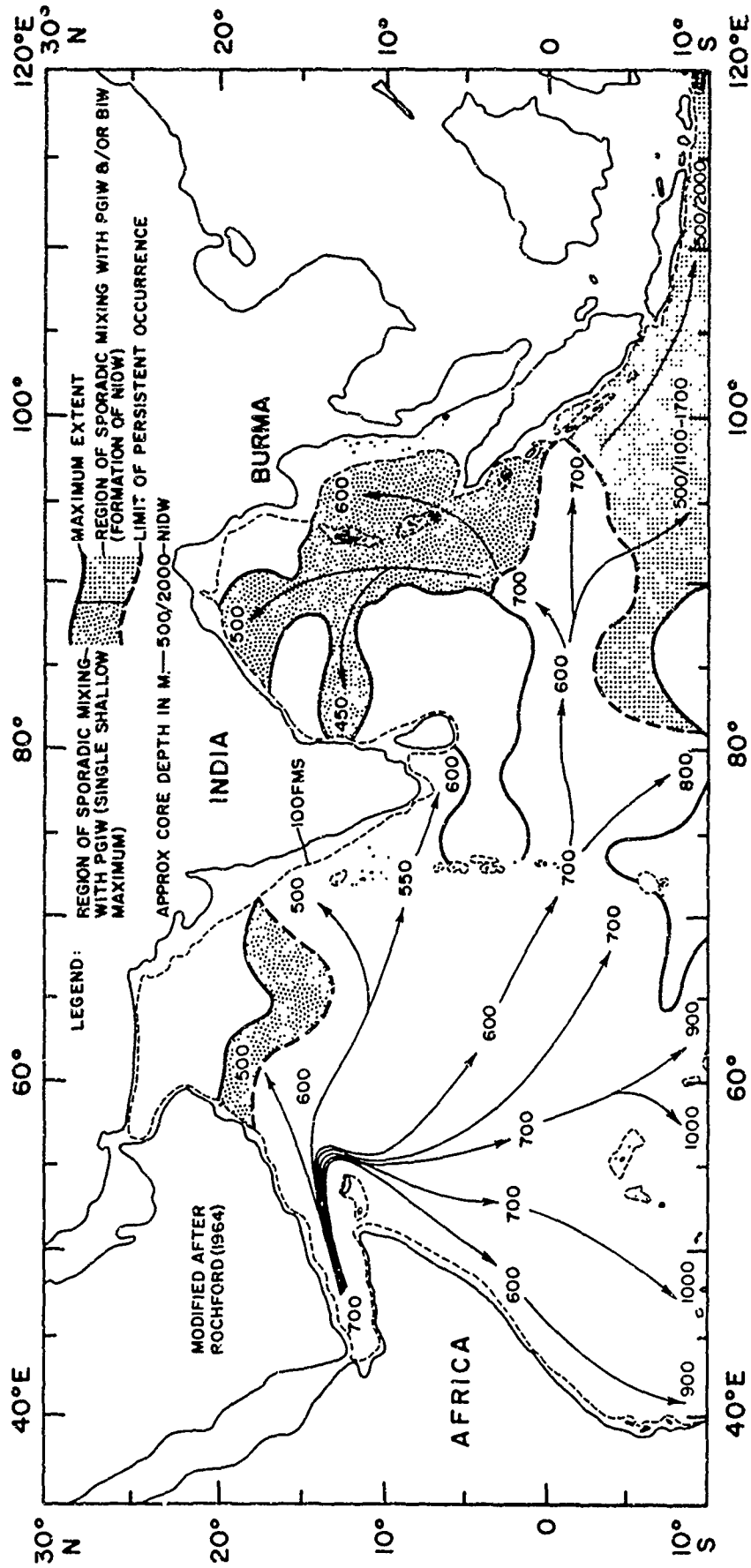


FIGURE C-5. GENERALIZED FLOW OF RED SEA INTERMEDIATE WATER (RSIW) HIGH SALINITY CORE

Basin that terminates in the region west of Ceylon; a strong, preferential flow between the Laccadive Islands and the Chagos Archipelago; a persistent flow along the Equator between the Chagos-Laccadive Ridge and Sumatra; and a more substantial flow into the Bay of Bengal and the Andaman Sea. All these flows occur during both monsoons. Seasonal independence of RSIW flow is in agreement with the findings of Duing, 1970 concerning vertical extent of monsoonal effects (less than 250 meters except in the western Somali Basin and off the southwest coast of India).

However, there is a monsoonal variation in RSIW concentrations in the Gulf of Aden (Figure B-7), western Somali Basin (Figures B-11 and B-25), southern Arabian Basin (Figure B-13), and Mid-Indian Basin (Figure B-35). On all these seasonal T-S comparisons, higher RSIW concentrations were found during the northeast monsoon. More RSIW enters the Gulf of Aden during the northeast monsoon due to the lack of a northward flowing current in Bab-el-Mandeb (Seriy, 1968). Therefore, relatively greater unmixed concentrations of RSIW are found during the northeast monsoon throughout the area. Seasonal reversal of RSIW may occur in the western Somali Basin south of the Equator as postulated by Warren, et al., 1966 and Krause, 1968. However, present data are inadequate to substantiate this reversal.

Figure C-6 (AAIW flow) is based on inadequate data south of about 5° S. latitude, particularly in the center of the area (Figure 4). Existing Nansen cast data often were taken at depths that missed the well mixed AAIW core. Based on all available data, the shoal bathymetry of the Chagos-Laccadive Ridge precludes an AAIW flow north along 70° E. longitude. In addition, the Seychelles Islands apparently cause a bifurcation in AAIW flow. When present, the AAIW salinity minimum generally occurs between two RSIW salinity maxima (Figures B-25, B-26, and B-33). This indicates that AAIW does not flow north between the PGIW and RSIW high salinity cores as postulated by Rochford, 1966b, but interfingers with RSIW below the 27.0 to 27.2 sigma-t surfaces as postulated by Warren, et al., 1966.

Figure C-7 (BIW flow) is similar to that of Rochford, 1966a in the region east of about 70° E. longitude. More extensive historical data in the southern Somali and North Mascarene Basins indicates that BIW occurs persistently due east and south of the Seychelles Islands (Figures B-31 and B-32) and sporadically to about 5° N. latitude (Figure B-19). As noted by Rochford, 1966a, BIW occurs on about the 27.4 sigma-t surface and often is separated from AAIW by a RSIW salinity maximum (Figure B-35). BIW probably is as influential as RSIW in blocking the northward spread of AAIW, and often mixes with AAIW to form a single salinity minimum (Figure B-36). RSIW inhibits the westward flow of BIW and often interfingers with BIW below the 27.4 sigma-t surface (Figure B-31).

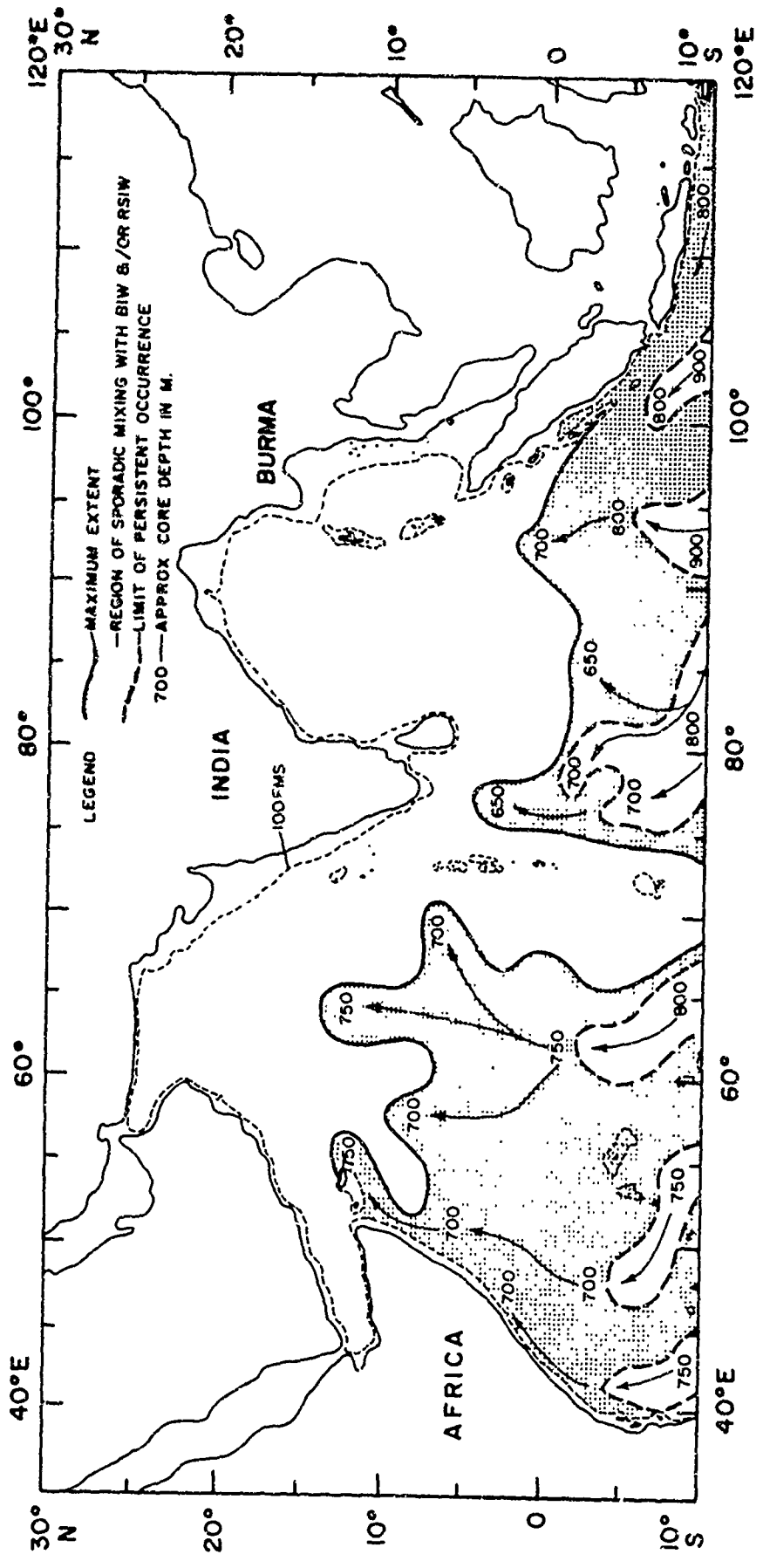


FIGURE C-6. GENERALIZED FLOW OF ANTARCTIC INTERMEDIATE WATER (AAIW) LOW SALINITY CORE

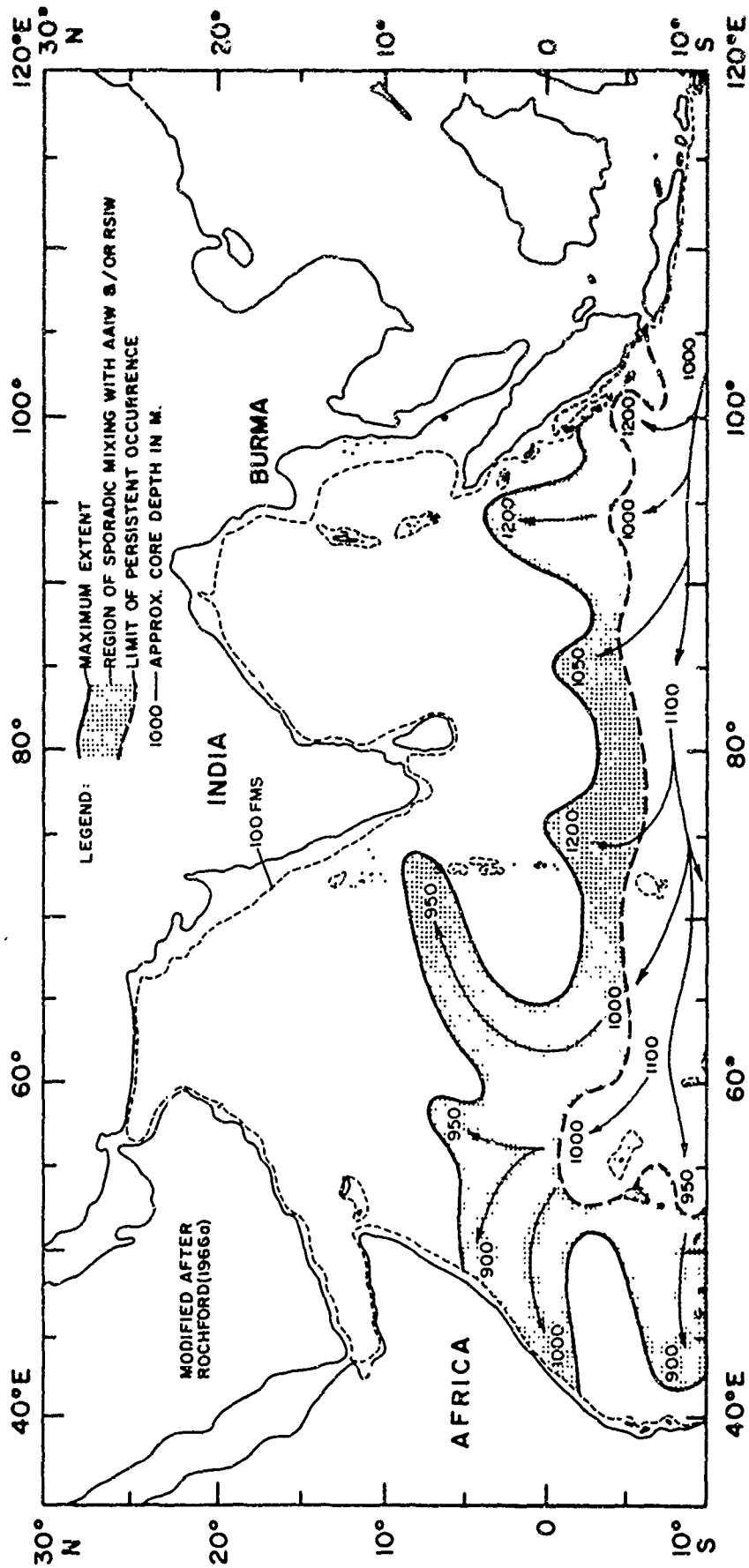


FIGURE C-7. GENERALIZED FLOW OF BANDA INTERMEDIATE WATER (BIW) LOW SALINITY CORE

NATIONAL OCEANOGRAPHIC ADMINISTRATION, U.S. DEPARTMENT OF COMMERCE, WASHINGTON, D.C. 20540

This process can lead to the formation of NIDW (Figure B-32), particularly in the region south of about 5° S. latitude and east of about 80° E. longitude (also see Figure C-5). As noted by Rochford, 1966a, the preferential westward flow of BIW is along or south of 10° S. latitude, particularly in the region west of the Chagos Archipelago.

REFERENCES

- Bruce, J. G., 1968, Comparison of near surface dynamic topography during the two monsoons in the western Indian Ocean: *Deep-Sea Res.*, v. 15, p. 665-677.
- Commonwealth Scientific and Industrial Research Organization, Australia, 1967, Oceanographical observations in the Indian Ocean in 1964, HMAS DIAMANTINA, Cruise DM2/64: CSIRO Aust. Oceanogr. Cruise Rept. no 36.
- Curry, J. R., and Moore, D. G., 1971, Growth of the Bengal Deep-Sea Fan and denudation in the Himalayas: *Geol. Soc. Am. Bull.*, v. 82, p. 563-572.
- Defant, A., 1961, *Physical oceanography*, v. 1: New York, Pergamon Press, 729 p.
- Deutsches Hydrographisches Institut, 1960, Monatskarten für den Indischen Ozean: Pub. no. 2422, Hamburg, unpaginated (in German).
- Duing, W., 1970, The monsoon regime of the currents in the Indian Ocean: IIOE Oceanogr. Monograph no. 1, Honolulu, East-West Center Press, 68 p.
- Duing, W., and Koske, P. H., 1967, Hydrographische Beobachtung im Arabischen Meer während der Zeit des Nordostmonsuns 1964/65: *METEOR Forsch. Erg.*, ser. A, no. 3, p. 1-44 (in German, English summary).
- Fenner, D. F., and Bucca, P. J., Dec 1969, The upper and deep sound channel in the northeast Atlantic: *Naval Oceanogr. Off. Informal Rept.* no. 69-94 (unpublished).
- Jan 1971, Sound velocity structure of the northwest Indian Ocean: prepared for Symposium on Indian Ocean and Adjacent Seas, Marine Biol. Assoc. India, Cochin (to appear in *Jour. Mar. Biol. Assoc. India*, V. 14).
- Nov 1971, The sound velocity structure of the North Atlantic Ocean: *Naval Oceanogr. Off. Informal Rept.* no. 71-13 (unpublished).
- Fisher, R. L., Engel, C. G., and Hilde, T. W. C., 1968, Basalts dredged from Amirante Ridge, western Indian Ocean: *Deep-Sea Res.*, v. 15, p. 521-534.

REFERENCES (CONTINUED)

- Fomicev, A. V., 1964, A study of the currents in the northern part of the Indian Ocean: *Trud. Inst. Okeanol.*, v. 64, p. 43-50 (in Russian, English abstract).
- Hamon, B. V., 1967, Medium-scale temperature and salinity structure in the upper 1500m in the Indian Ocean: *Deep-Sea Res.*, v. 14, p. 169-181.
- Ivanenkov, V. N., and Gubin, F. A., 1960, Water masses and hydrochemistry of the western and southern parts of the Indian Ocean: *Trud. Morsk. Gidrofiz. Inst.*, v. 22, p. 33-115 (translated from Russian by Am. Geophys. Union).
- Johnson, R. H., and Norris, R. A., Apr 1967, Geographic variation in SOFAR speed and axis depth in the Pacific: *Hawaii Inst. Geophys. Rept. no. HIG 67-7*.
- Krause, G., 1968, Struktur und Verteilung des Wassers aus dem Roten Meer im Nordwestern des Indischen Ozeans *METEOR Forsch. Erg.*, ser. A, no. 4, p. 77-100 (in German, English summary).
- LaViolette, P. E., Aug 1967, Temperature, salinity and density of the World's seas. Bay of Bengal and Andaman Sea *Naval Oceanogr. Off. Informal Rept. no. 67-57* (unpublished).
- LaViolette, P. E., and Froarenc, T. R., Aug 1967, Temperature, salinity and density of the World's seas. Arabian Sea, Persian Gulf, and Red Sea: *Naval Oceanogr. Off. Informal Rept. no. 67-49* (unpublished).
- Mamayev, O. I., 1969, Generalized T-S diagrams of the water masses of the World Ocean *Oceanology*, v. 9, no. 1, p. 49-55 (translated from Russian by Am. Geophys. Union).
- Matthews, S. W., Oct 1967, Science explores the monsoon sea: *Nat. Geographic Mag.*, v. 132, no. 4, p. 554-573.
- Moore, C. T., Nov 1965, Tables of sound speed at the bottom below 1,000 fathoms in the North Atlantic Ocean: *Naval Oceanogr. Off. Informal Manuscript Rept. no. 0-52-65* (unpublished).
- Olson, B. E., Jun 1968, On the abyssal temperatures of the World Oceans: PhD thesis, Oregon State Univ., Corvallis, 151 p.

REFERENCES (CONTINUED)

- Ovchinnikov, I. M., 1961, Circulation of waters in the northern part of the Indian Ocean during the winter monsoon: *Okeanol. Issled.*, v. 4, p. 18-24 (in Russian, English abstract).
- Rochford, D. J., 1964, Salinity maxima in the upper 1000 meters of the north Indian Ocean: *Aust. Jour. Mar. Freshw. Res.*, v. 15, p. 1-24.
- 1966a, Distribution of Banda Intermediate Water in the Indian Ocean: *Aust. Jour. Mar. Freshw. Res.*, v. 17, p. 61-76.
- 1966b, Source regions of oxygen maxima in intermediate depths of the Arabian Sea: *Aust. Jour. Mar. Freshw. Res.*, v. 17, p. 1-30.
- 1967, The phosphate levels of major surface currents of the Indian Ocean: *Aust. Jour. Mar. Freshw. Res.*, v. 18, p. 1-22.
- Rodolfo, K. S., 1969, Bathymetry and geology of the Andaman Basin, and tectonic implications for Southeast Asia: *Geol. Soc. Am. Bull.*, v. 80, p. 1203-1230.
- Ryther, J. H., and Menzel, D. C., 1965, On production, composition, and distribution of organic matter in the western Arabian Sea: *Deep-Sea Res.*, v. 12, p. 199-209.
- Scully-Power, P. D., Apr 1969, Oceanographic cruise, South China Sea and Indian Ocean, August-November 1966: Royal Aust. Navy Res. Lab. Tech. Memo. (external) 4/68.
- Seriy, V. V., 1968, The problem of water exchange between the Red Sea and the Gulf of Aden: *Okeanol. Issled.*, v. 19, p. 195-200 (translated from Russian as Naval Oceanogr. Off. Transl. no. 546, 1971).
- Shcherbinin, A. D., 1969a, Water structure of the equatorial Indian Ocean: *Oceanology*, v. 9, no. 4, p. 487-495 (translated from Russian by Am. Geophys. Union).
- 1969b, Deep waters of the Indian Ocean: *Oceanology*, v. 9, no. 6, p. 783-792 (translated from Russian by Am. Geophys. Union).

REFERENCES (CONTINUED)

- Sverdrup, H. U., Johnson, M. W., and Fleming, R. H., 1942, *The oceans, their physics, chemistry, and general biology*: Englewood Cliffs, Prentice Hall, 1087 p.
- Swallow, J. C., and Bruce, J. G., 1966, Current measurements off the Somali coast during the southwest monsoon of 1964: *Deep-Sea Res.*, v. 13, p. 861-868.
- Warren, B., Stommel, H., and Swallow, J. C., 1966, Water masses and patterns of flow in the Somali Basin during the southwest monsoon of 1964: *Deep-Sea Res.*, v. 13, p. 825-860.
- Wilson, W. D., 1960, Equation for speed of sound in seawater: *Jour. Acoustical Soc. Am.*, v. 32, no. 10, p. 1357.
- Wyrki, K., 1962, The upwelling in the region between Java and Australia during the south-east monsoon: *Aust. Jour. Mar. Freshw. Res.*, v. 13, p. 217-225.
- Zaklinskii, G. B., 1963, Deep circulation of water in the Indian Ocean: *Okeanologiya*, v. 3, no. 4, p. 591-598 (translated from Russian in *Deep-Sea Res.*, v. 11, p. 286-292, 1964).